Wenmin Xia, M.Sc.

The role of abhydrolase domain containing 15 (ABHD15) in lipid metabolism

---

DOCTORAL THESIS

to obtain the academic degree

Doktorin der Naturwissenschaften

submitted to

Graz University of Technology

Direct supervisor:

Assoc.Prof. Mag. Dr.rer.nat. Juliane Bogner-Strauss

Institute of Biochemistry

Co-supervisor:

Assoc. Univ.-Prof. Mag. Dr.rer.nat. Guenter Haemmerle

Institute of Molecular Biosciences, University of Graz

Graz, September 2018

AFFIDAVIT

I declare that I have authored this thesis independently, that I have not used other than the declared sources/resources, and that I have explicitly indicated all material which has been quoted either literally or by content from the sources used. The text document uploaded to TUGRAZonline is identical to the present doctoral thesis.

Date	Signature

Preface

This PhD project started in April 2015 and is enrolled in DK-MCD. The work has been performed under supervision of Associate Prof. Juliane G. Bogner-Strauss. Ten months were spent abroad at University of California, San Diego, in the laboratory of Prof. Alan R. Saltiel.

Acknowledgement

Three and half years ago, I made a brave and challenging decision to pursue my PhD degree at Graz. This was not an easy journey, but I was lucky enough to meet my supervisor-Juliane Bogner-Strauss. *A teacher affects eternity, she can never tell where her influence stops*. I still remember those moments when I was badly hurt/disappointed and she gave me a hug and supported me go through all the rocks; I still remember those moments when I was extremely anxious and she gave encouraging words to help me jump over those barriers. At this memorial date, I would like to give my most gratitude to Juliane, and wish her all success in the new field.

Another valuable appreciation goes to all members of the Bogner-Strauss lab. Thank you Ariane for guiding me through the beginning of my studies. Thank you Thomas and Wolfi for helping me with experiments. Thank you Dina, Kathi and Furkan for fruitful discussions and introducing me to your joyful life. Thank you Meli for being a reliable friend and labmate. Thank you Claudia, Flo and Su for all the administrative and miscellaneous stuff. Thank you Kathi (W.), Gabriel and Juergen for producing many cheerful moments.

Thanks to the big family of DK-MCD and Karin who always patiently answered my questions and who was helpful with setting down my life when I just arrived in Graz. Thanks to Dagmar and Gerald for sharing their experiences how to deal with stress from work. Thanks to Guenter for being my new supervisor in the last months. Thanks to all the members in my thesis committee for sharing their knowledge and helping me overcoming scientific difficulties.

I also want to give my special thanks to Alan Saltiel for his inspiring mentoring during my research stay at UCSD and for offering me a great chance to work with a group of talented scientists in the near future.

To the end, the warmest thanks I give to my parents, my sister, my fiancé and his parents. Thanks to my Dad for educating me, my Mom for loving me, my

sister for accompanying me. Thanks to Jianfeng for supporting and encouraging me to be the person I want to be.

Abstract

Adipose tissue (AT) is an important multifunctional organ which serves as a commander of energy homeostasis. Dysregulated lipid and glucose metabolism in AT result in insulin resistance and the development of obesity and type 2 diabetes. There are still remaining questions on insulin-regulated lipolysis, which is highly relevant as elevated circulating fatty acids (FA) contribute to obesity-associated metabolic complications..

My thesis shows that α/β-hydrolase domain-containing 15 (ABHD15) is indispensable for the stability of phosphodiesterase 3B (PDE3B) and insulin-inhibited lipolysis in white adipose tissue (WAT). ABHD15 is highly expressed in energy metabolism tissues, such as brown adipose tissue (BAT) and WAT. WAT ABHD15 expression is strongly downregulated by fasting, while upregulated by refeeding. The nutritional transition from fasting to refeeding is tightly controlled by insulin in WAT. Thus we applied insulin injection and glucose gavage to investigate which insulin-related pathways are changed by Abhd15 *deletion* in mice. We found that neither insulin nor glucose treatments can suppress FFA release in total and AT-specific *Abhd15* knockout (*Abhd15*-ko and *Abhd15*-ako) mice. In addition, insulin-regulated glucose uptake via protein kinase B (PKB/Akt) signaling was impaired in *Abhd15*-ko adipocytes, thus *de novo* lipogenesis from glucose was also reduced. Our *in vitro* data revealed that ABHD15 associates with PDE3B to stabilize its protein level. Consistently, PDE3B expression is decreased in the absence of ABHD15 in mouse. This mechanistically explains the increased protein kinase A (PKA) activity, HSL phosphorylation and undiminished FA release by insulin in *Abhd15*-ko mice. Due to the unsuppressed FFA release and disrupted insulin signaling, *Abhd15*-ko mice eventually develop insulin resistance upon aging and high fat or glucose diet. To further support our animal results, we found that *ABHD15* expression is decreased in obese, diabetic patients compared to obese, non-diabetic patients. Our results

identified ABHD15 as a potential therapeutic target to mitigate insulin resistance.

Despite the fact that ABHD15 plays a key role in the node of insulin-regulated lipolysis pathway in WAT, ABHD15 might play a different role in BAT. We found that *Abhd15*-ako mice are catecholamine sensitive. With an acute β_3 adrenergic receptor agonist administration, *Abhd15*-ako showed a higher O_2 consumption and energy expenditure than control mice. Our preliminary data suggest that this might be due to the increased FFA release in WAT which promotes the FA oxidation in BAT of *Abhd15*-ako mice.

In summary, my studies provide an important contribution to understand the physiological function of ABHD15, also including comprehensive information on the newly generated *Abhd15* total and AT-specific deleted animal models which will benefit future studies.

Kurzfassung

Fettgewebe ist ein multifunktionelles Organ, das eine wichtige Rolle im Lipid- und Glukosemetabolismus spielt. Störungen dieser Stoffwechselwege können Insulinresistenz verursachen und die Entstehung von Adipositas bzw. Diabetes mellitus Typ 2 begünstigen. Erhöhte Level an freien Fettsäuren (FFA) im Blutkreislauf korrelieren mit Fettleibigkeit-assoziierten metabolischen Komplikationen, trotzdem ist weiterhin unbekannt, wie Insulin an der Regulation der Lipolyse beteiligt ist.

Diese Arbeit zeigt, dass α/β-hydrolase domain-containing 15 (ABHD15) essentiell für die Stabilität von Phosphodiesterase 3B (PDE3B) Proteinlevel ist und daher wichtig für die anti-lipolytische Wirkung von Insulin im weißen Fettgewebe (WAT). ABHD15 ist stark exprimiert in Geweben, die am Energiehaushalt beteiligt sind, wie dem braunen Fettgewebe (BAT) und WAT. Die Expression ist stark reduziert während des Fastens und erhöht im gefütterten Zustand. Auf zellulärer Ebene ist der Übergang vom gefasteten in den gefütterten Zustand im WAT maßgeblich von Insulin kontrolliert. Daher nutzten wir Insulininjektionen und Glukose-Sondenernährung, um zu untersuchen welche Insulin-abhängigen Signalwege in *Abhd15*-deletierten Mäusen verändert sind. Wir konnten zeigen, dass weder das Verabreichen von Insulin, noch von Glukose, die Freisetzung von FFA ins Plasma in totalen und fettgewebsspezifischen *Abhd15* knock-out (*Abhd15*-ko und *Abhd15*-ako) Mäusen reduziert. Außerdem war die Glukoseaufnahme mittels dem Akt-Signalweg in *Abhd15*-ko Adipozyten gestört, wodurch die Neusynthese von Lipiden aus Glukose vermindert war. Unsere in vitro Daten zeigten, dass ABHD15 durch direkte Interaktion die Proteinlevel von PDE3B stabilisiert. Dementsprechend ist die Expression von PDE3B in *Abhd15*-deletierten Mäusen verringert,was auch mechanistisch erklärt, warum die Proteinkinase A (PKA) – Aktivität und die Hormon-sensitive Lipase (HSL) Phosphorylierung in *Abhd15*-ko Mäusen gesteigert ist, während Insulin nicht in der Lage ist die

Lipolyse zu supprimieren. Durch die unkontrollierte Freisetzung von FFA und der Störung des Insulin-Signalweges entwickelten die *Abhd15*-ko Mäuse schließlich Insulinresistenz auf fettreicher/glukosereicher Diät im Alter. Zur Untermauerung dieser Daten fanden wir verminderte *ABHD15* Expression in adipösen, diabetischen Patienten, verglichen mit adipösen, nicht-diabetischen Patienten. Diese Daten stellen ABHD15 als mögliches Zielprotein zur Therapie der Insulinresistenz dar.

Obwohl ABHD15 eine Schlüsselrolle in der Insulin-induzierten Suppression der Lipolyse spielt, sind *Abhd15*-ako Mäuse katecholaminsensitiv. Die Verabreichung eines β_3-adrenergen Rezeptoragonisten resultierte in erhöhtem O_2-Verbrauch und Energieverbrauch in *Abhd15*-ako Mäusen gegenüber Kontrolltieren. Vorläufige Daten lassen darauf schließen, dass dies auf Grund der erhöhten Freisetzung von FFAs ist, wodurch die Fettsäureoxidation im BAT begünstigt wird.

Zusammenfassend liefert diese Arbeit einen wichtigen Beitrag zum Verständnis der Funktion von ABHD15 im Insulin-Signalweg, aber auch umfangreiche Information über die neugenerierten *Abhd15* total KO und fettgewebsspezifischen KO Mausmodelle, was zukünftige Studien unterstützen wird.

Table of Contents

I. Introduction

1. Introduction

1.1 The function of adipose tissues

Obesity has reached epidemic proportions globally, with at least 2.8 million people dying each year as a result of being overweight or obese (http://www.who.int/features/factfiles/obesity/en/). Worldwide obesity has nearly tripled over the past five decades. Obesity, partially due to an overabundance of fat cells, is frequently associated with several complications, the most devastating of which may be type 2 diabetes[1]. Both obesity and type 2 diabetes are associated with the dysfunction of adipose tissue (AT)[2]. Originally, AT has been considered simply as a storage organ for energy in form of triacylglycerols (TAGs), however, since then the interest in AT biology increased substantially. Over the last decades we have gained considerable amount of knowledge about the biology and biochemistry of AT. It is now generally recognized that AT is a significant organ of a complex network that involves the regulation of diverse biological functions. In mammals, there are two distinct types of AT: white adipose tissue (WAT) and brown adipose tissue (BAT)[3]. The adipocytes in WAT and BAT display distinct morphology and functions. WAT serves as a storage depot of lipids whereas BAT burns lipids to generate heat through mitochondrial oxidation. WAT is also a remarkable endocrine organ secreting a number of hormones, known as adipokines, involved in the regulation of diverse metabolic functions and immune responses[4], the endocrine function of BAT has been suggested[5,6], while still unclear.

WAT consists of mature adipocytes and is characterized by unilocular lipid droplets and very few mitochondria, preadipocytes, fibroblasts, small blood vessels, and nerve cells[7]. Mature adipocytes have an important role in buffering nutrient availability and demand by storing excess calories and preventing the toxic accumulation in other types of cells. Upon energy demand, stored TAGs in mature adipocytes are rapidly hydrolyzed by lipases

(a process known as lipolysis). After food digestion, blood glucose levels increase and activate insulin secretion from pancreatic islets; a rise of postprandial insulin inhibits AT lipolysis and promotes glucose uptake for *de novo* lipogenesis (DNL).

BAT, which is specialized in producing heat, is almost degenerated in adult humans but found at birth[8]. The average diameter of brown adipocytes is smaller than white adipocytes. Brown adipocytes have a number of cytoplasmic lipid droplets of different sizes, a spherical core and numerous mitochondria that release heat by fatty acids oxidation. BAT also stores energy as TGs, but more frequently produces heat by oxidizing fatty acids, rather than supplying energy substrates for other organs. The heat production from BAT is highly dependent on uncoupling protein 1 (UCP1) which is a unique protein located in the inner mitochondrial membrane[9]. It has been known for long time that respiration and mitochondrial ATP synthesis are coupled[10]. It was demonstrated that the mitochondrial electrochemical proton gradient, generated when electrons are passed down the respiratory chain, is the primary source for cellular ATP synthesis[11] (fig.1). The mitochondrial

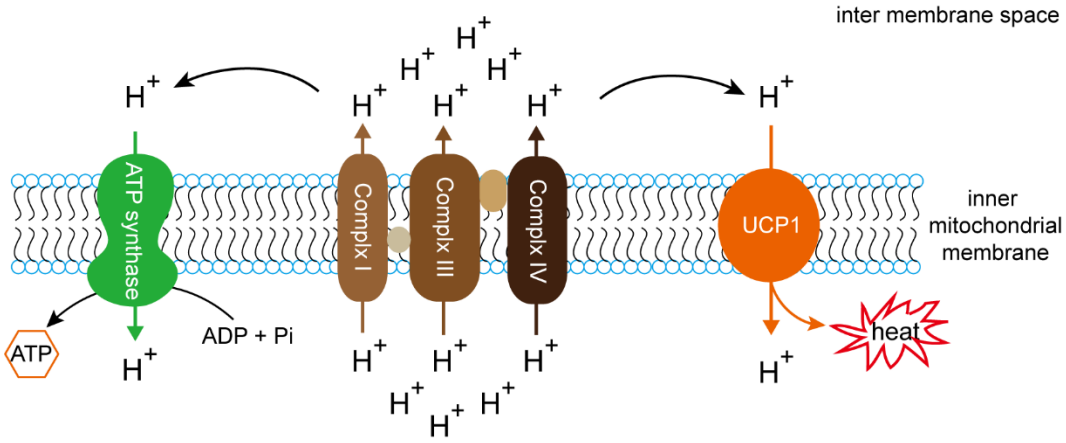

Figure 1. The mechanism of coupled energy production and uncoupled heat production.

respiratory chain is made of five complexes. Complexes I, III, and IV pump protons outside the inner membrane and generate a proton gradient which allows the protons to reenter the mitochondria bypassing the ATP synthase[10]. In addition to this coupled proton reentry, an uncoupled proton leak via UCP1

is another mechanism consuming the mitochondrial proton gradient and producing heat which is named non-shivering thermogenesis (NST).

In addition to white and brown adipocytes, another intensively studied cell type are beige adipocytes which are UCP1 positive but predominant in subcutaneous WAT (sWAT)[12]. Similar to brown adipocytes, beige adipocytes also contain multilocular lipid droplets and plentiful mitochondria that express UCP1. Different from the intrinsic brown adipocytes in BAT, beige adipocyte biogenesis in sWAT is strongly induced in response to some environmental conditions and external cues, including chronic cold stimulation, exercise, long-term treatment of β_3-adrenergic receptor (AR) agonists or peroxisome proliferator-activated receptor γ (PPARγ) agonists, and cancer cachexia. This accumulation of beige adipocytes in WAT is often referred to as “browning” or “beiging” of WAT[13]. The idea of activating beige adipocytes and browning of WAT therapeutically has gained a lot of attention, since brown and beige adipocytes play a key role in the regulation of systemic energy homeostasis in mammals[14-16], and the active BAT in adults is barely low and inversely correlated with BMI and age[15,17-23]. For a quite long time, UCP1 has been considered to be the only thermogenic protein that is responsible for NST. However, genetic studies in rodent models suggested an unexpected metabolic phenotype in UCP1-deficient mice. The sWAT of cold-acclimated *Ucp1*$^{-/-}$ mice exhibits increased oxygen consumption in response to succinate administration[24]. Further, chronic treatment with β3-AR agonists increases respiration of epididymal WAT (eWAT) of *Ucp1*$^{-/-}$ mice[25]. The creatine-driven substrate cycle[26] has been reported as a novel nonshivering thermogenic mechanism in brown and beige fat further demonstrating that a UCP1-independent thermogenic mechanism exists. A recent study reported sarcoplasmic/endoplasmic reticulum calcium ATPase 2 (SERCA2b)-mediated calcium cycling regulates beige fat thermogenesis[27], which experimentally confirmed the existence of UCP1-independent thermogenesis in beige fat. Although UCP1 is thermogenic indispensable in BAT, the anti-obesity and

anti-diabetic action of beige fat are UCP1-independent.

1.2. Energy metabolism in AT

As the fuel reservoir, AT conserves the heat of the body and controls energy mobilization. As an energy storage organ, AT releases energy and stores excess energy through lipolysis and lipogenesis, respectively. Systemically, feeding stimulates the lipogenic pathway and storage of TAGs in AT, while fasting induces the activation of the lipolytic pathway and promotes the breakdown of TAGs and the release of FFA from AT[28] (fig. 2).

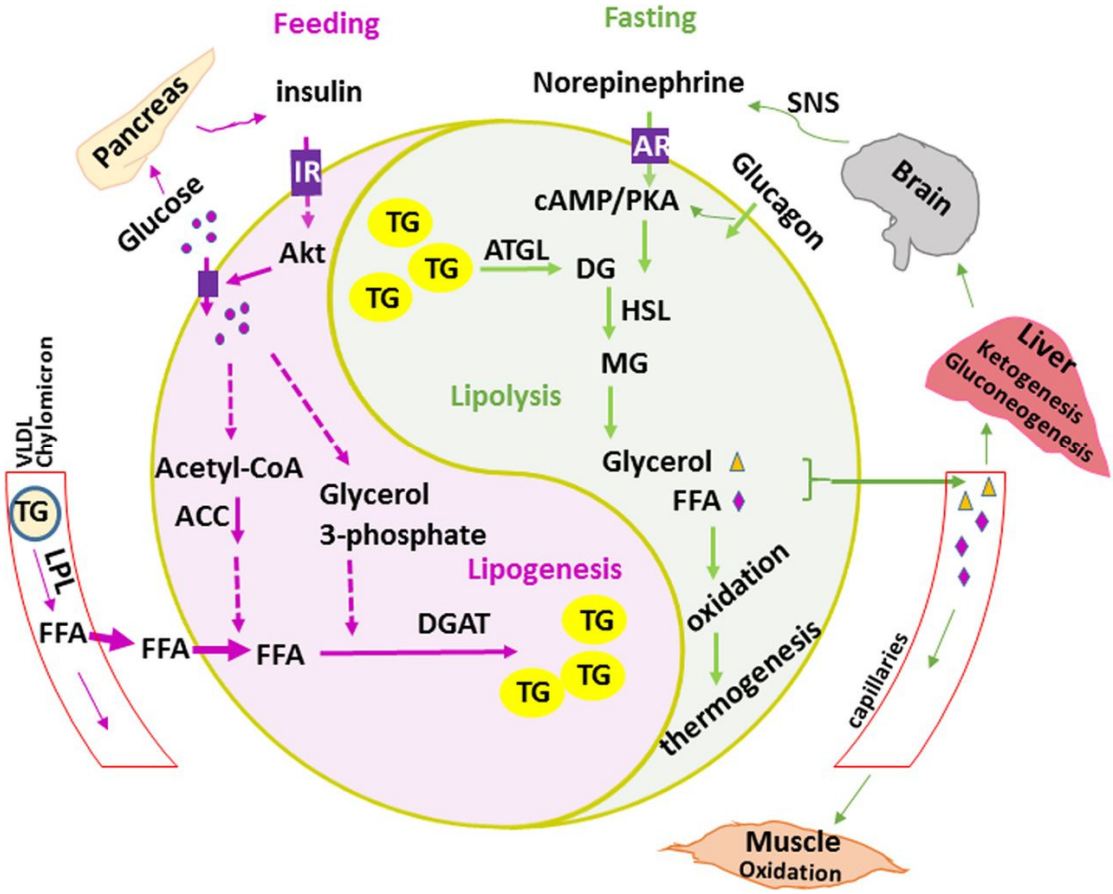

Figure 2. Lipid metabolism controlled by adipose tissue[26]. Abbreviations: VLDL: very low density lipoprotein; TG: triglyceride; LPL: lipoprotein lipase; ACC: acetyl-CoA carboxylase; DGAT: diglyceride acyltransferase 1; AR: adrenergic receptor; ATGL: adipose triglyceride lipase; DG: diglyceride; HSL: hormone sensitive lipase; MG: monoglyceride; SNS: sympathetic nervous system.

Lipolysis is the catabolic process leading to the breakdown of TAGs stored in adipocytes and the subsequent release of FFAs and glycerol[29-32]. This catabolic pathway is activated by fasting and supplies glycerol for hepatic gluconeogenesis and FFAs for oxidation according to energy needs in other organs[33]. Several hormones have been shown to regulate the lipolytic pathway. During fasting, decreased circulating levels of insulin result in suppression of lipogenesis as well as activation of the lipolytic pathway. Consistently, elevated circulating glucagon during fasting is also responsible for the activation of cyclic AMP (cAMP)-dependent protein kinase A (PKA) pathway and lipolysis in adipocytes. Additionally, catecholamines release by the sympathetic nervous system (SNS) is also stimulated by fasting; those

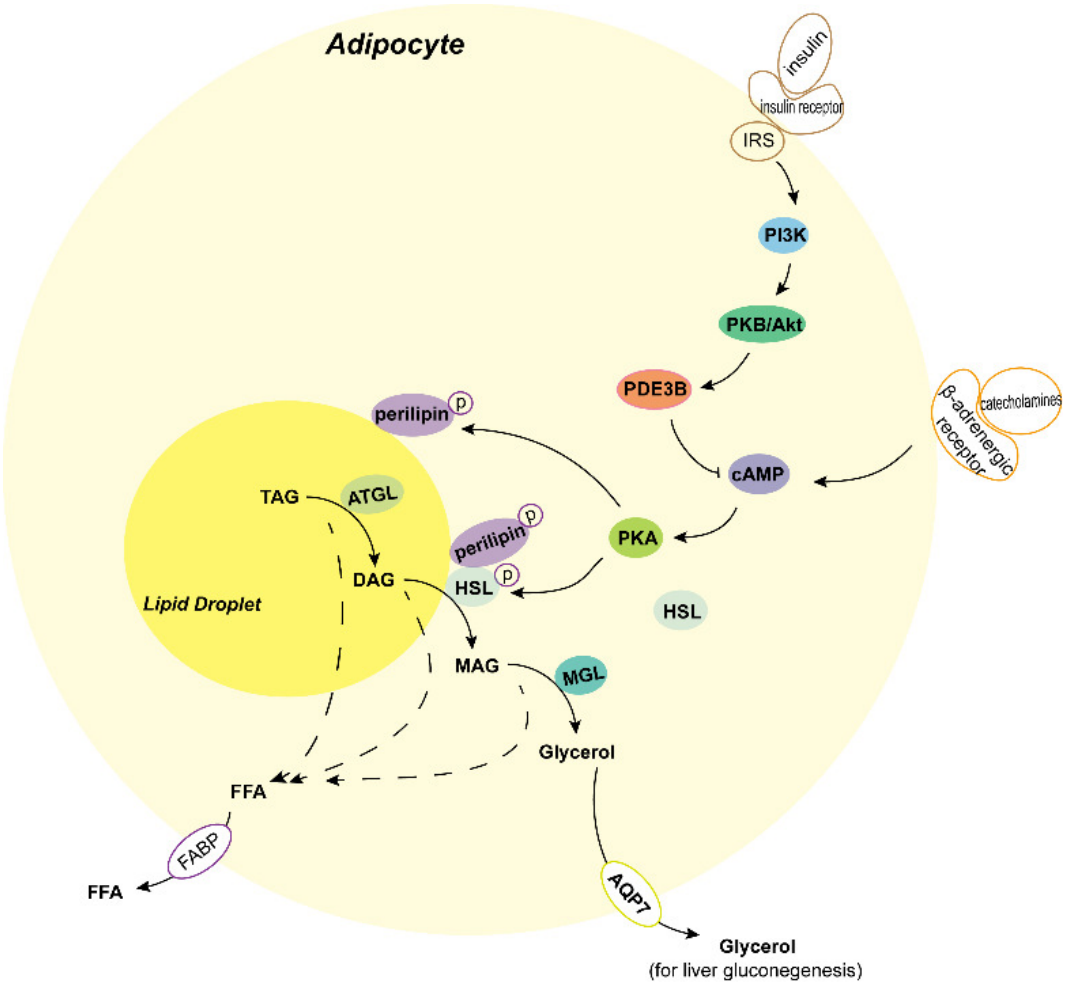

Figure 3. The regulation of lipolysis in adipocytes. Abbreviations: IRS: insulin receptor substrate; PI3K: phosphoinositide 3-kinase; PKB/Akt: protein kinase B; PDE3B: phosphodiesterase 3B; PKA: protein kinase A; MGL: monoglyceride lipase; FABP: fatty acids binding protein; AQP7: aquaporin 7.

catecholamines bind to the β-AR and activate PKA and lipolytic pathways[31,34]. Lipolysis proceeds in a precisely regulated manner, with different enzymes acting at each step (fig. 3). TAG is sequentially hydrolyzed into diacylglycerol (DAG), then monoacylglycerol (MAG), with the liberation of one FFA at each step. MAG is hydrolyzed to release the final FFA and glycerol[34]. While adipose triglyceride lipase (ATGL) is mainly responsible for the first step of TAG breakdown, hormone-sensitive lipase (HSL) mainly converts DAGs to MAGs[35,36]. The lipid droplet-associated protein perilipin is phosphorylated by PKA and then recruits activated HSL to lipid droplets for lipolysis[37,38]. Monoglyceride lipase (MGL) hydrolyzes the 1(3) and 2-ester bonds of MAG at equal rates but owns no *in vitro* catalytic activity against TAG, DAG, or cholesteryl esters[39].

Lipogenesis is the process that encompasses *de novo* fatty acid synthesis from acetyl-coenzyme A (acetyl-CoA), eventually also leading to the synthesis of TAGs. After a meal, increased blood glucose is transported into adipocytes,

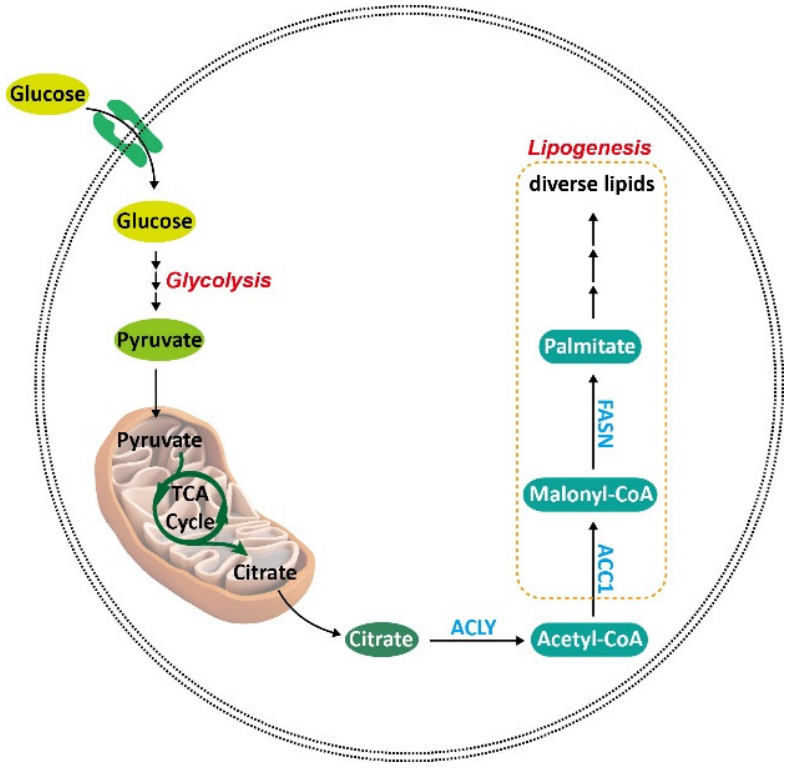

Figure 4. *De novo* lipogenesis from glucose. Abbreviations: TCA: tricarboxylic acid; ACLY: ATP-citrate synthase; FASN: fatty acid synthase.

then oxidized to acetyl-CoA, which is further converted to malonyl-CoA and then to palmitate. Palmitate is modified by elongases and desaturases to produce diverse fatty acids and derivatives (fig. 4). Glucose provides its own metabolite acetyl-CoA as the substrate for *de novo* synthesis of fatty acids, induces the expression of acetyl-CoA carboxylase (ACC), the rate-limiting enzyme of lipogenesis and stimulates the release of pancreatic insulin which promotes lipogenesis (fig. 2). As a result, insulin stimulates glucose uptake into adipocytes, activates glycolytic and lipogenic enzymes, and stimulates expression of the lipogenic gene sterol regulatory element-binding protein 1 (SREBP1) that further controls expression of genes required for cholesterol, fatty acid, TAG, and phospholipid synthesis[40,41]. In addition to SREBP1, another transcriptional factor namely carbohydrate response element binding protein (ChREBP) promotes DNL genes expression and has been shown to modulate both lipid and glucose metabolism in AT and substantially impacts whole-body insulin sensitivity[42-44]. Under normal conditions, DNL is relatively low in WAT compared with liver and BAT in rodents and even lower in humans[45,46]. By contrast, BAT can take up a decent amount of glucose during the cold exposure or after fasting[14,47-49]. Thereby, BAT has been considered as an important glucose sink able to defend against the negative effects of obesity on glucose homeostasis.

1.3 Phosphodiesterase 3B (PDE3B) and its role in lipolysis pathway.

Phosphodiesterases (PDEs) were identified right after the discovery of cAMP[50-52]. PDEs represent a super family of widely expressed hydrolases that regulate the intracellular levels of cyclic nucleotides by hydrolyzing cAMP and cGMP to 5'AMP and 5'GMP, respectively[53]. PDE3s contain a transmembrane region and multiple phosphorylation sites at the N-terminus, and they have a unique C-terminal structure that contains a 44-amino acid insert[54-56]. The PDE3 subfamily consists of two proteins: PDE3A and PDE3B. PDE3A is mostly expressed in heart and smooth muscles, while PDE3B is

more abundant in energy metabolism tissues including AT, liver, pancreatic β cells and hypothalamus[54,57]. Studies with *Pde3b* knockout (*Pde3b*-ko) mice demonstrate that PDE3B plays a crucial role in the regulation of energy metabolism[58]. In adipocytes, insulin activates PDE3B is a major mechanism whereby insulin acutely inhibits lipolysis[59,60]. Rapid, acute suppression of lipolysis by insulin involves both cAMP-dependent and -independent mechanisms. cAMP-independent regulation of insulin involves the direct downregulation of *Atgl* expression and 5'AMP-activated protein kinase (AMPK) pathways. The underlying molecular mechanisms are yet to be fully understood. cAMP-dependent inhibition of lipolysis by insulin involves PDE3B activation[58] which is well understood. Insulin binds to insulin receptor (IR) and leads to the phosphorylation of insulin receptor substrate (IRS). Phosphorylated IRS activates class IA phosphatidylinositol-3-kinase (PI3K) and subsequent the interaction of its subunits p110 and p85, which promotes the generation of phosphatidylinositol 3,4,5-triphosphate (PIP3) at the plasma membrane (PM). PIP3 then recruits protein kinase B (PKB/Akt) to the PM where it will be fully activated by phosphoinositide-dependent kinase-1 (PDK1) and mTOR complex 2 (mTORC2). Akt phosphorylates/activates PDE3B which hydrolyze cAMP to 5'AMP thus decreases cAMP levels in adipocytes, leading to the inactivation of protein kinase A (PKA) and suppression of lipolysis through a reduction of the phosphorylation of HSL and perilipin. It has been generally accepted that insulin-activated Akt phosphorylates and activates PDE3B is the key node of insulin-suppressed lipolysis. However, it has been argued that phosphorylation of PDE3B at its Akt and PKA sites is dispensable for the anti-lipolytic action of insulin, whereas those phosphorylation sites are still necessary for the full activation of PDE3B´s enzymatic activity by insulin[60]. The experimental evidence is still missing, but one explanation from literature supporting this discrepancy is that both, Akt-dependent and -independent activation of PDE3B exists in adipocytes, and depending on the experimental condition, one of the pathways

predominate.

1.4 Abhydrolase domain containing 15 (ABHD15) and its regulation of lipid metabolism in AT

Our lab utilized high through techniques to uncover novel players in adipogenesis[61,62]. Based on previous observations, α/β-hydrolase domain containing protein 15 (ABHD15) was found strongly increased during adipocyte differentiation[63,64]. ABHD15 belongs to the α/β-hydrolase superfamily which consist of various lipases, esterases, and proteases that share a common structural feature[65]. Typically, ABHD proteins harbour a catalytic triad build up with a nucleophile (Ser, Cys, or Asp), an acid (aspartate or glutamate), and a conserved histidine residue enabling hydrolase activity[65] (fig. 5). However, ABHD15 lacks the nucleophile; therefore a hydrolytic activity is less possible. Moreover, ABHD15 misses the Ser-X4-Asp motif, making a prediction of its enzymatic function difficult[65]. In human tissues, *ABHD15* is widely expressed, with highest expression in AT and to a lower level in liver[64,65]. Those tissues are primary sites of postprandial insulin action, and ABHD15 has been described as a potential novel player in insulin signalling[63,66]. Our previous publication showed ABHD15 as a direct and functional target gene of PPARγ, the master regulator of adipogenesis[64]. In 3T3-L1 adipocytes, ABHD15 has been identified as a phosphorylation substrate of Akt[66]. ABHD15 also forms a protein complex with PDE3B in 3T3-L1 adipocytes, and PDE3B protein expression is related to ABHD15 expression[63]. Although those studies proposed ABHD15 as a substrate of Akt and an interacting protein with PDE3B in adipocytes, *in vivo* studies to confirm those assumptions and studies on its physiological function were still missing. Therefore, our lab generated global *Abhd15* knockout mice and *Abhd15* floxed mice to produce tissue specific knockout mice.

In this thesis, I mainly focused on *in vivo* studies to explore the physiological function(s) of ABHD15 in WAT and BAT by using global and conditional knockout models. In addition, I also included *in vitro* assays to show the role of ABHD15 in the interaction with PDE3B in adipocytes.

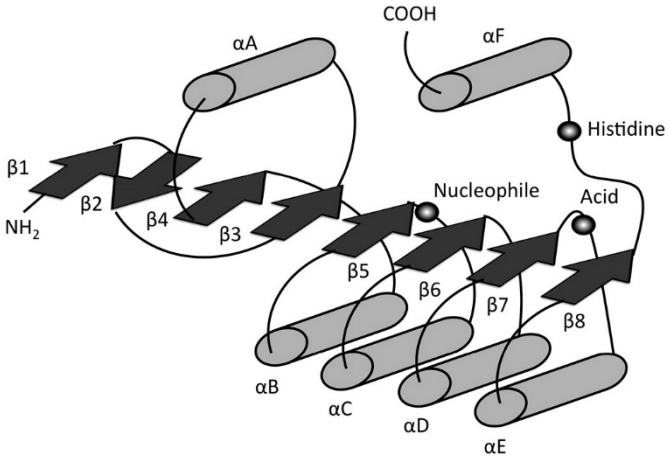

Figure 5. Canonical structure of the α/β hydrolase fold[52].

II. Material and Methods

2. Material and Methods

2.1 Reagents.

All chemicals were obtained from Sigma-Aldrich unless otherwise stated. All cell culture reagents were purchased from Invitrogen. The following primary antibodies were used in this study: Anti-Flag and anti-βACTIN (Sigma), anti-HIS (GE Healthcare), anti-ABHD15 (ProteinTech). Anti-GAPDH, Anti-phospho-PKA substrate, anti-AKT, anti-phospho-AKT (Ser473), anti-HSL, anti-phospho-HSL (Ser660) antibodies were from Cell Signaling Technology. Anti-PDE3B antibody and pAcSG2-mPde3b plasmid were generous gifts from Dr. Vincent Manganiello (NHLBI, NIH) and Dr. Eva Degerman (Lund University). Abhd15-his and LacZ-his plasmids were constructed in our lab. Enhanced chemiluminescence (ECL) reagents were purchased from GE Healthcare. EDTA-free protease inhibitor cocktail (PIC) tablets, phosphatase inhibitor cocktail (PhosSTOP®) tablets, Collagenase D and Dispase II were purchased from Roche Diagnostics.

2.2 Western blot analysis.

Cell were lysed by scraping with RIPA buffer supplemented with PIC. Frozen tissues were minced and homogenized with an electrical homogenizer in RIPA buffer supplemented with PIC and PhosSTOP®. Cell or tissue lysates were incubated on ice for 30 min, then centrifuged at 16,000 g, 4 °C for 30 min and the clean middle layer were collected and frozen at -20 °C until usage. Protein concentrations were determined with the BCA protein assay kit (Pierce). Protein samples were diluted in sodium dodecyl sulfate (SDS) loading buffer and boiled for 10 min at 80 °C. Proteins were resolved by SDS-polyacrylamide gel electrophoresis and transferred to nitrocellulose membranes. Individual proteins were detected with the specific antibodies and visualized on film using horseradish peroxidase-conjugated secondary antibodies (DAKO) and ECL reagents with the G:Box detection system

(Syngene).

2.3 Cell culture.

3T3-L1 fibroblasts (American Type Culture Collection) were cultured and differentiated as described previously[62]. Control non-targeting siRNA and siRNA directed against *Abhd15* were purchased from Sigma (MISSION siRNA NM_026185), Control non-targeting siRNA (cat mo. D-001810-10) and siRNA corresponding to murine *Pde3b* mRNA (cat no. L-043781-00) were purchased from (Dharmacon). 450,000 differentiated 3T3-L1 cells (5 days after differentiation start) were electroporated per 100 µL reaction with control siRNA or a mixture of siAbhd15 #1 and #2 (400 nM) using the Neon Transfection System (Invitrogen), at 1400 V, 20 ms, 2 pulse. Cells were harvested for lipolysis and western blotting 72 hours after electroporation. The cDNA of mouse Pde3b-flag was cut from pAcSG2-mPde3b plasmid with XhoI and inserted into a murine stem cell virus vector (pMSCVpuro; BD Biosciences Clontech). The generation of Pde3b-flag recombinant retrovirus was described before[64]. Viral supernatants were supplemented with 8 µg/mL polybrene and added to 3T3L-L1 cells (30 % confluence) for infection for 18-24 hours. Cells were selected with 3 µg/mL puromycin, expanded, and seeded for further experiments. If not otherwise stated, cells were used 7 days after induction of differentiation. Successful overexpression of PDE3B protein was confirmed by Western blot analysis. COS7 and BnlCl.2 cells (American Type Culture Collection) were maintained in DMEM (4.5 g/L glucose, glutamine) supplemented with 10% fetal bovine serum (FBS) and penicillin-streptomycin at 37 °C, 5% CO_2. For transfection, 200,000 cells per well were seeded into 12-well plates, the cells were transfected with 1 µg DNA together with 2 µL metafectene overnight (o/n) in complete DMEM medium. 48 hours after transfection, cells were harvested for co-immunoprecipitation or treated with 5 µg/mL cycloheximide (CHX) for indicated times.

2.4 Primary cell culture.

The isolation of adipocytes and stromal vascular cells (SVCs) was described previously[67] with the following modifications. 1g sWAT from 8-10 weeks old female mice was dissected, washed, minced, and digested in 1 mL PBS containing 0.125 U/mL Collagenase D, 2.4 U/mL Dispase II, 10 mM $CaCl_2$ (added just prior to digestion of the tissue) at 37 °C with constant agitation at 180 rpm for 25-30 min. To stop digestion, complete DMEM/F12 media containing Glutamax (LifeTechnology), 10 % FBS, 1% P/S was added to the digestion mixture then filtered through a 100-µm cell strainer to remove undigested tissue. The flow-through was centrifuge for 10min at 200 g, the floating adipocyte layer was collected for protein isolation, while the left medium and cells was re-suspended and filtered through a 70-µm cell strainer. After centrifugation for 10 min at 700 g, the cell pellet containing the SVCs was resuspended in complete DMEM/F12 and seeded on a 10-cm cell culture dish. At a confluency of ~80%, cells were propagated and seeded for further experiment. To re-express Abhd15 in KO-SVCs, 50,000 cells in 12-well plates were subjected to either pMSCV-puro or pMSCV-Abhd15 retrovirus medium (prepared as described above). 48 hours after reaching confluency, adipocyte differentiation was induced by using complete DMEM/F12 media supplemented with 1 µM dexamethasone, 0.5 mM isobutylmethylxanthine (IBMX), 5 µg/mL insulin, and 1 µM rosiglitazone. Three days after induction, medium was changed to complete DMEM/F12 supplemented with 5 µg/mL insulin for two days, afterwards cells were maintained in complete DMEM/F12 medium. On day 7, fully differentiated cells were harvested for Western Blotting.

2.5 Membrane isolation.

Cells from 10-cm dishes were washed with ice-cold PBS, then scraped in 1 mL hypotonic lysis medium (HLM) containing 50 mM HEPES, 50 mM sucrose, 1 mM EDTA, 100 mM NaCl and 1 x PIC and were lysed using a Dounce

homogenizer (~50 strokes). Around 50 mg frozen tissue were minced in 1 mL HLM, and thoroughly dounced. Lysates were centrifuged at 5000 g, 4 °C for 10 min. The supernatant was centrifuged at 100,000 g, 4 °C for 30 min. The resulting supernatant represented the cytosolic fraction; membrane pellets were resuspended in RIPA buffer with 1 x PIC for Western blotting.

2.6 Co-immunoprecipitation.

Pde3b-Flag overexpressing cells in 35-mm dishes were washed twice with ice-cold PBS and then lysed in 1mL pulldown buffer (50 mM Tris-HCl pH 7.4-7.5; 300 mM NaCl; 1% Triton X-100; 1x PIC and PhosSTOP$^{@}$). Lysates were cleared from cell debris via centrifugation and protein content was measured by BCA as described above. 1 mg protein lysate was used for pulldown with Anti-FLAG M2 affinity gel (Sigma Aldrich) according to manufacturer's guidelines. After o/n incubation, beads were washed thoroughly and affinity-bound proteins were eluted by boiling the samples with 2x SDS lysis buffer (100 mM Tris/HCl pH 6.8, 10% glycerol, 2.5% SDS, 1 x PIC). Pulldown-products were directly subjected to Western blot analysis.

2.7 Human study.

Omental white adipose tissue (OWAT) samples from severely obese human subjects (BMI > 40 kg/m^2; n = 11) were collected as part of previous trial of a collaborator group[68]. As described, anthropometric parameters and blood sampling for laboratory analysis were determined at inclusion. Patients underwent a 75 g standardized 2 hours oral glucose tolerance test (OGTT). Estimators of systemic insulin sensitivity and insulin resistance were calculated such as the oral glucose insulin sensitivity (OGIS)[69], the composite insulin sensitivity index (ISI)[70], the clamp-like index (CLIX)[71], first and second phase response to glucose challenge, area under the curve (AUC) during OGTT and HOMA-IR[72]. The study was performed in accordance with the Helsinki Declaration of 1975 as revised in 1983 and with Good Clinical Practice guidelines and was approved by the Ethics Committee of the

Medical University of Vienna and Göttlicher Heiland Hospital (EK Nr. 963/2009, EK Nr. 488/2006 and E10-N01-01). All subjects provided written informed consent.

2.8 Animal study.

We flanked exon 2 of the *Abhd15* gene with 2 loxP sites and cloned the homologous regions into a targeting vector that was electroporated into 129 HM-1 embryonic stem (ES) cells. Homologous and Cre recombined ES cells haboring the floxed allele were injected into C57BL/6 blastocysts, and chimeric males were tested for germ-line transmission. Heterozygous floxed mice were bred with *CMV*-Cre mice[73], *Adiponectin*-Cre[74] and *Ucp1*-Cre/ERT2[75] mice to gain heterozygous total knock-out, adipose tissue and brown adipose tissue specific knock-out mice. Mice were backcrossed to the C57BL/6J background for at least 10 generations. Homozygous *Abhd15*-ko, *Abhd15*-ako and *Abhd15*-bko mice were fertile and were used for breeding. Mice were housed in groups of 2–4 in filter-top cages in a pathogen-free barrier facility. The animals were maintained in a 14 hours light/ 10 hours dark cycle, light on at 7:00 a.m., and had *ad libitum* access to food and water, except when food was restricted during fasting. The o/n fasting is around 12 to 14 hours during the dark cycle. At the age of 8-10 weeks, they were either fed a chow diet (calories 11 kJ% from fat, 53 kJ% from carbohydrates, and 36 kJ% from protein, #V1126, Ssniff Spezialdiäten, Germany) or put, at the age of 8-10 weeks on HGD (calories 7 kJ% from fat, 72 kJ% from carbohydrates, and 21 kJ% from protein, #E15629-34, Ssniff Spezialdiaten, Germany) or on HFD (Sniff, Germany, #E15744-34, 45 kJ% calories from fat, 35 kJ% from carbohydrates, and 20 kJ% from protein) until experiments were done. Experiments were performed after 12 weeks on the according diet, or mice were maintained on diets until experiments were finished. If not otherwise stated, age matched male *Abhd15*-ko and wild-type (WT) mice, *Abhd15*-flox, *Abhd15*-ako and *Abhd15*-bko mice (except for SVC

isolation we used female, 10 weeks old mice) were used for each experiments in this study (age and number of mice used are noted in figure legends). The study was approved by the institutional ethics committee and experiments were performed according to the guidelines of the Austrian Federal Ministry of Science and Research. Experiment licenses were granted under BMWF-68.205/0258-II/3b/2011, BMWF-66.007/0026-WF/V/3b/2015 and BMWF-66.007/0008-WF/V/3b/2016.

2.9 Microarray experiments and functional annotation.

Male mice at age of 14 weeks on chow diet after o/n fasting and one hour of refeeding were harvested for microarray analysis. Total RNA was isolated from eWAT as described above. Two-hundred ng of total RNA were prepared for Affymetrix hybridizations on Mouse Gene 2.1 ST arrays. Raw array data was analyzed using the R package oligo, normalized using the robust multi-array average (RMA) method, and log10-transformed. Data was deposited in NCBI gene expression omnibus (GEO) with the accession number GSE98321. Probe sets were filtered for inter-quartile range (IQR) > 0.5 and Refseq annotation. Significantly differentially expressed genes were identified using the R package limma and p-values were adjusted for multiple testing according to the Benjamini-Hochberg method and considered if $p<0.01$ (FDR<0.1) and fold-change >1.5. Functional annotation (gene ontology biological process and KEGG pathways) were performed using DAVID[76]. Heatmap was generated using Genesis[77] based on gene-wise z-score of expression levels .

2.10 Gene expression analysis.

Human *ABHD15* mRNA expression raw data from the microarray with accession number GSE16415 published by Agarwal *et al* was analyzed with GEO2R online tool[78]. As output, fold change and p-value were obtained. Tissue RNA was isolated with TRIzol® reagent (Invitrogen) according to the manufacturer's protocols. cDNA was generated using the cDNA Reverse

Transcription Kit (Thermo Fisher Scientific). mRNA expression was assessed using real-time PCR using the StepOne Plus Detector system and SYBR Green PCR master mix (Invitrogen). Gene expression was normalized to *TfIIß* in murine tissues and *βACTIN* in human tissues. Relative mRNA expression levels were calculated using averaged 2^{-ddCt} values for each biological replicate[79]. Primers are listed in Table 1.

Gene	Forward	Reverse
Dgat1	GACGGCTACTGGGATCTGA	TCACCACACACCAATTCAGG
Acsl1	TCCTACAAAGAGGTGGCAGAACT	GGCTTGAACCCCTTCTGGAT
Acot3	GCTCAGTCACCCTCAGGTAA	AAGTTTCCGCCGATGTTGGA
Acot4	ACATCCAAAGGTAAAAGGCCCA	TCCACTGAATGCAGAGCCATT
Ldlr	GCTTCATGTACTGGACAG	CTGGAAAGATCTAGTGTGA
Abcg1	CTCCTATGTCAGATACGG	CTCTGACTTCTGGAAGTG
Hmgcs1	GTCTGATCCCCTTTGGTG	GGTGAAAGAGCTGTGTGA
Gck	CCGTGATCCGGGAAGAGAA	GGGAAACCTGACAGGGATGAG
Pck	GGCCACAGCTGCTGCAG	GGTCGCATGGCAAAGGG
Pepck	CCACAGCTGCTGCAGAACA	GAAGGGTCGCATGGCAAA
Fas	GCTGTAGCACACATCCTAGGCA	TCGTGTTCTCGTTCCAGGATC
AceCS	GCTGCCGACGGGATCAG	TCCAGACACATTGAGCATGTCAT
AceCC	TGACAGACTGATCGCAGAGAAAG	TGGAGAGCCCCACACACA
Gpat	GCGGAAAAACTACGGCTACGT	TCTGACTCTGGCCTTCTAAATATTCCT
Srebp-1c	GGAGCCATGGATTGCACATT	GCTTCCAGAGAGGAGGCCAG
Scd1	ATCGCCTCTGGAGCCACAC	ACACGTCATTCTGGAACGCC
Acsl1	TCCTACAAAGAGGTGGCAGAACT	GGCTTGAACCCCTTCTGGAT
Pde3b	ATTCAATGCCAAGGCCAATG	AATTTGATGCACACCTGGCAG
Pde3a	CGTCTGTCATATGTAGCA	GTGTCATCTGTTCTGTTTG
Abhd15	TATGAACGTGGGTTCTTGCT	TTGGTGTGACAGAACAGGGT
ABHD15	CCGTGCTGCGCTGCCGAGAGTGG	GGCTGTGGCATACCTGCTGAGGGCG
TFIIß	TCAATAACTCGGTCCCCTACAA	GTCACATGTCCGAATCATCCA

Table 1. Murine and human primer sequences used for qRT-PCR.

2.11 Blood parameters.

Whole blood was taken from facial vein and blood glucose was measured with a glucose meter (Calla light, Wellion) from the tail vein. Plasma was collected after centrifugation at 1200 rpm, 4 °C for 10 min. Plasma

triglycerides (TG) and FFA levels were measured with Infinity™ triglycerides kit (Thermo Fisher) and NEFA kit (WAKO). Plasma insulin levels were measured with the Mouse Ultrasensitive Insulin ELISA (Alpco Diagnostics, Salem, NH, USA) and the Adiponectin and Leptin with Mouse ELISA (Crystal Chem, Downers Grove, IL, USA) kits.

2.12 *In vivo* and *ex vivo* lipolysis.

To determine *in vivo* lipolysis, circulating plasma FA levels were measured after o/n fasting (12-14 hours). Mice were then given an intraperitoneal (i.p.) injection of human insulin (Sigma) at a dose of 0.3 U/kg for HGD, 0.35 U/kg for HFD or an oral gavage of glucose at a dose of 2.5 g per kg body weight. During both procedures, mice were continuously fasted. Plasma FAs were measured after 15, 30, 60, 90 min post injection or gavage. To determine *ex vivo* lipolysis, the release of FA and free glycerol from AT explants was measured as previously described[80]. For chow diet mice, o/n-fasted mice were injected intraperitoneally with 0.6 U/kg insulin or saline. Twenty minutes thereafter, mice were sacrificed and eWAT was excised. The fat pads were washed in pre-warmed 2% BSA (FFA free)-DMEM medium (BSA medium). AT explants (20 mg) were incubated in 200 µL BSA medium in the presence or absence of 25 µM HSL inhibitor 76-0079 (NNC 0076-0000-0079, Novo Nordisk) or 40 µM Atglistatin[81] for 1 hour at 37 °C, 5% CO_2 and 95% humidified atmosphere. After this pre-incubation, the AT explants were transferred into identical, fresh medium containing the appropriate lipolysis inhibitors and incubated for another hour at 37 °C. For HFD mice, eWAT and sWAT were excised from o/n fasted mice. The fat pads were washed in pre-warmed BSA medium. AT pieces (20 mg) were incubated in 200 µL BSA medium with 5 µM Triacsin C (Sigma) in the presence or absence of 100 nM insulin for 4 hours at 37 °C. Thereafter, the medium was removed and used to measure FA (NEFA Kit, WAKO) and glycerol (free glycerol kit, Sigma-Aldrich) release. For protein determination, AT explants were first incubated in 400 µL

extraction solution (chloroform:methanol, 2:1) for 1 hour. Then the tissue pieces were transferred in 400 µL lysis solution (NaOH/SDS, 0.3N/0.1%) and incubated o/n at 56 °C under vigorous shaking. Protein content was determined using BCA reagent (Pierce) and BSA as standard.

2.13 Histology and Oil-red O staining.

sWAT were fixed in 4% buffered formaldehyde and embedded in paraffin. Sections were stained with hematoxylin and eosin or Trichrome according to standard protocols. Adipocyte size was assessed by NIS-Element software (Nikon Instruments, Tokyo, Japan). At least 3 areas per individual section per mouse fat pad were analyzed at ×200 magnification. Adipocytes size was analysis with Adiposoft[82]. Fully differentiated SVCs were fixed (10% formalin in PBS for 30 min), rinsed in PBS, and stained with oil-red O (0.25% in 60% isopropyl alcohol stock solution diluted 3:2 with distilled H_2O) for 30 min.

2.14 Glucose uptake and incorporation assay.

Mice were fasted o/n for 14-16 hours, glucose spiked with [^{3}H]-deoxy-glucose was administrated by oral gavage (2.5 g/kg glucose, ~10 µCi per mouse). 20 min post-gavage, the mice were perfused with ice-cold PBS and tissue were collected and snap frozen until further processing. The accumulation of [^{3}H]-deoxy-glucose-phosphate (deoxy-glc-P) in different organs was determined as described[83]. SVCs isolated from WT and *Abhd15*-ko mice were seeded in 12-well plates and used for glucose incorporation assay that was performed as described by us elsewhere[84].

2.15 Insulin tolerance test (ITT) and glucose tolerance test (GTT).

Mice were fasted prior to GTT and ITT for 6 or 4 hours, respectively. 1.0-2.5 g/kg glucose or 0.25-0.5 U/kg human insulin were i.p. injected and blood glucose levels from tail vein were monitored after 15, 30, 60, 90, and 120 min. The respective dose of glucose or insulin was indicated in the figure legends.

2.16 Cold exposure experiments

Prior the cold exposure experiments, the metal ear tags were removed and mice were single housed for 3 days without nesting material and had free access to food and water unless otherwise stated. Thereafter, the mice were maintained at 5 °C for 2 weeks. At the beginning and ending of the experiments, body weights were recorded, and food intake was measured during the experiment. After animal protocols were completed, mice were anesthetized using isoflurane and blood was collected via the retro-orbital sinus. Mice were euthanized by cervical dislocation; tissues were dissected and immediately processed or flash-frozen in liquid N_2. Plasma and tissue samples were stored at –80 °C until further analyses.

2.17 Tissue O_2 consumption measurement

Tissues were isolated freshly from mice and weighed. 50-100 mg of tissue pieces were stored in closed tubes until the measurement at RT. Tissues were minced and placed in 100% air saturated respiration buffer (2% BSA in DMEM medium). The oxygen concentration in the chamber over time was measured with Strathkelvin Instruments 782 System. A decrease of oxygen is recorded as measure of respiration rate, O_2 consumption was normalized to tissue weight and calculated as µg O_2/min/mg tissue.

2.18 Tissues and cells lipids extraction

To isolate the lipids from frozen tissues, weigh and homogenize the tissue in 1 mL PBS. Add 800 µL lysates into 4 mL chloroform/methanol/acetic acid solution (2:1:1%) and rotate the pyrex tube at room temperature. The remaining tissue lysates were used to measure protein content. 60 min after rotation, centrifuge the samples at 3000 rpm for 20 min to separate the organic and aqueous phases. Withdraw ~2 mL organic phase from the bottom, and evaporate it under N_2 stream. Resolve lipids in chloroform or 2% Triton-X 100 for further analysis. For isolating lipids from seeded cells, cells in

6-well plate were washed with PBS and lipids were extracted twice with hexane/isopropanol (3:2, v/v). Lipid extracts were dried using N_2, re-suspended in chloroform for further analysis. Cells were lysed in NaOH/SDS (0.3N/0.1%) for protein measurement.

2.19 Thin layer chromatography (TLC)

Thin layer chromatography on Silica Gel 60 plates (Merck) was used to separate lipids by polarity. The dried sample lipids were dissolved in 10 uL chloroform and loaded slowly onto the plate. To separate neutral lipids, the spotted TLC plate was placed in a developing chamber containing and was pre-saturated with hexane/diethyl ether/acetic acid (70:29:1) solution. When the solvent front (the boundary where the wet part of the adsorbent ends) is 5–10 mm from the top the plate, remove the TLC plate from the developing chamber and mark the solvent front with a pencil before the solvent dries. Lipids were visualized by incineration and with iodine.

2.20 Targeted lipidomic analysis.

Total plasma lipids (70 µL) were extracted twice according to Folch et al.[85] using chloroform/methanol/water (2:1:0.6, v/v/v) containing 500 pmol butylated hydroxytoluene, 1% acetic acid, and 100 pmol of internal standards (ISTD, 17:0 FA, Avanti Polar Lipids) per sample. Extraction was performed under constant shaking for 60 min at room temperature (RT). After centrifugation at 1,000 x *g* for 15 min at RT the lower organic phase was collected. 2.5 mL chloroform were added to the remaining aqueous phase and the second extraction was performed as described above. Combined organic phases of the double-extraction were dried under a stream of nitrogen and resolved in 200 µL methanol/2-propanol/water (6:3:1, v/v/v) for UPLC-TQ analysis. Chromatographic separation was modified after[86] using an AQUITY-UPLC system (Waters Corporation), equipped with a Kinetex C18 column (2.1 x 50 mm, 1.7 µm; Phenomenex) starting a 20 min gradient with 100% solvent A (MeOH/H_2O, 1/1, v/v; 10 mM ammonium acetate, 0.1%

formic acid). A EVOQ Elite™ triple quadrupole mass spectrometer (Bruker) equipped with an ESI source was used for detection. FA species were analyzed by selected reaction monitoring (FA: [M-H]- to [M-H]-, 0eV). Data acquisition was done by MS Workstation (Bruker). Data were normalized for recovery and extraction- and ionization efficacy by calculating analyte/ISTD ratios.

2.21 Body mass composition and indirect calorimetric measurements.

Body mass composition was assessed in non-anesthetized mice by using the time-domain NMR minispec (Live Mice Analyzer system, Model LF90II, Bruker Optik). For indirect calorimetric measurements, mice were individually housed in metabolic cages for 3-4 days at 20 to 22 °C on a 14 hours light/10 hours dark cycle starting at 7:00 am. Prior to the experiment, mice were adapted to the metabolic cages for 2 days. Food intake, locomotor activity, oxygen consumption, and carbon dioxide production of animals were monitored by using a laboratory animal monitoring system (PhenoMaster, TSE Systems). Respiratory exchange ratio (RER, VCO_2/VO_2) was measured by the system, and energy expenditure (EE) was calculated from indirect calorimetry data using the formula: EE (kcal per h) = $(15.818*VO_2+5.176*VCO_2)/4.1868/1000$[87]. Mice were provided with drinking water *ad libitum* during the whole measurement, and were either fed *ad libitum* or o/n fasted and then refed with the diet mentioned in the figures.

2.22 Reesterification assay.

Primary SVCs were isolated, seeded and differentiated as described in the Main Methods. On day 7 of differentiation, cells were pre-incubated with 5 µM DGAT1 and DGAT2 inhibitors (iDGATs, Sigma) for 30 min in complete media. Thereafter, cells were washed twice with PBS, therafter lipolysis was induced by 10uM isoproterenol in media without serum or BSA. Thirty minutes upon induction of lipolysis, 0.5 µCi ^{14}C-labeled oleic acid (Cat#MC406, American Radiochemicals) were added to each well. Two hours upon induction of

lipolysis, cells were washed with PBS and lipids were extracted twice with hexane/isopropanol (3:2, v/v). Lipid extracts were dried using N_2, re-suspended in chloroform, and one half of the extracted lipids was separated by TLC using hexane/diethyl ether/acetic acid (80:20:1) as mobile phase. TLC spots corresponding to TG were cut out and the co-migrating radioactivity was determined by scintillation counting. Cells were lysed in NaOH/SDS (0.3N/0.1%) for 3 hours and protein content was determined by BCA protein assay using BSA as standard. Reesterification was analyzed as the incorporation of ^{14}C-labeld oleic acids into TG and is expressed as cpm/mg cellular protein. Analyses of WT and knockout cells (*Abhd15*-ko) were run in parallel.

2.23 Statistical analysis

If not otherwise stated data are shown as mean values ± SD of at least three independent experiments or results show one representative experiment out of at least three. Statistical significance was determined using the unpaired 2-tailed student's t-test or the two-way ANOVA test. For statistical analysis GraphPad prism software was used. §, #, * ($p < 0.05$), ** ($p < 0.01$), *** ($p < 0.001$). Correlations of the human dataset in Table 4 were explored by Spearman's method. Statistical significance was set at $p < 0.05$. All statistical analyses were performed with IBM SPSS Statistics for Windows, Version 21.0. Armonk, NY: IBM Corp.

III. Results

3 Results

3.1 The expression pattern of ABHD15 *in vivo* and *in vitro*.

3.1.1 The tissue and cellular expression of ABHD15.

In agreement with published results on murine and human mRNA expression[64,65], we found that murine ABHD15 protein was mainly expressed in adipose depots, among them BAT had the highest expression, followed by a weak expression in liver (fig. 6, A). However, unlike the human *ABHD15* mRNA expression in muscle[65], we did not detect murine ABHD15 protein in skeletal (SM) and cardiac muscle (CM) (fig. 6, A). In WAT, ABHD15 was only expressed in mature adipocytes and primary adipocytes differentiated from SVCs, but not in undifferentiated SVCs, suggesting that ABHD15 is unlikely expressed in macrophages (fig. 6, B). Previously, we showed that *Abhd15* mRNA expression is upregulated during 3T3-L1 adipocyte differentiation[64]. Here, we confirm that ABHD15 protein expression is detectable 2 days after adipogenic induction, and maximal expression is reached in fully differentiated 3T3-L1 adipocytes (fig. 6, C&E). Like in differentiating 3T3-L1 cells, ABHD15 expression was also increasing during beige adipocyte differentiation of SVCs (fig. 6, D). Therefore, in my thesis we applied animal models and cell line models to comprehensively investigate the contribution of ABHD15 to AT function.

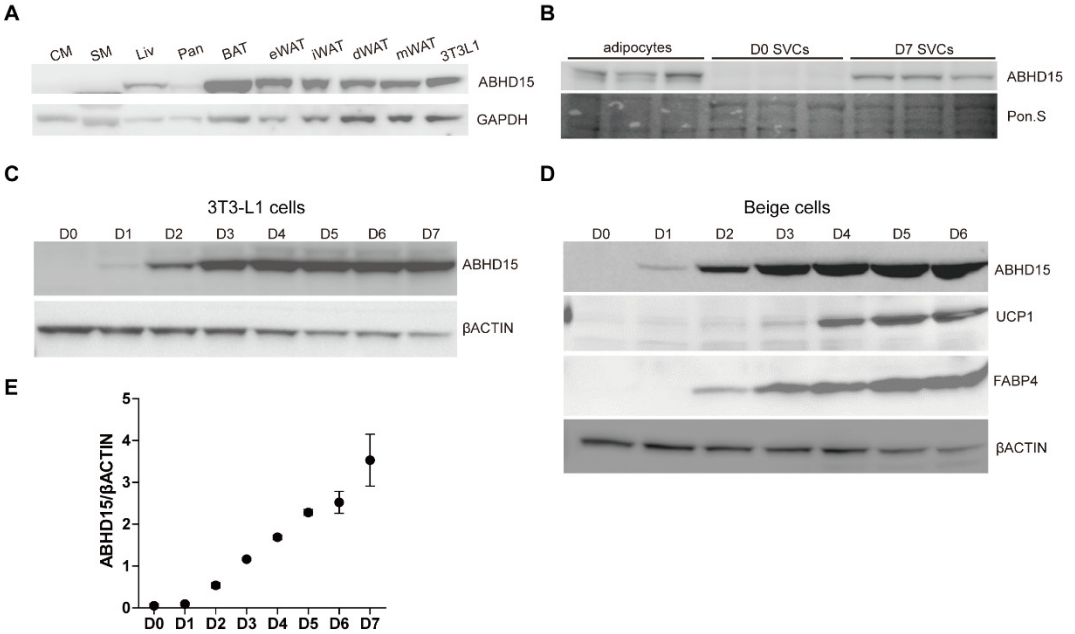

Figure 6. The tissue and cell expression profile of ABHD15. (A) ABHD15 expression in cardiac muscle (CM), skeletal muscle (SM), liver (Liv), pancreas (Pan), brown AT (BAT), eWAT, inguinal WAT (iWAT), dorsal WAT (dWAT), and mesenteric WAT (mWAT) of 18 weeks old CD fed C57BL6/J mice and in 3T3-L1 adipocytes. (B) ABHD15 expression in mature adipocytes and SVCs isolated from sWAT of 10 weeks old female C57BL6/J mice. SVCs were differentiated into adipocytes and harvested on day 7 (n = 3). (C&E) ABHD15 expression in murine 3T3-L1 cells during differentiation from day 0 to 7 (D0-D7). One representative replicate is shown. (D) ABHD15 expression in SVCs during the differentiation into beige cells.

3.1.2 The nutritional regulation of ABHD15 expression *in vivo*.

Based on our preliminary study[64], we further explored the regulator(s) of ABHD15 expression in WAT. Since *Abhd15* expression is upregulated in WAT of obese and insulin resistant *ob*/*ob* mice[64], we also checked the protein expression in similar insulin resistant models. Thus we fed C57BL/6J mice with high fat diet (HFD, 45% fat) and high glucose diet (HGD, 50% glucose) for 12 weeks when the insulin sensitivity decreased in those mice, and collected the tissues at fed *ad libitum*, o/n fasted and refed states. In comparison to chow diet (CD)-fed C57BL/6J mice, 12 weeks of either HFD or HGD feeding massively induced ABHD15 protein expression in WAT (fig. 7, A&B). The abundant expression of ABHD15 in AT and its robust increase upon HGD or HFD feeding indicate that this protein might play an important

role in AT function and diet-related diseases. In mouse eWAT, ABHD15 expression was reduced after o/n fasting, while it is significantly increased upon 1 and 2 hours of refeeding (fig. 7, C&D). Food intake increases circulating glucose levels and stimulates pancreatic insulin secretion; the dramatic increase of ABHD15 expression by refeeding indicates that ABHD15 might be an important regulator of insulin signaling.

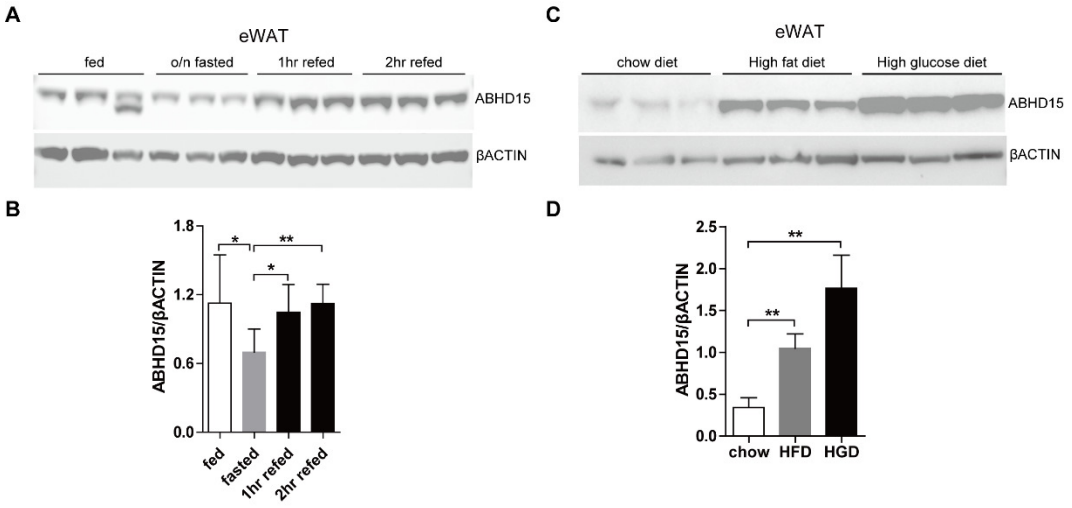

Figure 7. The regulation of ABHD15 expression in eWAT. (A-B) ABHD15 expression in eWAT of 18 weeks old CD fed C57BL6/J mice harvested at fed *ad libitum*, o/n fasted, 1 hour refed and 2 hours refed states. (C-D) ABHD15 expression in eWAT of 20 weeks old C57BL6/J mice fed with CD, HGD and HFD for 12 weeks.

3.1.3 The regulation of ABHD15 expression *in vitro*.

To further investigate whether the nutritional regulation of ABHD15 expression at different physiological conditions is a fat cell autonomous effect, we designed nutritional fasting or drug induced fasting and glucose/insulin refeeding experiments with 3T3-L1 adipocytes. In the first experiment, fully differentiated 3T3-L1 adipocytes were serum and glucose starved for 12 hours, then refed with 4.5 g/L glucose, or 100 nM insulin, or glucose together with insulin for 1 hour and 2 hours. Although we observed the reduced ABHD15 expression after starving, 1-2 hours refeeding with glucose and insulin didn't recover the ABHD15 level to fed state (fig. 8, A left and middle) We proposed that the 1-2 hours refeeding time may not be enough for protein

synthesis in cells. Thereby in the second experiment, we prolonged the refeeding time to 6 hours and added 3% BSA in the starving medium to avoid the lipotoxicity of FA during lipolysis. However, also with the addition of BSA, long time starving did not reduce ABHD15 levels and 6 hours refeeding also did not impact ABHD15 levels (fig. 8, A right). There is discussion about the benefits of 3T3-L1 mouse cell line in various studies, also we have to be aware that this cell line do not necessarily recapitulate the results from primary cell culture and physiological conditions[88,89]. However, these results suggest that the regulation of ABHD15 expression *in vitro* is different from what we observed in mice AT.

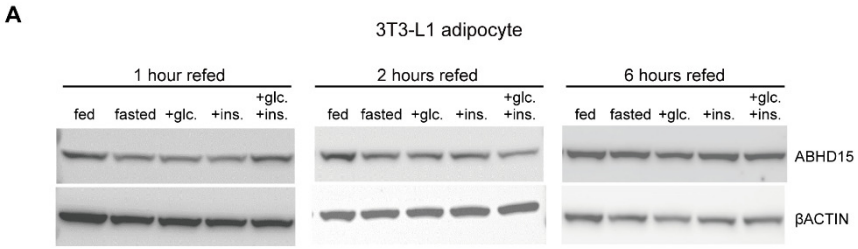

Figure 8. The regulation of ABHD15 expression in 3T3-L1 adipocytes. (A) ABHD15 expression in 3T3-L1 adipocytes at fed (normal medium), fasted (serum and glucose starving medium with or without BSA) and refed (4.5 g/L glucose or 100nM insulin medium or both) states. One representative replicate is shown. (n = 2)

3.2 Elucidation of the physiological role of ABHD15 with animal models.

3.2.1 Generation of *Abhd15* deficient mice models.

The generation of total *Abhd15* (*Abhd15*-ko) and AT-specific knockout (*Abhd15*-ako) mice has been described in our recently published paper in detail[49]. In addition to the published knockout models, we also generated Abhd15 BAT-specific knockout (*Abhd15*-bko) mice by cross breeding the *Abhd15*-flox mice with inducible *Ucp-1* promoter driven *Cre* transgenic mice[75]. The deletion of *Abhd15* was confirmed by PCR (fig. 9, A-D). Further, successful deletion of ABHD15 protein was confirmed by immunoblotting (fig. 9, E-G). Newborn *Abhd15*-ko, *Abhd15*-ako and *Abhd15*-bko pups exhibited

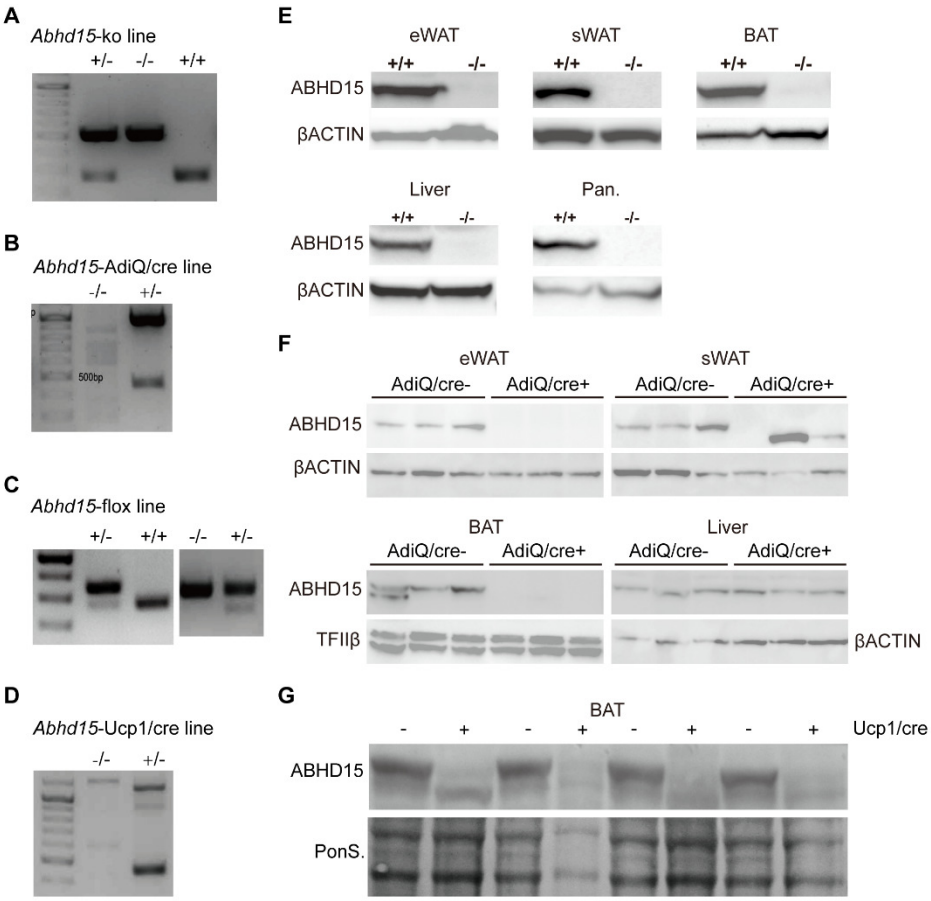

Figure 9. The confirmation of *Abhd15* deletion in mice models. (A) Tailtip PCR of wildtype (+/+), heterozygous (+/-), and homozygous (-/-) *Abhd15*-ko mice. (B) Tailtip PCR of cre negative (-/-) and positive (+/-) mice. (C) Tailtip PCR of wildtype (+/+), heterozygous (+/-), and homozygous (-/-) *Abhd15*-flox mice. (D) Tailtip PCR of cre negative (-/-) and positive (+/-) mice. (E-G) ABHD15 expression in tissues harvested from wildtype (+/+) and *Abhd15*-ko (-/-) mice, cre negative (AdiQ/cre- or Ucp1/cre-) and positive (AdiQ/cre+ or Ucp1/cre+) homozygous *Abhd15*-flox mice.

no obvious developmental defects and adult mutants of both sexes were fertile.

3.2.2 The metabolic characterization of *Abhd15*-ko mice fed with CD, HGD and HFD.

Based on our observation, ABHD15 expression was highly increased by HGD and HFD feeding in C57BL/6J mice (fig. 7, C&D), thus, we assumed that ABHD15 might play a role inr protecting mice from diet-related diseases. To explore the effect of *Abhd15* deficiency on those diets, we fed*Abhd15*-ko and wildtype control (WT) mice with HGD, HFD and CD for 12 weeks, and then the metabolic cage analysis was performed. During the feeding period, body weight was measured every second week. Body mass composition was measured with NMR right after 12 weeks feeding with the respective diets. *Abhd15*-ko mice did not significantly differ from WT mice regarding to body weight, fat and lean mass composition on chow (fig. 10, A&B), HGD (fig. 10, C&D), and HFD (fig. 10, E&F) at fed *ad libitum* state.

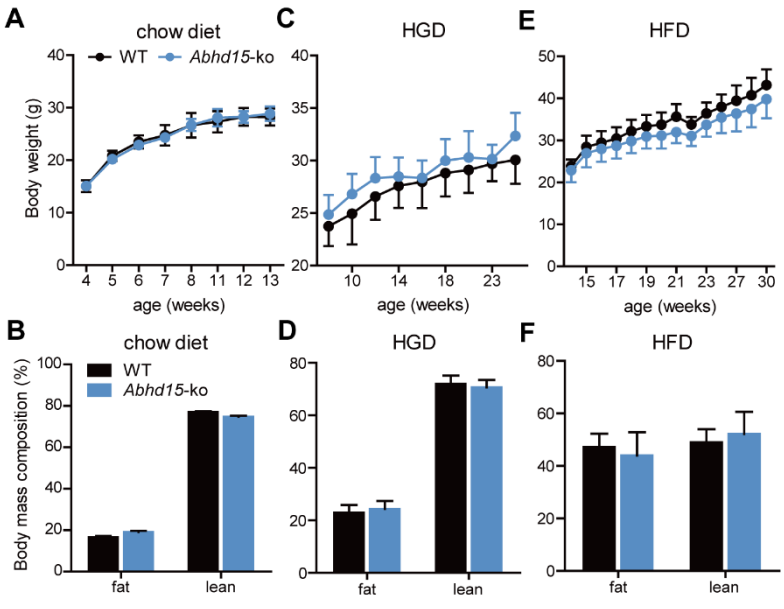

Figure 10. Body parameters of *Abhd15*-ko and WT mice fed with CD, HGD and HFD. (A-F) Body weight and body mass composition of mice at the age of 20 weeks on CD, HGD and HFD when fed *ad libitum* (n = 6-13).

With no restrictions to food and water, food intake, energy expenditure, and respiratory exchange ratio (RER) were similar in WT and *Abhd15*-ko mice on CD, HGD, and HFD (fig. 11, A-I). For CD, HGD and HFD fed mice, energy expenditure and RER were comparable during o/n fasting between both genotypes (fig. 11, B-I). Of note, the RER was significantly lower in HGD-fed *Abhd15*-ko mice than in WT mice when refeeding them after an o/n fasting period (fig. 11, F). This result suggest that lipids are the predominant energy source in *Abhd15*-ko mice during the refeeding phase and further suggest that food intake prohibited utilization of lipids was unsuppressed in *Abhd15*-ko mice when fed with HGD.

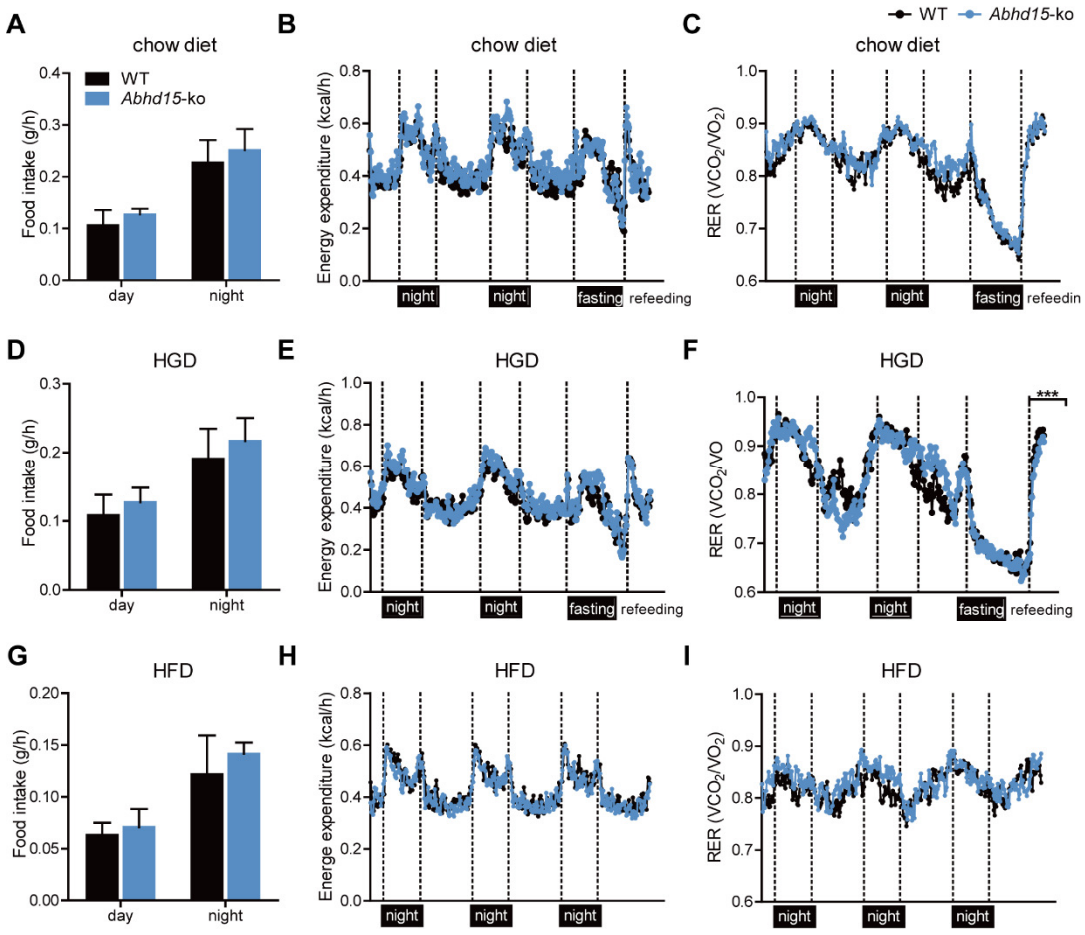

Figure 11. Metabolic parameters of *Abhd15*-ko and WT mice fed with CD, HGD and HFD. (A-I) Food intake was measure at fed state over 3 days, energy expenditure and RER were measured over 3 days including o/n fasting and 6 hours refeeding period (except for HFD) (n = 6). ***<0.001.

Since ABHD15 expression was dramatically regulated by nutritional changes (fig. 7, A&B), we performed the fasting/refeeding experiments with *Abhd15*-ko and WT mice fed with CD, HGD or HFD. In those experiments, mice were o/n fasted, then refed with the same diet as they had before the experiment for 1 hour. Blood was taken after fasting and refeeding. Blood glucose, plasma FFA and TAG levels were measured in the fasted and in the refed state on all diets (Table 2). After fasting, all plasma parameters were unchanged between *Abhd15*-ko and WT mice fed with CD, HGD and HFD. At refed state, there was no significant differences on plasma FFA levels between the two genotypes on CD, HGD and HFD. Refed blood glucose was unchanged when fed with CD and HFD, whereas glucose was increased in Abhd15-ko mice fed with HGD. Except in HGD fed mice, refed plasma TAG levels were increased in *Abhd15*-ko mice compared to WT mice (Table 2).

Measurement	fasted			refed		
	WT	**KO**	***P***	**WT**	**KO**	***P***
Glucose (mg/dL)						
CD	128 ± 10.3	120.6 ± 17.3	0.41	198.2 ± 18.9	183.5 ± 35.4	0.41
HGD	90.9 ± 11.5	90.4 ± 8.9	0.95	194.3 ± 20.2	265.1 ± 32.7	**0.0004**
HFD	172.7 ± 14.8	171.4 ± 26.6	0.93	163.7 ± 24.5	171.2 ± 36.2	0.72
FA (mM)						
CD	1.34 ± 0.18	1.24 ± 0.14	0.33	0.62 ± 0.15	0.79 ± 0.15	0.08
HGD	1.00 ± 0.07	0.95 ± 0.09	0.3	0.73 ± 0.16	0.68 ± 0.10	0.58
HFD	1.16 ± 0.14	1.04 ± 0.12	0.21	0.60 ± 0.12	0.67 ± 0.17	0.5
TG (mM)						
CD	2.01 ± 0.24	2.22 ± 0.36	0.28	1.8 ± 0.24	2.82 ± 0.58	**0.003**
HGD	1.18 ± 0.42	0.80 ± 0.09	0.07	0.79 ± 0.35	1.08 ± 0.44	0.23
HFD	1.55 ± 0.70	1.84 ± 0.30	0.42	0.90 ± 0.20	1.32 ± 0.26	**0.02**

Table 1. Blood parameters of global *Abhd15*-ko compared to WT mice on chow, HGD and HFD. Blood was taken from 20 weeks old mice, HGD and HFD feeding was start from 8 weeks old, 6-8 WT and *Abhd15*-ko mice were used in each group.

To examine whether ABHD15 plays a predominant role in insulin-mediated alterations in glucose and lipid metabolism, we performed a classic o/n fasting and a 12 hours high carbohydrates diet (HGD) refeeding experiment

with those mice. The detailed protocol was described elsewhere[90]. Comparable to above results in Table 2, body weight, blood glucose, plasma FFA, and TG levels were unchanged in *Abhd15*-ko mice at fed and fasted states in this experiment (fig. 12, A-E). Although blood glucose and plasma FFA were unchanged after 12 hours HGD refeeding (fig. 12, C&D), we found that *Abhd15*-ko mice consumed more food, thus those mice were heavier than WT mice (fig. 12, A&B). Of note, after 12 hours HGD refeeding, the plasma TG levels in Abhd15-ko mice were strongly reduced, this might result from a reduced hepatic lipoprotein secretion (fig. 12, E).

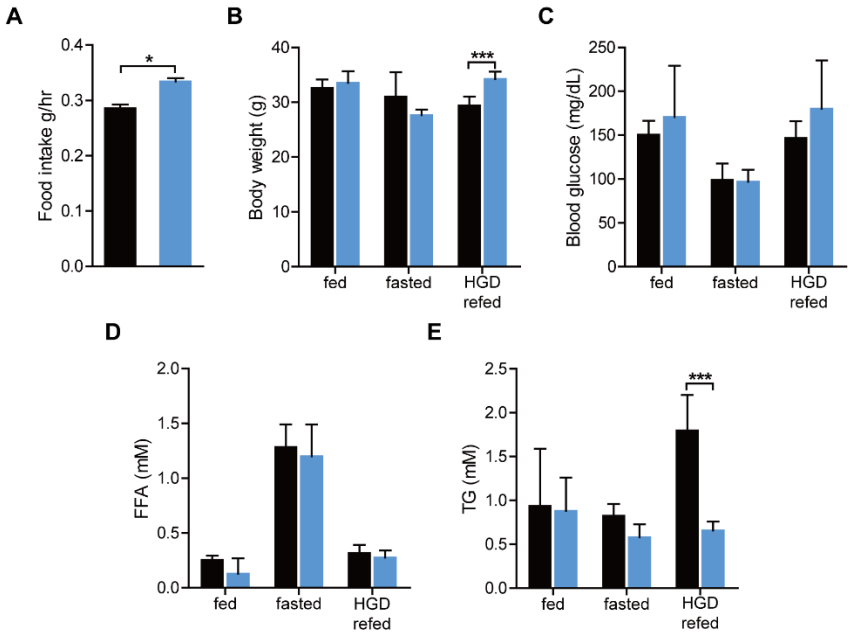

Figure 12. The classic fasting/refeeding experiment with *Abhd15*-ko and WT mice. (A) Food intake during 12 hours HGD refeeding; (B-E) Body weight, blood glucose levels, plasma FFA and TG levels of *Abhd15*-ko and WT mice at fed ad libitum, o/n fasted and 12 hours HGD refed states (n = 5-6). *<0.05, ***<0.001.

3.2.3 The metabolic characterization of *Abhd15*-ako mice fed with CD and HGD.

To elusively investigate the effect of *Abhd15* deletion in AT, we further generated the AT-specific *Abhd15* knockout mice. When fed *ad libitum*, *Abhd15*-ako and control mice had comparable body weight on both CD and HGD (fig. 13, A&C). There is no difference on food intake between *Abhd15*-ako and control mice when fed with CD (fig. 13, B). Fat mass in *Abhd15*-ako mice was lower than in control mice upon CD feeding, while no differences between knockouts and controls were visible when fed with HGD (fig. 13, D&E).

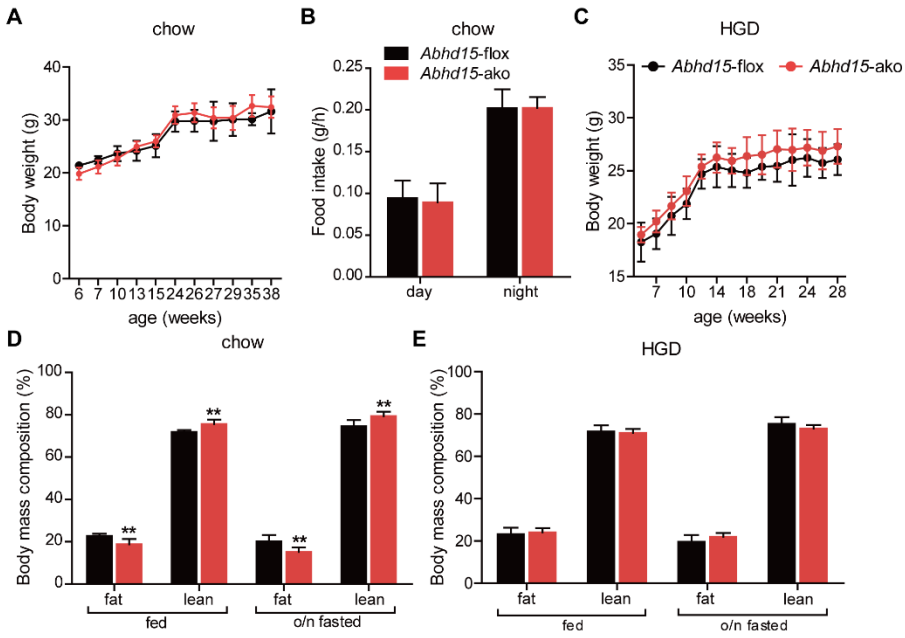

Figure 13. Body parameters of *Abhd15*-ako and control mice fed with CD and HGD. (A) Body weight of *Abhd15*-flox (control) and *Abhd15*-ako mice fed with CD (n = 5-7). (B) Food intake was measured over 3 days (n = 5-7). (C) Body weight of *Abhd15*-ako mice fed with HGD (n = 3-5). (D-E) Body mass composition of CD and HGD fed control and *Abhd15*-ako mice at indicated states (n = 3-7). **<0.01.

We also put those mice into metabolic cages to analysis their metabolic parameters during feeding/fasting/refeeding conditions. There was no differences on energy expenditure between *Abhd15*-ako and control mice when fed with CD and HGD (fig. 14, A&B). *Abhd15*-ako mice displayed a lower RER than control mice when fed with HGD (fig. 14, D), whereas RER were comparable between those mice when fed with CD (fig. 14, C). The reduced RER in HGD-fed *Abhd15*-ako indicated a preference of lipids oxidation during refeeding.

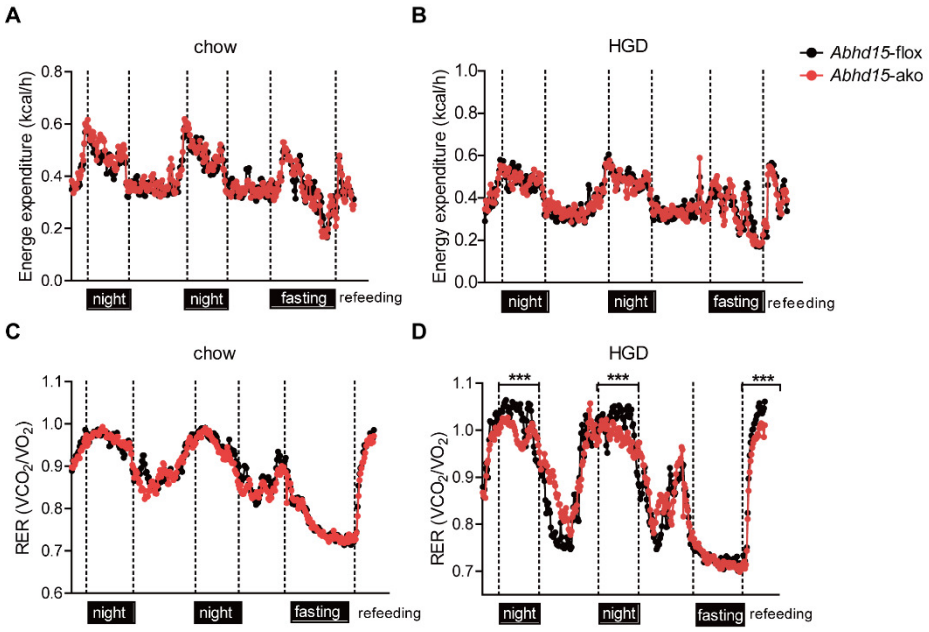

Figure 14. Metabolic parameters of *Abhd15*-ako and control mice fed with CD and HGD. (A-D) Energy expenditure and RER were measured over 3 days including o/n fasting and 6 hours refeeding (n = 3-7). ***<0.001.

In addition, we performed the same classic fasting/refeeding experiment[90] with *Abhd15*-ako mice. Unlike in *Abhd15*-ko mice, *Abhd15*-ako mice did not consume more food (fig. 15, A), thereby the body weights were unchanged (fig. 15, B). The blood glucose, plasma FFA and free glycerol levels in *Abhd15*-ako mice changed to the same extend with control mice during the experiment (fig. 15, C-E).

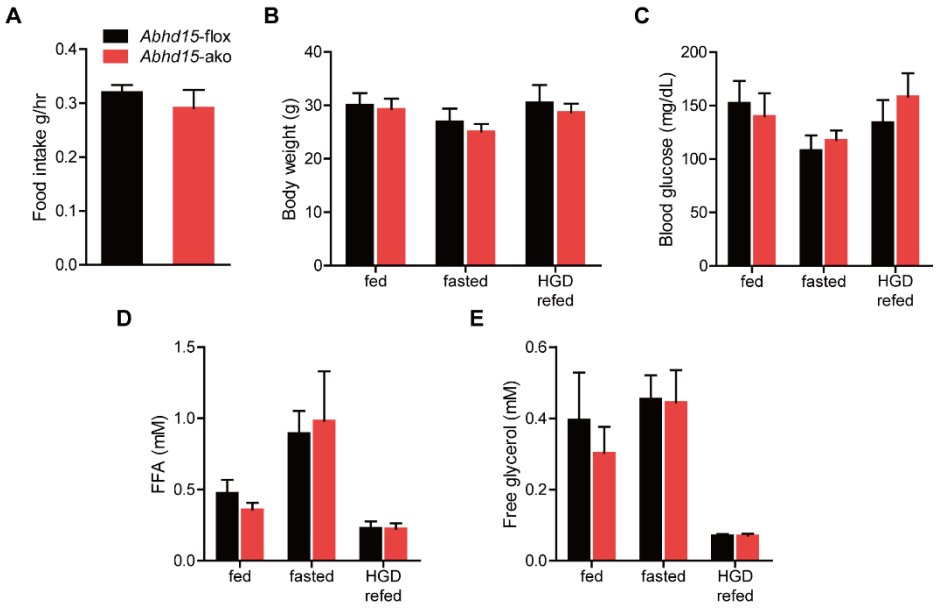

Figure 15. The classic fasting/refeeding experiment with *Abhd15*-ako and control mice. (A) Food intake during 12 hours HGD refeeding; (B-E) Body weight, blood glucose levels, plasma FFA and free glycerol levels of *Abhd15*-ako and control mice at fed ad libitum, o/n fasted and 12 hours HGD refed states (n = 6).

3.3 The impact of *Abhd15* deletion on lipid metabolism *in vivo* and its contribution to insulin resistance

3.3.1 Downregulated lipid metabolism pathways and *Pde3b* expression in *Abhd15* deleted AT.

To narrow down possible pathways that might be affected upon the deletion of *Abhd15*, we performed RNA microarray analysis with eWAT from CD-fed WT and *Abhd15*-ko mice, which were fasted o/n and then harvested at 1 hour refeeding state (Database: GSE98321). The result showed that 241 genes were more than 1.5-fold dysregulated in eWAT of *Abhd15*-ko compared to WT mice ($p < 0.01$) (fig. 16, A) and 90 genes thereof with a false discovery rate (FDR) < 0.1. Among these dysregulated genes, 81 were upregulated and 160 downregulated in *Abhd15*-ko eWAT. Gene ontology / pathway analysis revealed that lipid metabolism-associated pathways were the most significantly downregulated processes in *Abhd15*-ko compared to WT mice (fig. 16, B). We could confirm the expression of several downregulated genes with qRT-PCR (*Dgat1*, *Acsl1*, *Acot3*, *Acot4*, *Ldlr*, *Abcg1* and *Hmgcs1*), further corroborating that lipid synthesis pathways were strongly downregulated in *Abhd15*-ko WAT tissue (fig. 16, C). In order to figure out the factor causes deregulated lipid metabolism pathway in *Abhd15*-ko WAT, we have systemically analyzed the dysregulated genes from our microarray data. Consistent with the downregulated lipid metabolism pathway, we found that *Pde3b*, encoding the PDE3B protein, was strongly reduced in WAT of *Abhd15*-ko and *Abhd15*-ako mice (fig. 16, D&E). PDE3B and PDE3A are two isoforms of the PDE3 subfamily and they are structurally similar, it is very likely that a compensatory rise from PDE3A when PDE3B is reduced. However, *Pde3a* was unchanged in both knockout mouse lines suggesting that there is no compensatory expression of *Pde3a* when *Pde3b* is strongly reduced in knockout animals (fig. 16, D&E). Due to the cAMP hydrolyzing activity of PDE3B in AT, it plays an important role in the regulation of a variety

of metabolic processes such as lipolysis and glucose uptake[91]. *Pde3b*–ko mice or deficient adipocytes have been reported to be resistant to insulin-inhibited lipolysis[58,60]. Next, we investigated the insulin-mediated lipid and glucose metabolism pathways in *Abhd15* deficient mice models.

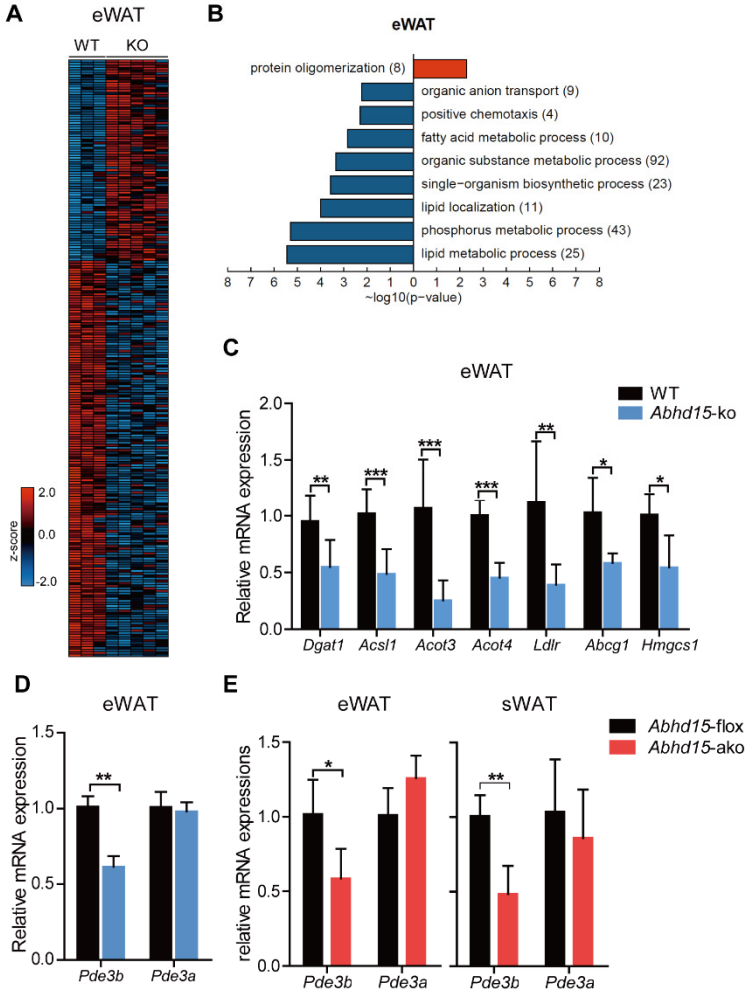

Figure 16. The dysregulated pathways and genes in WAT of *Abhd15* deficient mice. (A) Heatmap of dysregulated genes from microarray of eWAT from 1 hour-refed WT and *Abhd15*-ko mice at the age of 14 weeks on CD (n = 3-5). (B) Gene ontology (GO) analysis was performed with -log10 (p value) plotted (x axis) as a function of classification meeting a p value < 0.001. Upregulated (red) and downregulated (blue) genes in eWAT of *Abhd15*-ko mice are compared to controls (n = 3-5). (C) Lipid metabolism related genes expression in eWAT of the samples used for microarray, Dgat1: diacylglycerol O-acyltransferase 1; Acsl1: acyl-CoA synthetase long chain family member 1; Acot3: acyl-CoA thioesterase 3; Acot4: acyl-CoA thioesterase 4; Ldlr: low density lipoprotein receptor; Abcg1: ATP binding cassette subfamily G member 1; Hmgcs1: 3-hydroxy-3-methylglutaryl-CoA synthase 1. (D-E) *Pde3b* and *Pde3a* relative expression in WAT of WT and *Abhd15*-ko mice fed with CD, control and *Abhd15*-ako mice fed with HGD (n = 5-9). *<0.05, **<0.01, ***<0.001.

3.3.2 Unsuppressed FFA release by insulin in *Abhd15*-ko mice.

The requirement of PDE3B in the regulation of lipolysis by insulin is well investigated[58,60]. Based on the information of our microarray and qPCR data, we assumed that the reduced *Pde3b* expression in AT will lead to a defect on insulin-regulated lipolysis in our knockout models. To investigate the impact of *Abhd15* deletion on the anti-lipolytic action of insulin *in vivo*, we intraperitoneally (IP) injected insulin to o/n fasted mice and plasma FFA levels were determined to indicate insulin response. Consistent with above results (Table 2), the fed *ad libitum* plasma FFA levels were unchanged in *Abhd15*-ko mice when compared to WT animals (fig. 17, A&B). And o/n fasting stimulated FFA release to the same extent in both genotypes (fig. 17, A&B). Expectedly, injected insulin potently reduced plasma FFA in WT mice, while plasma FFA levels in *Abhd15*-ko mice remained the same level as in the fasted state, and this result is the same in both young and old mice (fig. 17, A&B). A targeted lipodomics analysis of the plasma from above experiments further proved an unsuppressed lipolysis, evidenced by that both saturated and unsaturated fatty acids were higher in *Abhd15*-ko mice after insulin treatment (fig. 17, C&D). To mimic the IP insulin injection, we orally gavaged glucose to increase the circulating insulin levels which were secreted from pancreas (fig. 17, E). This endogenous insulin also resulted in strongly reduced FFA level in WT mice and unsuppressed FFA release in *Abhd15*-ko mice (fig. 17, F). Comparing to the IP injected insulin, endogenous insulin seems to have a weaker anti-lipolytic action, this is possible due to murine insulin undergoes degradation easier than human insulin in mouse body. These data indicate that insulin cannot suppressed lipolysis in WAT of *Abhd15*-ko mice.

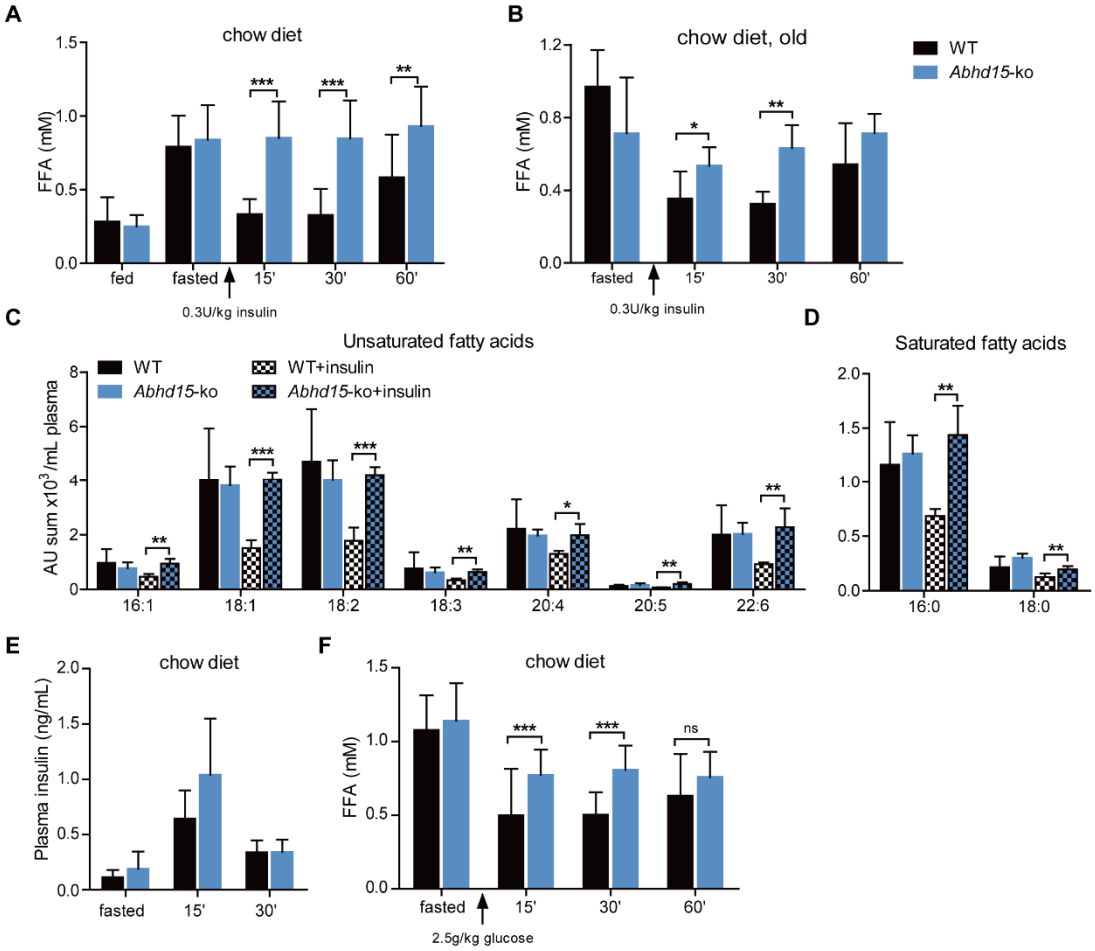

Figure 17. The unsuppressed FFA release in *Abhd15*-ko mice. (A-B) WT and *Abhd15*-ko mice (20 weeks and 44 weeks old) were fasted o/n and i.p. injected with 0.3 U/kg insulin; blood was taken at the indicated time points and plasma FAs were determined (n = 6). (C-D) Plasma from (A) was used for lipid extraction and classes of FFA determined by using UPLC-MS (n = 4-5). (E-F) Mice were o/n fasted and then gavaged with 2.5 g/kg glucose (n = 8). *<0.05, **<0.01, ***<0.001.

The unsuppressed lipolysis by insulin might be the consequence of decreased PDE3B protein activity, thus we examined the PDE3B protein level and cAMP concentrations in WAT as a read out of PDE3B activity. We isolated the membrane fraction of eWAT from HGD-fed WT and *Abhd15*-ko mice. Immunoblotting result showed that PDE3B protein was strongly reduced in *Abhd15*-ko mice (fig. 18, A&B). The elevation and degradation of cAMP levels are very quick, after an o/n fasting we observed that the cAMP levels showed only trends to be elevated in *Abhd15*-ko mice (fig. 18, C). PKA is commonly known as cAMP-dependent protein kinase, its activity is positively related with cellular levels of cAMP. Upon activation of PKA, it further phosphorylates its substrates. Therefore, we checked the phosphorylation of PKA substrates to reflect the PKA activity. Immunoblotting results showed that the phosphorylation of PKA substrates was increased in eWAT and sWAT of *Abhd15*-ko mice after o/n fasting (saline) and insulin stimulation (fig. 18, D&E). HSL is one of the PKA substrates that regulates lipolysis[92,93]. Accordingly, phosphorylation of HSL at Ser660 (S660), the major HSL phosphorylation site that control HSL activity[94], is markedly increased in *Abhd15*-ko mice when compared to WT mice (fig. 18, F-I).

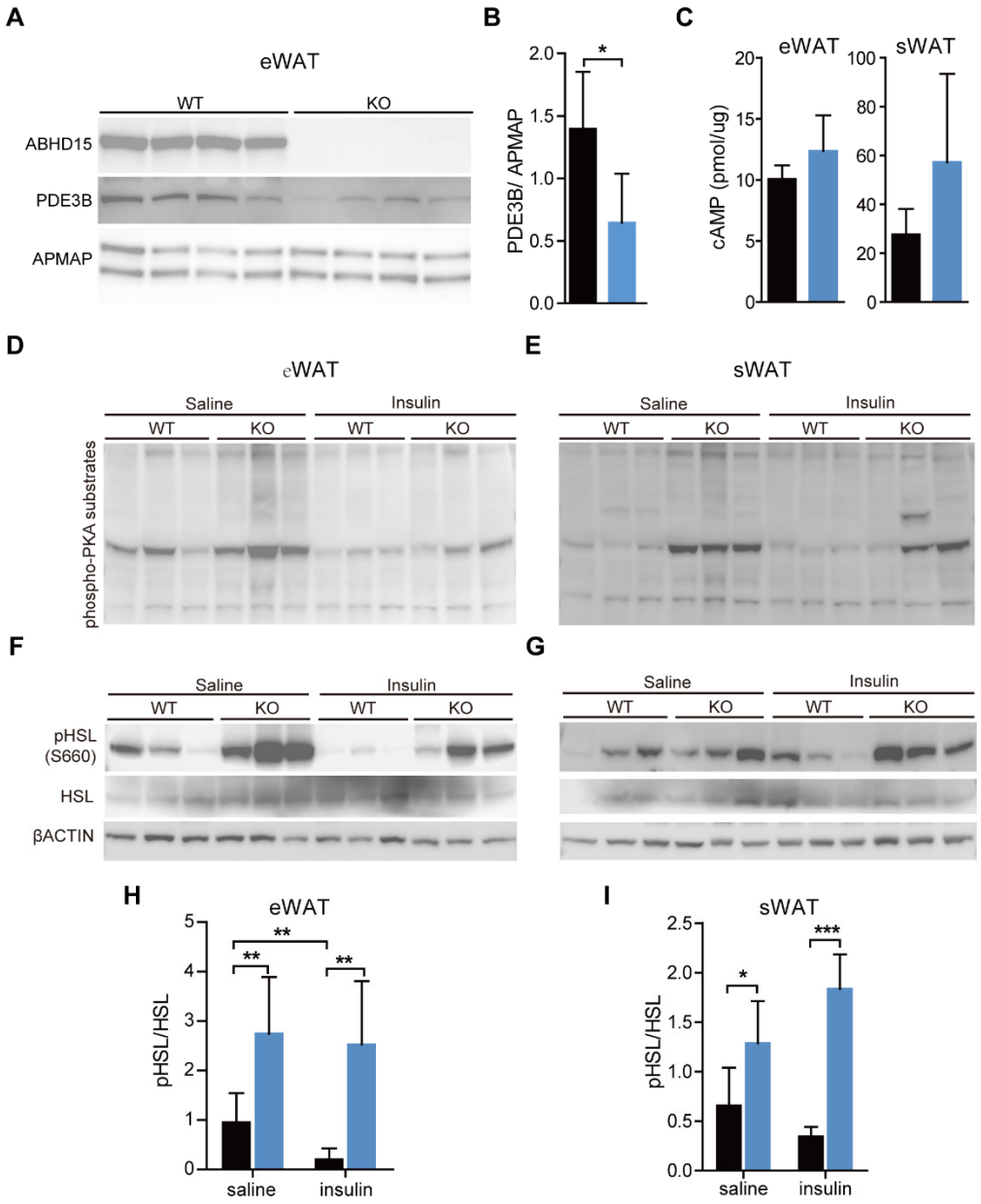

Figure 18. The reduced PDE3B levels and increased PKA/HSL pathway in *Abhd15*-ko mice. (A-B) ABHD15 and PDE3B expressions in the membrane faction of eWAT from Abhd15-ko and WT mice fed with HGD. (C) cAMP levels measured from eWAT and sWAT of o/n fasted mice (n = 4). (D-I) o/n fasted mice were injected with 0.6 U/kg insulin, 20 min later eWAT and sWAT were collected and used for blotting phosphorylated PKA substrates and HSL, total HSL. *<0.05, **<0.01, ***<0.001.

To exclude the effects of *in vivo* FFA uptake by other organs, we measured lipolysis in *ex vivo* fat pads isolated from WT and *Abhd15*-ko mice. FFA release from WT fat pads was normally inhibited by insulin (fig. 19, A). Consistently, there was no insulin-mediated inhibition of FFA release in *Abhd15*-ko fat pads (fig. 19, A). In addition, we also measured the lipase activity by adding small molecule inhibitors for ATGL and HSL (iATGL and iHSL) during lipolysis assay. In the presence of iATGL and iHSL, FFA release from *Abhd15*-ko and WT fat pads was both decreased with the same significance (fig. 19, A). *Ex vivo* glycerol release was comparable between WT and *Abhd15*-ko mice with or without iATGL and iHSL (fig. 19, B). These results indicate that the unsuppressed FFA release by insulin in *Abhd15*-ko mice is not due to the ATGL and HSL lipases activity.

As the major energy storage, WAT is the predominant energy substrates (e.g. FFA and glycerol) supplier to other tissues during fasting. The activated FFA release from WAT causes its weight loss and the shrink of adipocytes size. Another evidence to confirm the disrupted anti-lipolytic action of insulin in *Abhd15*-ko WAT, sWAT weight was lighter in *Abhd15*-ko than in WT mice after insulin bolus. Since there was no differences with plasma parameters (e.g. glucose, FFA and TG levels) at fasted (Table2) and fed state (fig. 12, fig. 15), we did not detect the differences on sWAT, eWAT and liver weights at those states (fig. 19, C). Unlike the high lipolysis activity in WAT, the lipolytic activity was much less in BAT. However, we observed that BAT weight was slightly reduced in *Abhd15*-ko mice when fasted or injected with insulin. To figure out the cause of weight loss, we performed histology staining with sWAT from fed, fasted and insulin injected states. The results showed that the adipocytes look similar between WT and *Abhd15*-ko mice at fed and fasted states, while the adipocytes in *Abhd15*-ko was obvious smaller than WT mice (fig. 19D). We further analyzed the adipocytes size with Adiposoft[82], and the result indicated unchanged adipocytes size at fed and fasted states, but a significant adipocytes size reduction in *Abhd15*-ko mice injected with insulin

(fig. 19E). These results collectively evidencing that ABHD15 plays a role in insulin-mediated suppression of lipolysis.

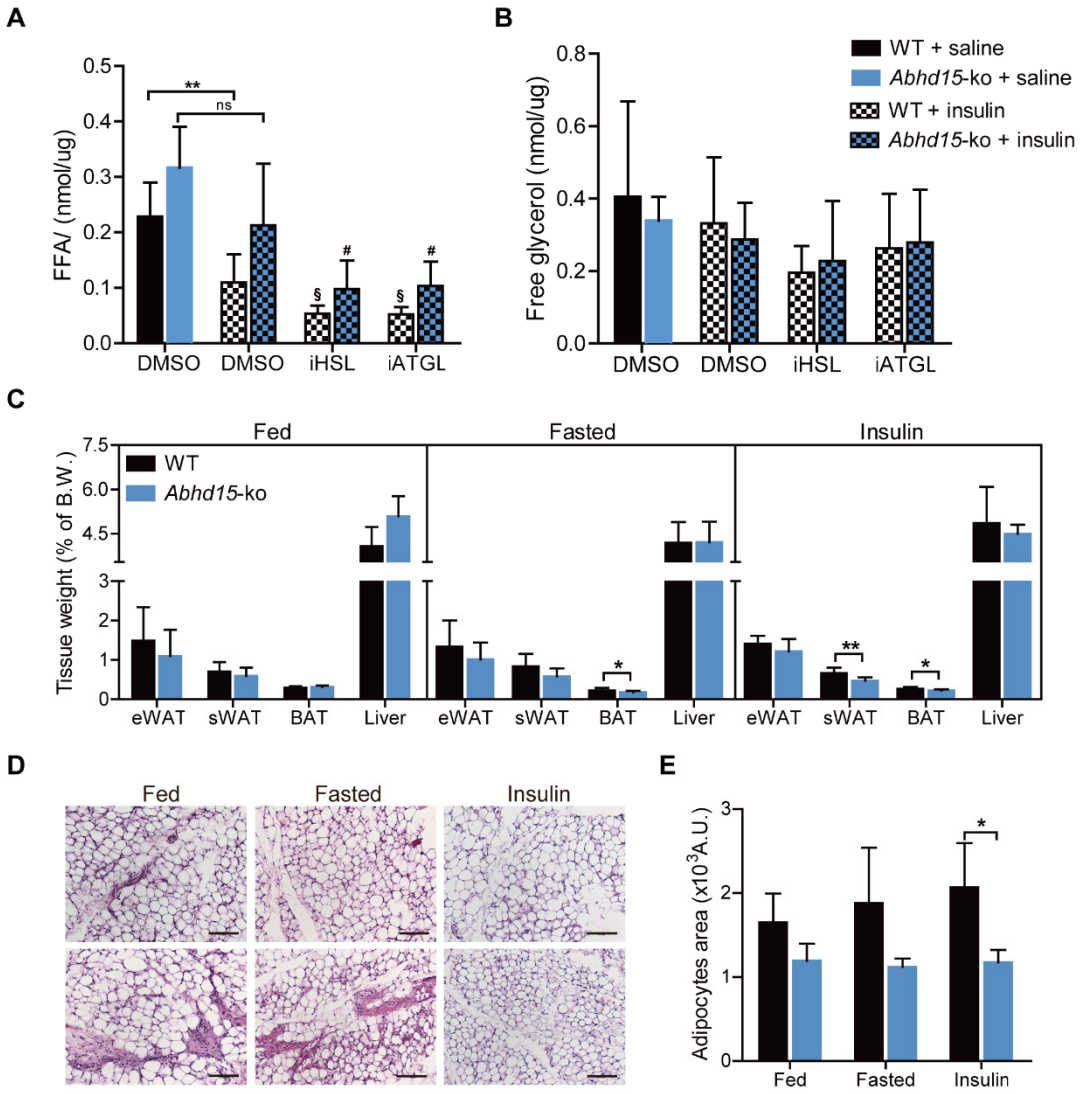

Figure 19. The reduced tissue weight and adipocytes size in sWAT of *Abhd15*-ko mice. (A-B) FA and glycerol release from eWAT explants of saline or insulin injected mice. Explants were treated with 25 µM HSL inhibitor (HSLi) or 40 µM ATGL inhibitor (ATGLi) for 1 hour in the medium (n = 4-7). § and # indicates the significance of inhibitors treatment compare to DMSO in WT and KO, respectively. (C) Mice were harvested at 7 a.m. fed *ad libitum*, 12 hours fasted, or 20 min after 0.6 U/kg insulin injection. Tissues weight were analyzed (n = 4-5). (D&E) sWAT from (C) was used for H&E staining, and adipocytes size was analyzed. Scale bar, 100 µm. §, #, *<0.05, **<0.01, ***<0.001.

3.3.3 *Abhd15* deletion did not impact adipocytes re-esterfication.

Besides the increased lipolysis and lipases activity, elevated plasma FFA levels might also due to the reduced FFA re-esterification in *Abhd15*-ko mice upon insulin signaling. We thereby isolated RNA from eWAT which was collected from the 12 hours refeeding experiment described in **3.2.2** and performed qRT-PCR with those samples. Gene expression data suggested a possible reduced re-esterification in *Abhd15*-ko WAT, because mRNA expression of *Pepck* which is related with re-esterification and lipogenesis (*Srebp1c, Scd1, Acsl1, and Dgat1*) was reduced in the fasted state (fig. 20, A-C), when re-esterification is highly active[95]. However, fasted plasma FFA levels were not differ in *Abhd15*-ko and WT mice (Table 2), opposing the possible reduced re-esterification in *Abhd15*-ko mice. Except for *Scd1*, expression levels of those genes were unchanged in *Abhd15*-ko mice during refeeding when insulin signaling is activated (fig. 20, C). Recently, it has been revealed that DGAT1 mediates the FFA re-esterification to protect adipocytes from ER stress[95]. We observed a reduced *Dgat1* level in Abhd15-ko WAT at refed state, but anyway *Dgat1* expression is inhibited during refeeding and its activity is increased at fasting state[95]. Thus the downregulated genes expression could not tell whether there is a reduction on re-esterification in *Abhd15*-ko adipocytes. To directly exam whether ABHD15 has an effect on FFA re-esterification in adipocytes, we analyzed the incorporated TG from radiolabeled oleic acid in differentiated primary *Abhd15*-ko and WT adipocytes stimulated with isoproterenol in the presence and absence of DGAT inhibitors (iDGATs)[95] (fig. 20, D). And we did not observe any differences between WT and Abhd15-ko cells which demonstrating *Abhd15* deletion in adipocytes did not affect, at least, DGAT-mediated re-esterification. These data further confirm that diminished anti-lipolytic action of insulin is responsible for elevated circulating FFA level in *Abhd15*-ko mice.

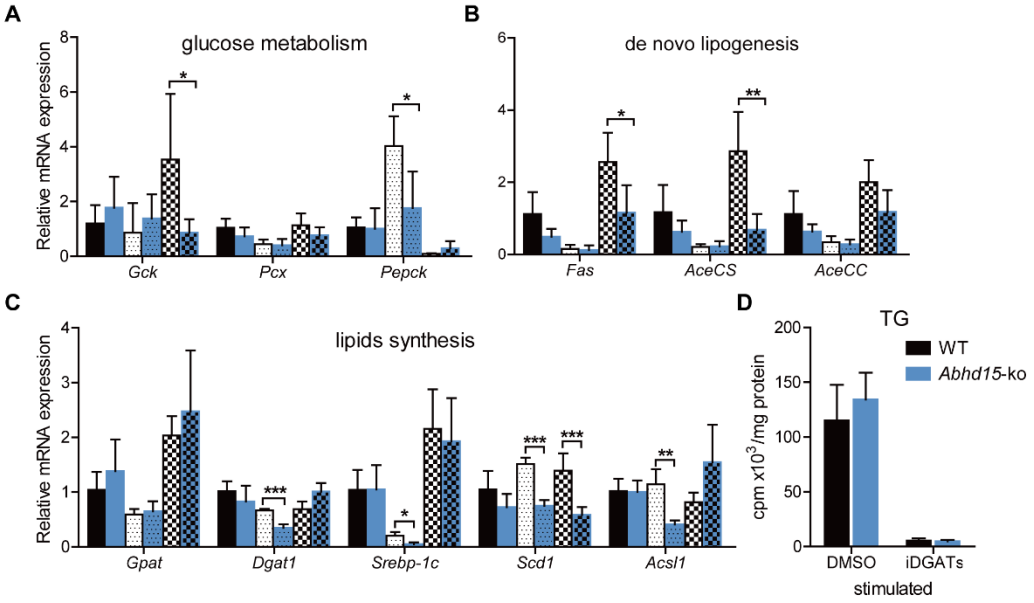

Figure 20. The downregulated expression of genes related with glucose and lipid metabolism. (A-C) Relative expression of genes involved in glucose and lipid metabolism in eWAT. (d) Incorporation of ^{14}C-oleic acid into TG of differentiated SVCs upon isoproterenol stimulation (n = 3). *<0.05, **<0.01, ***<0.001.

3.3.4 Impaired glucose uptake and development of insulin resistance in *Abhd15*-ko mice.

Except for FFAs, glucose is another important energy substrate for the body. Increased circulating FFA (especially saturate FAs) levels contribute largely to the development of insulin resistance[96,97], as well as disrupted glucose homeostasis triggers obesity and type 2 diabetes[98,99]. Therefore, we examined whether *Abhd15* deletion also impacts the glucose metabolism in AT. In CD fed mice, there was a moderately increased plasma insulin level (62%, $p = 0.068$) in *Abhd15*-ko mice 15 min after glucose gavage (fig. 17, E). But the increased insulin levels failed to reduce plasma FFA levels in *Abhd15*-ko mice (fig. 17, F). Akt is a master regulator in insulin signaling and plays multiple roles via activating different downstream substrates. Insulin stimulated Akt not only activates PDE3B to inhibit lipolysis, but also promotes the translocation of glucose transporter 4 (Glut4) to plasma membrane[98,100,101] for importing glucose into cells. The accumulation of glucose inside the cells will be oxidized and its metabolites will be used for lipid synthesis, a process known as *de novo* lipogenesis (DNL).

To check the impact of *Abhd15* deficiency on glucose metabolism, we firstly checked tissues glucose uptake in WT and *Abhd15*-ko mice. After o/n fasting, we orally gavaged both *Abhd15*-ko and WT mice with ^{3}H-deoxyglucose that cannot be further metabolized after uptake. The results show that glucose uptake into eWAT, heart was decreased in *Abhd15*-ko mice compared to WT mice, while there were no differences in sWAT, SM (quadriceps) and BAT (fig. 21, A). We also saw that glucose uptake in liver was reduced in Abhd15-ko mice after ^{3}H-deoxyglucose administration, but the clamping method will be more accurate to tell us the glucose turnover in liver.

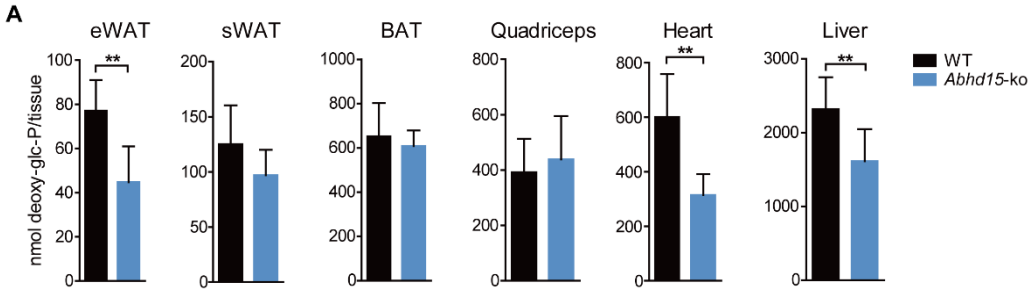

Figure 21. The glucose uptake in *Abhd15*-ko and WT mice. (A) Mice were o/n fasted and then gavaged with 2.5 g/kg glucose (spiked with 10 µCi ^{3}H-deoxyglucose per mouse). 20 min after gavage, tissues were collected, and uptake of radioactive glucose was determined (n = 7).

Next we examined whether DNL is changed in *Abhd15*-ko adipocytes. We used the isolated primary stromal vascular cells to directly investigate DNL in adipocytes. After isolation, we differentiated those cells into mature adipocytes. Contrast to the results of Abhd15 silenced 3T3-L1 cells, *Abhd15*-ko SVCs had no defects on differentiation capacity and can differentiate into mature adipocytes as the same as WT SVCs. For instance, there was no differences on adipogenesis marker expression and lipid accumulation between WT and *Abhd15*-ko cells (fig. 22, A-B).

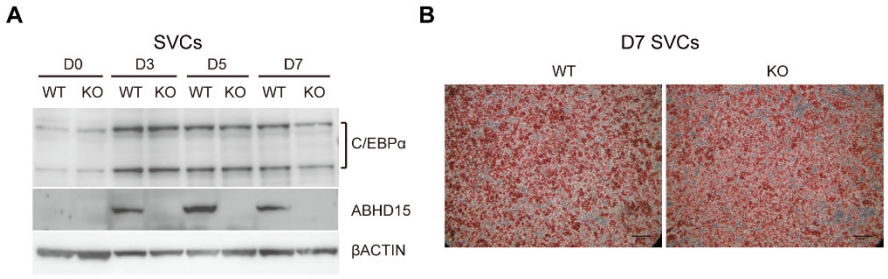

Figure 22. The differentiation of primary SVCs from sWAT of *Abhd15*-ko and WT mice. (A) C/EBPα and ABHD15 expression in SVCs during differentiation. (B) Representative oil-red-O staining of fully differentiated SVCs (D7), scale bar: 100 µm.

Since there is no adipogenic differences between WT and *Abhd15*-ko adipocytes, we following investigated the DNL with those cells. Without insulin, there is same amount of glucose converted into lipids in WT and *Abhd15*-ko adipocytes (fig. 13E). With insulin, it strongly promotes the conversion of glucose into lipids in both genotypes, but *Abhd15*-ko adipocytes had much less amount of converted lipids than WT (fig. 23, A). In particular, there was reduced levels of FFA, MAG, and DAG in *Abhd15*-ko cells (fig. 23, B), while the amount of TGs and cholesteryl esters (CE) was the same in both cells (fig. 23, C). In line with these data, gene expression related with glucose metabolism and DNL, such as glucose kinase (*Gck*), fatty acid synthase (*Fas*) and acetyl-coenzyme A synthetase (*AceCS*) was reduced in *Abhd15*-ko WAT after refeeding (fig. 20, A&B). Moreover, phosphorylation of Akt was strongly decreased in eWAT and sWAT of *Abhd15*-ko mice when compared to controls (fig. 23, D-F). These results strongly suggest that *Abhd15* deletion not only affects insulin-regulated lipolysis, also glucose uptake and DNL in AT.

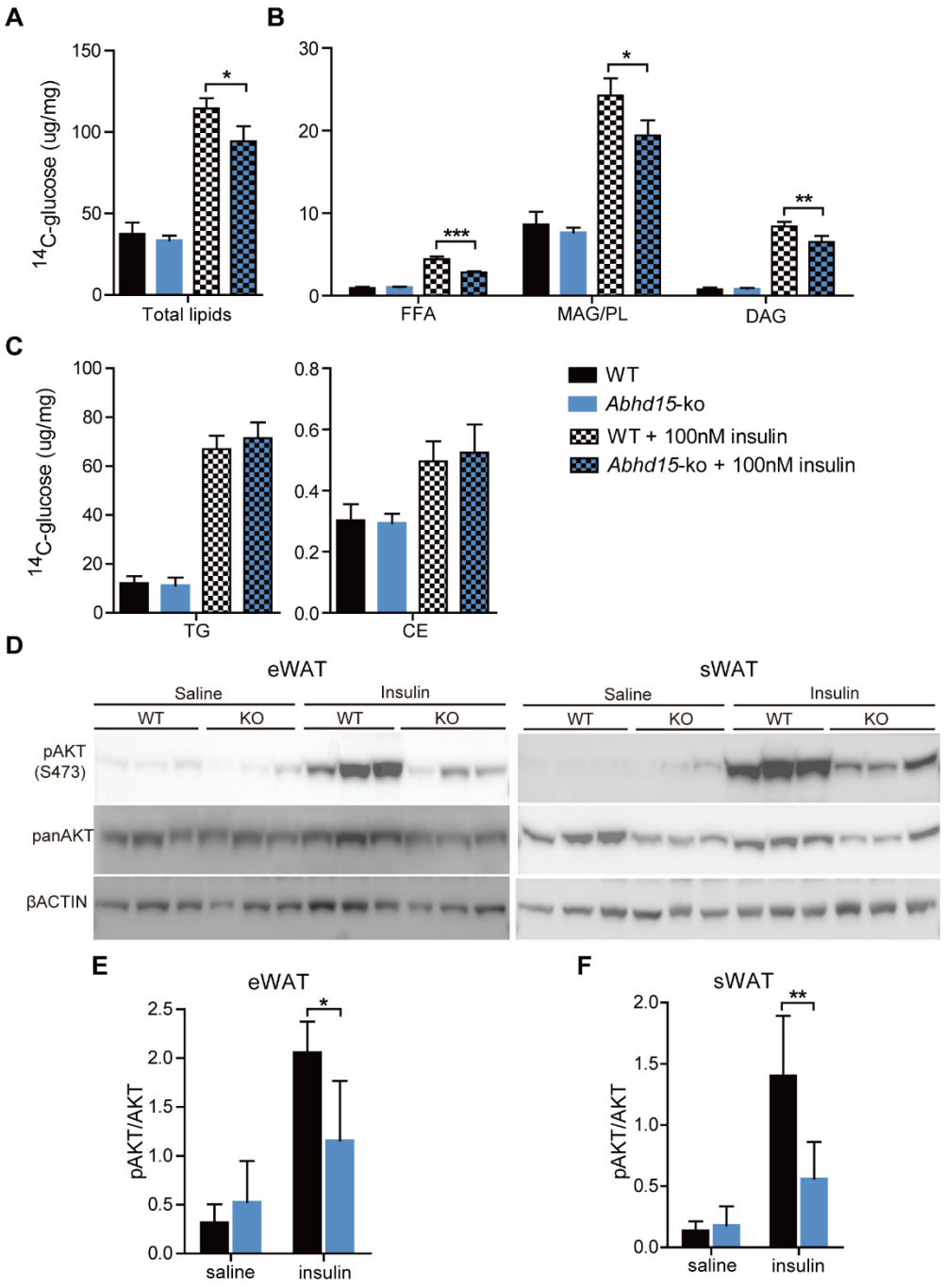

Figure 23. The impaired glucose metabolism in *Abhd15*-ko mice. (A-C) ^{14}C-glucose incorporation into lipids of fully differentiated SVCs treated with or without 100 nM insulin. (D-F) Phosphorylation of Akt and Akt expression of eWAT and sWAT from insulin injected (20 min) mice. *<0.05, **<0.01.

Decreased adiponectin levels are regarded as an early indicator of insulin resistance[102,103]. We found that plasma adiponectin levels were markedly reduced in *Abhd15*-ko compared to WT mice independent of age (fig. 24, A). Upon aging, insulin sensitivity decreases which correlates with lower adiponectin levels[104]. Indeed, young *Abhd15*-ko mice showed moderately reduced insulin sensitivity with a normal glucose tolerance (fig. 24, B&C), while old *Abhd15*-ko mice (over 60 weeks) showed strongly reduced insulin sensitivity and impaired glucose tolerance when compared to WT mice (fig. 24, D&E). Together, these data demonstrate that ABHD15 ablation impairs glucose metabolism and subsequently leads to insulin resistance.

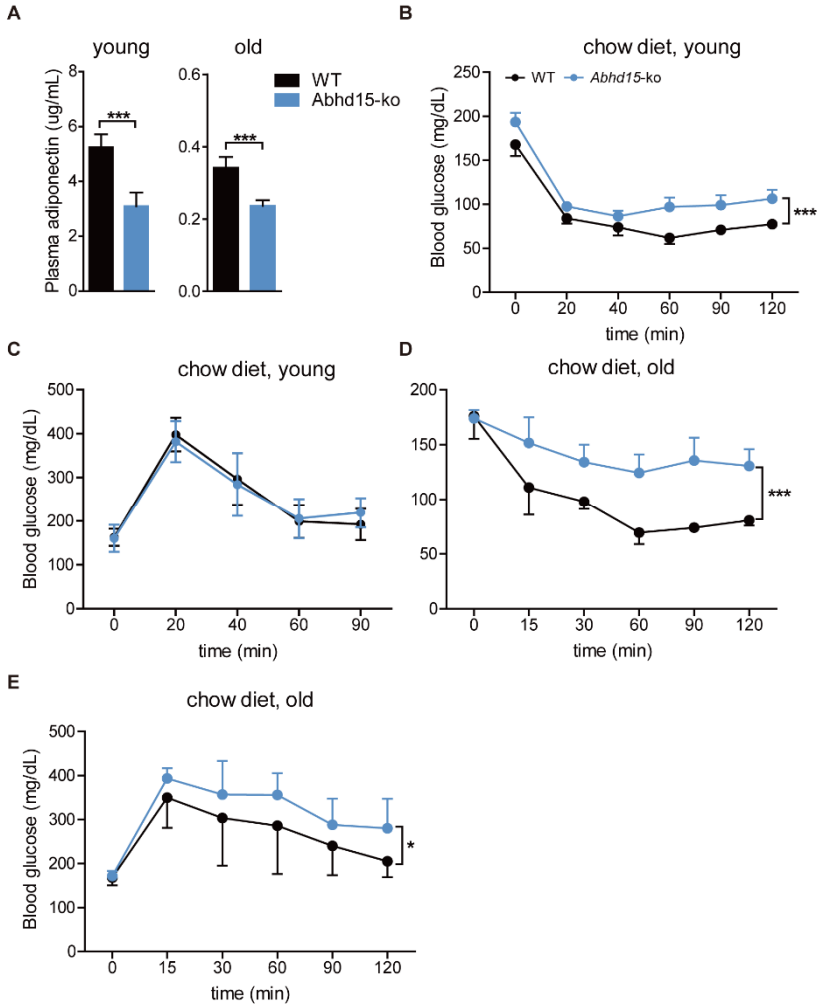

Figure 24. The development of insulin resistance in *Abhd15*-ko mice fed with CD. (A) Plasma adiponectin levels after 1-hour refeeding at the age of 20 and 54 weeks respectively. (B-C) Insulin tolerance and glucose tolerance test of 12 and 13 weeks old mice separately (n = 6-7). (D-E) Insulin tolerance and glucose tolerance test of 60 and 80 weeks old mice separately (n = 4-6). *<0.05, ***<0.001.

3.3.5 HFD and HGD accelerate insulin resistance in *Abhd15*-ko mice.

HFD has been widely used to induce obesity in C57BL/6 mouse and once the mice became obese they show severely insulin resistance[105,106], HGD feeding can also cause insulin resistance[107] and we found that ABHD15 expression was induced by HGD to a higher extent in WAT than HFD (fig. 7, C). Thus, we fed those mice with HFD or HGD to study the impact of *Abhd15* knockout on insulin resistance. After a 12 weeks (short term) HFD or HGD feeding, the disrupted anti-lipolytic effect of insulin was also evident from elevated plasma FFA levels in *Abhd15*-ko mice (fig. 25, A&B). When fed with HFD, basal FFA release was increased in *Abhd15*-ko fat pads, which could not be diminished by insulin addition (fig. 25, C). These results again confirm the role of ABHD15 as a regulator of insulin-suppressed lipolysis.

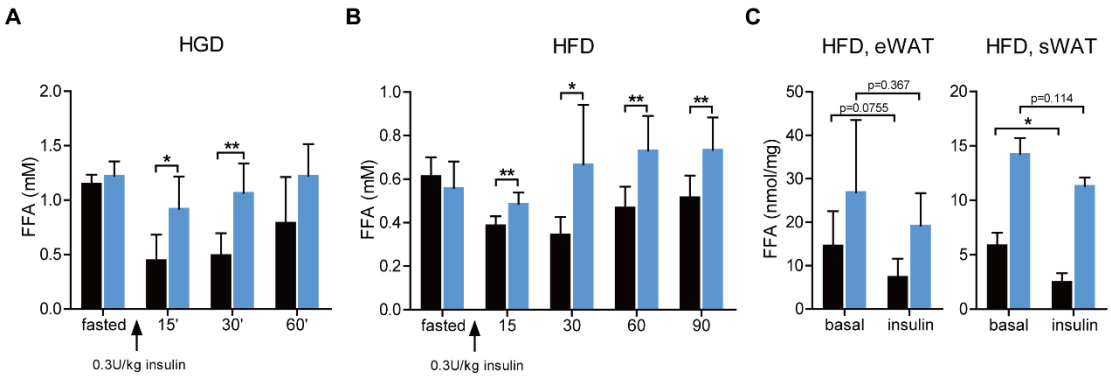

Figure 25. The unsuppressed FFA release by insulin in *Abhd15*-ko mice fed with HGD and HFD. (A&B) mice were o/n fasted and injected with 0.3 and 0.35 U/kg insulin respectively, plasma FA levels were determined as indicated (n = 5-8). (C) FA release from explants of eWAT and sWAT of mice on HFD with or without 100 nM insulin in the medium (n = 4). *<0.05, **<0.01.

Although the insulin-suppressed lipolysis was consistently abrogated in *Abhd15*-ko mice fed HGD and HFD (fig. 25, A&B), they did not suffer from severely impaired insulin sensitivity after short term feeding with these diets (fig. 26, A&C). Though there was an impaired glucose tolerance in HFD-fed *Abhd15*-ko mice (fig. 26, D), glucose tolerance was not yet unchanged upon HGD feeding (fig. 26, B).

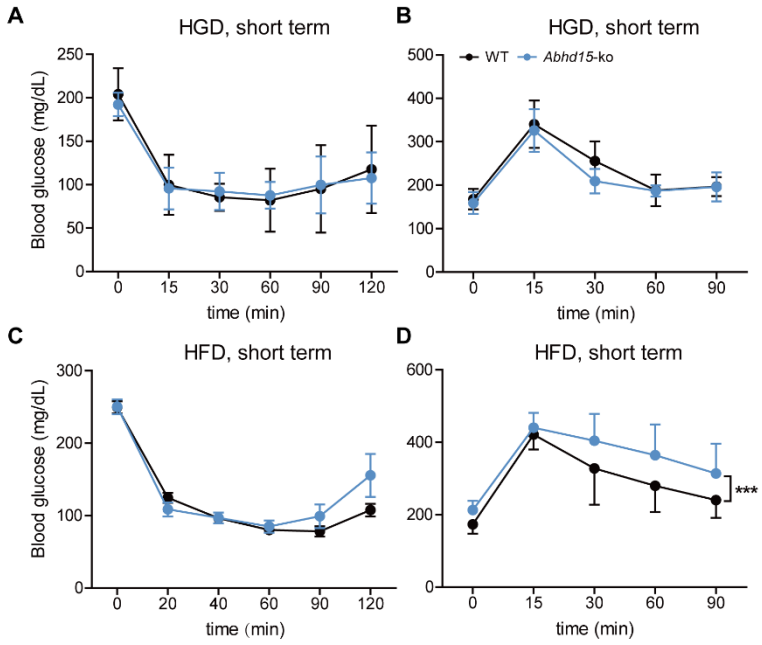

Figure 26. The insulin and glucose tolerance tests in *Abhd15*-ko and WT mice fed with HGD and HFD for short term. (A-D) Insulin and glucose tolerance test of mice on short term (12 weeks) HGD and HGF (n = 4-6). ***<0.001.

After HGD feeding for longer than 18 weeks (long term), at the age of between 30-44 weeks old, *Abhd15*-ko mice displayed reduced adiponectin levels, and increased postprandial insulin and glucose levels. Importantly, leptin levels were unchanged, as well as food intake in HGD-fed WT and *Abhd15*-ko mice (fig. 27, A-E). Long term HGD-fed *Abhd15*-ko showed a reduced insulin sensitivity (fig. 27, F). Long term HFD feeding (30 weeks) also evoked a strongly reduced glucose tolerance in *Abhd15*-ko mice (fig. 27, G). Unexpectedly, the insulin tolerance was similar between Abhd15-ko and WT mice, this might be due to the fact that long term HFD feeding makes both, WT and ko miceseverely insulin intolerant. Together, these result demonstrate that *Abhd15* ablation leads to insulin resistance and HFD/HGD accelerate insulin resistance development.

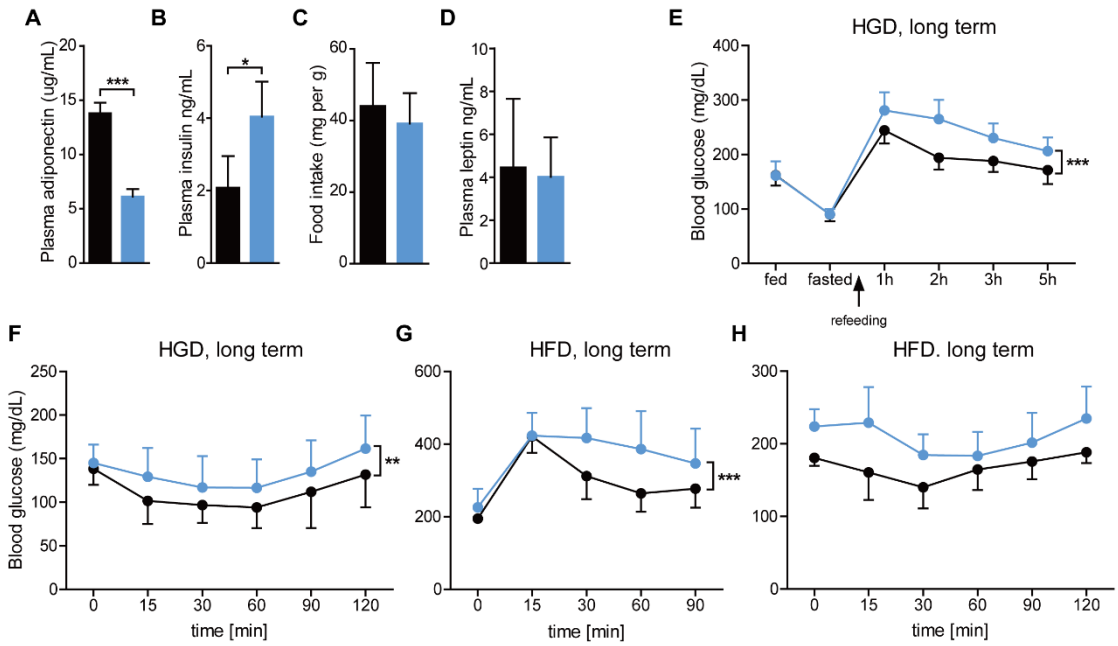

Figure 27. The development of insulin resistance in *Abhd15*-ko mice fed with HGD and HFD for long term. (A-B, D) Refeeding plasma adiponectin, insulin and leptin levels in Abhd15-ko and WT mice fed long term HGD. (C, E) Food intake and blood glucose levels during the refeeding. (F) Insulin tolerance test of mice on long term (30-44 weeks) HGD feeding (n = 5). (G-H) Insulin and glucose tolerance test of mice on long term (30-44 weeks) HFD feeding (30-44 weeks) (n = 4-6). *<0.05, **<0.01, ***<0.001.

3.3.6 Exclusive deletion of *Abhd15* in WAT contributes to the development of insulin resistance.

To delineate the contribution of ABHD15 in WAT for developing insulin resistance, we generated AT-specific *Abhd15* knockout mice (*Abhd15*-ako). In o/n fasted *Abhd15*-ako mice, neither IP insulin injection nor oral glucose gavage was able to suppress FFA release on chow and HGD (fig. 28, A&B). To further confirm that this phenotype is due to the loss of ABHD15 in WAT, we cross bred the *Abhd15*-flox mice with tamoxifen inducible *Ucp1*-cre transgenic mice[75] to get BAT-specific knockout mice (*Abhd15*-bko). After 5 constitutive days of tamoxifen gavage, *Abhd15*-flox (as control) and *Abhd15*-bko mice were o/n fasted, and insulin injection (with male) as well as glucose gavage (with female) reduced FFA release comparable to control mice (fig. 28, C&D). These results confirm the phenotype of unsuppressed FFA release by insulin we observed in conditional and total knockout mice is due to the loss of ABHD15 in WAT, but not in BAT.

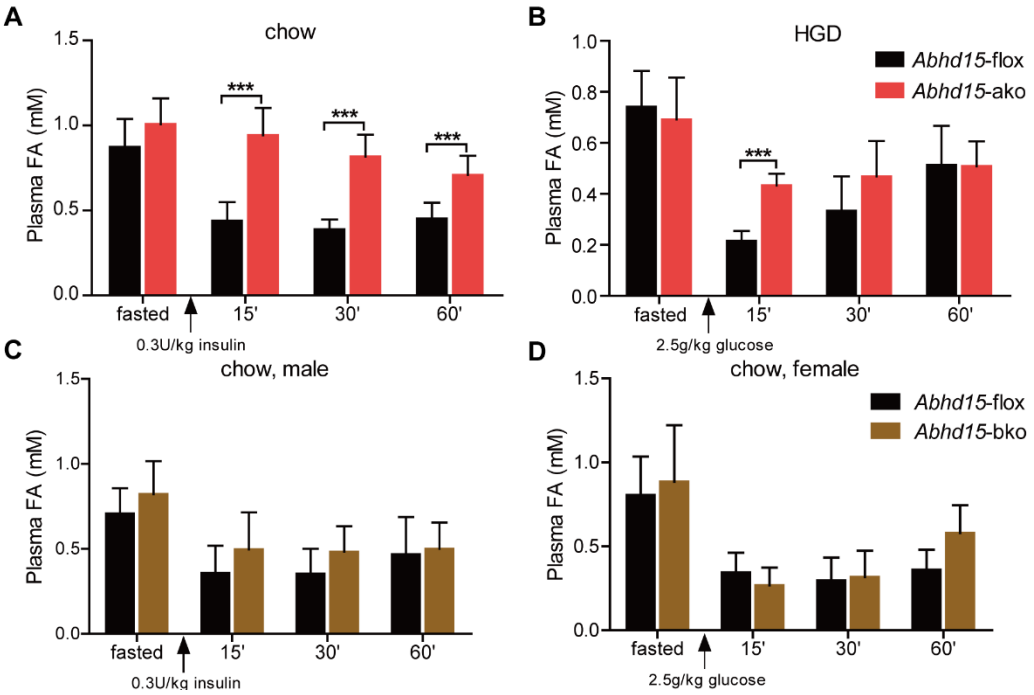

Figure 28. The unsuppressed FFA release by insulin in *Abhd15*-ako mice not in *Abhd15*-bko mice. (A&B) CD and HGD fed mice were o/n fasted and injected with insulin or gavaged with glucose, plasma FA levels were measured at indicated time (n = 6-8). (C&D) CD fed male or female mice were o/n fasted and injected with insulin or gavaged with glucose, plasma FA levels were measured at indicated time (n = 4-5). ***<0.001.

Comparable to the changes in *Abhd15*-ko mice (fig.16, C), *Abhd15*-ako mice fed with HGD showed the same decreased expression of the genes related with lipid synthesis (fig. 29, A), PDE3B content (fig. 29, B) and plasma adiponectin levels (fig. 29, C). Consistent with *Abhd15*-ko mice, HGD fed *Abhd15*-ako mice displayed an obviously reduced glucose tolerance and insulin sensitivity (fig. 29, D&E). These results show the impaired insulin-regulated pathways in both *Abhd15*-ko and *Abhd15*-ako mice, and strongly suggest an exclusive role of ABHD15 for insulin-mediated suppression of lipolysis in WAT, thereby influencing whole body lipid and glucose metabolism.

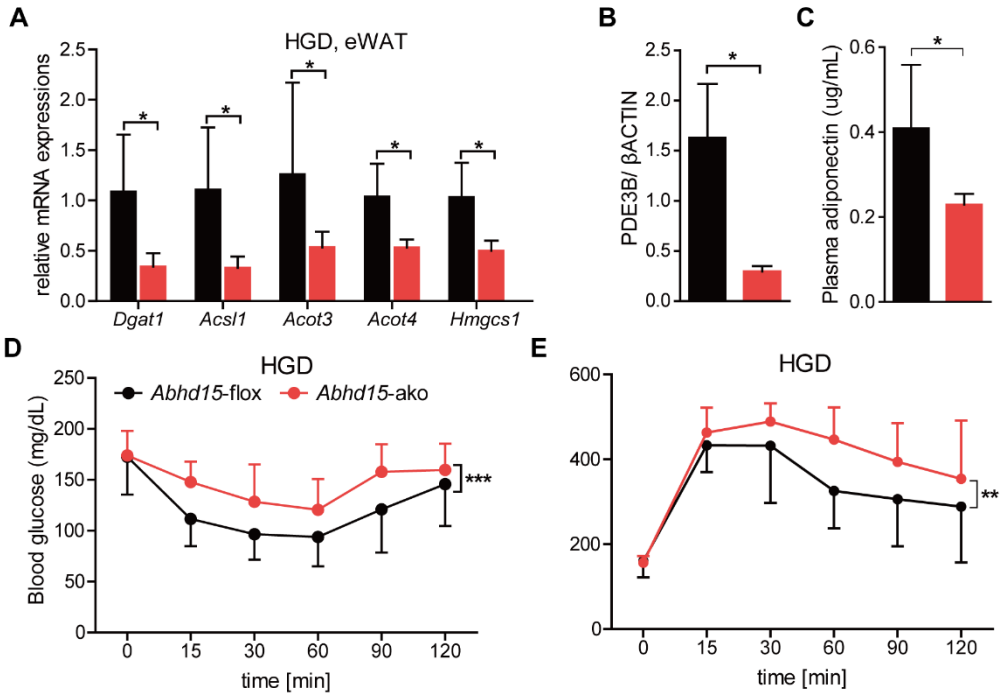

Figure 29. The downregulation of genes related with lipid metabolism and development of insulin resistance in *Abhd15*-ako mice fed with HGD. (A) Relative expression of genes involved in lipid metabolism from eWAT. (B) Quantification of PDE3B protein expression in mice fed with HGD. (C) Plasma adiponectin levels after 1-hour refeeding on HGD. (D-E) Insulin and glucose tolerance test of HGD fed mice (n = 7-8). (F) RER was measured over 3 days including o/n fasting and 6-hour refeeding period (n = 3-5). *<0.05, **<0.01, ***<0.001.

3.4 The impact of ABHD15 on lipid metabolism *in vitro*.

To apply a different but complementary approach to study the impact of ABHD15 on lipolysis, we generated an *Abhd15* (or puro as control) stable overexpressing 3T3-L1 fibroblast cell line. The adipogenic markers, lipogenic genes expression and lipid accumulation in ABHD15 overexpressed cells did not differ from control cells during differentiation (fig. 30, A-E). Overexpression of ABHD15 *per se* had no influence on basal or stimulated (with insulin or isoproterenol) FA and glycerol release (fig. 30, F-G), however under the co-treatment of insulin and IBMX, a non-selective PDE inhibitor, *Abhd15* overexpressing adipocytes had higher glycerol release than control cells (fig. 30, G).

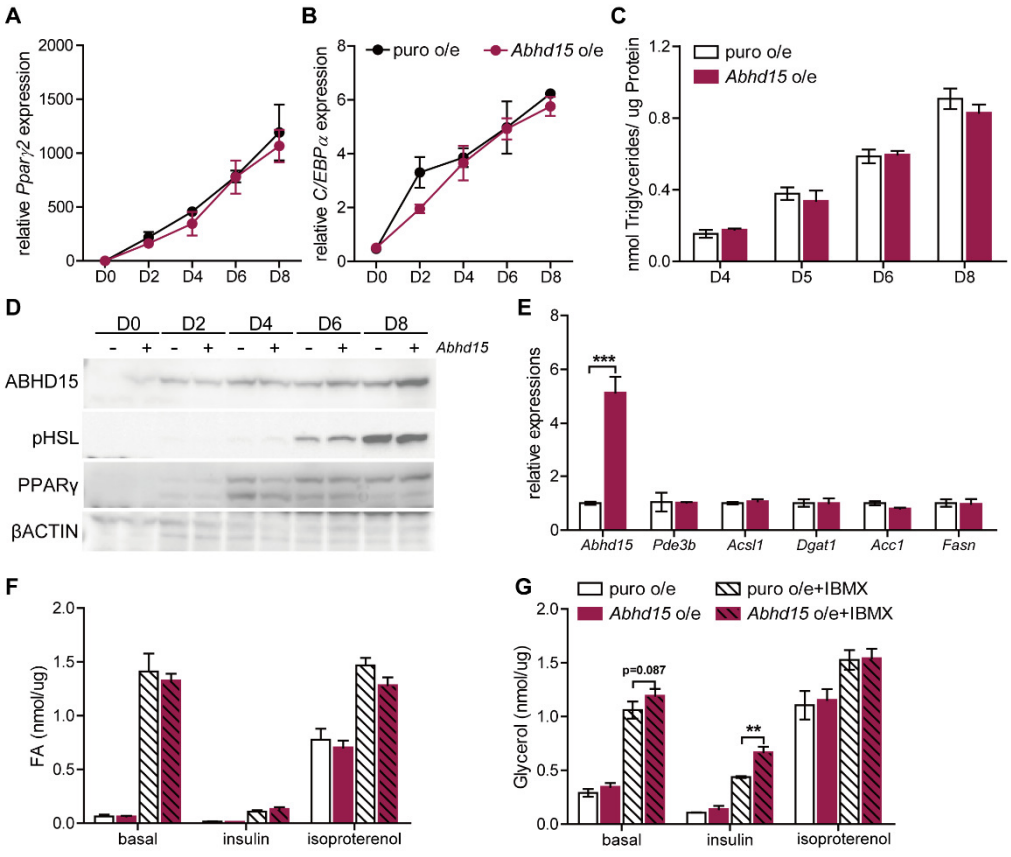

Figure 30. The overexpression of ABHD15 in 3T3-L1 adipocytes. (A-B) Relative *Pparγ2* and *C/EBPα* expression during the differentiation of cells (day 0-8) (n = 3). (C) Intracellular TG content during the differentiation of cells (day 4-8) (n = 3). (D) PPARγ and phosphorylated HSL expression during the differentiation. (E) Relative genes expression in fully differentiated cells (day 8). (F-G) FA and glycerol release in control and Abhd15 o/e cells under basal, insulin and isoproterenol stimulation with or without 50 µM IBMX treatment (n = 3). **<0.01, ***<0.001.

3.5 Correlation of *ABHD15* expression in WAT with human disease.

Our mice models provide comprehensive evidence to support that ABHD15 knockout leads to the insulin resistance in mice. To further confirm whether this is the same with human disease, we first evaluated published microarray data (GSE16415) from human omental AT (OWAT). Bioinformatics analysis of this data revealed that *ABHD15* expression was two-fold lower in obese, diabetic women (BMI > 30, age > 55) compared to age-matched obese but glucose-tolerant women (Table 3). Interestingly, *PDE3B* and *ABHD5* (ATGL-coactivator, also named as *CGI-58*) were decreased four-fold and three-fold respectively (Table 3). And the other *PDE* and *ABHD* family members showed no deregulation or were not detected in this human cohort (Table 3). To further looking for convincing evidence and validate the data generated by other group, we isolated mRNA and measured *ABHD15* gene expression of OWAT from eleven severely obese patients. Later, *ABHD15* expression was correlated with insulin resistance markers and other metabolic parameters via Spearman's rank. The results showed that *ABHD15* expression in OWAT positively correlated with several insulin sensitivity indicators, for instance oral glucose insulin sensitivity (OGIS), insulin sensitivity index (ISI), clamp-like index (CLIX) and negatively correlated with insulin resistance indicators, like 1st, 2nd phase response and the area under the curve (AUC) during the oral glucose tolerance test (OGTT). Interestingly, *ABHD15* expression is negatively correlated with serum IL-6 and FFA concentrations (Table 4).

GSE16415											
down-regulated			up-regulated			down-regulated			up-regulated		
ABHD Family						PDE Family					
Member	FC	P	Member	FC	P	Member	FC	P	Member	FC	P
ABHD1	-2.02	0.067	*ABHD3*	1.28	0.54	*PDE2A*	-1.48	0.38	*PDE1A*	1.72	0.21
ABHD5	-3.03	**0.0012**	*ABHD4*	1.14	0.61	***PDE3B***	**-4.19**	**0.001**	*PDE3A*	1.62	0.16
ABHD6	-1.17	0.54	*ABHD8*	1.09	0.71	*PDE4C*	-1.54	0.08	*PDE4A*	1.41	0.18
ABHD10	-1.26	0.27	*ABHD11*	1.01	0.94	*PDE4D*	-1.82	0.98	*PDE4B*	1.54	0.25
ABHD12B	-2.14	0.081	*ABHD12*	1.23	0.57	*PDE6A*	-3.03	0.67	*PDE5A*	1.16	0.73
ABHD13	-1.27	0.42	*ABHD16A*	1.46	0.084	*PDE8A*	-1.38	0.28	*PDE7*	1.63	0.23
ABHD14A	-1.1	0.75	*ABHD17A*	1.53	0.16	*PDE8B*	-3.55	**0.013**	*PDE10*	1.12	0.78
ABHD14B	-1.69	0.11									
ABHD15	**-1.98**	**0.0376**									
ABHD16B	-1.08	0.74									
ABHD17B	-1.09	0.78									

Table 2. *ABHD* and *PDE* family members expression in diabetic versus non-diabetic obese women. mRNA expression as fold-change (FC) and p values (P) in visceral AT from microarray data (GSE16415) comparing diabetic with non-diabetic obese women (n = 5).

Insulin sensitivity			Insulin resistance			Other parameters		
	Spearman's rho	*p*		Spearman's rho	*p*		Spearman's rho	*p*
OGIS	0.66	0.02	1st phase response	-0.62	0.04	IL6	-0.70	0.02
ISI	0.68	0.03	2nd phase response	-0.62	0.03	FFA	-0.69	0.02
CLIX	0.64	0.03	AUC OGTT	-0.65	0.02			
			HOMA-IR	-0.53	0.07			

Table 3. Correlations of *ABHD15* gene expression in OWAT from severely obese patients and several metabolic parameters. BMI > 40 kg/m^2 designed as severely obese (n = 11).

3.6 The mechanism whereby ABHD15 regulates PDE3B.

3.6.1 The association between ABHD15 and PDE3B *in vitro*.

Previously, the interaction of ABHD15 with PDE3B was proposed[63], here we confirmed the interaction in 3T3-L1 adipocytes again with a specific antibody of murine ABHD15. We also show here that the interaction of ABHD15 and PDE3B is not affected by insulin or isoproterenol treatment (fig. 31, A). We also co-transfected *Pde3b* and *Abhd15* in COS7 cells and Bnlcl2 hepatocytes and confirmed the interaction in non-adipocytes (fig. 31, B&C). Although the evidence for direct interaction remains elusive, fractionation experiments revealed that both ABHD15 and PDE3B are enriched in membrane fraction (fig. 31, D) which makes the interaction of those two protein reasonably.

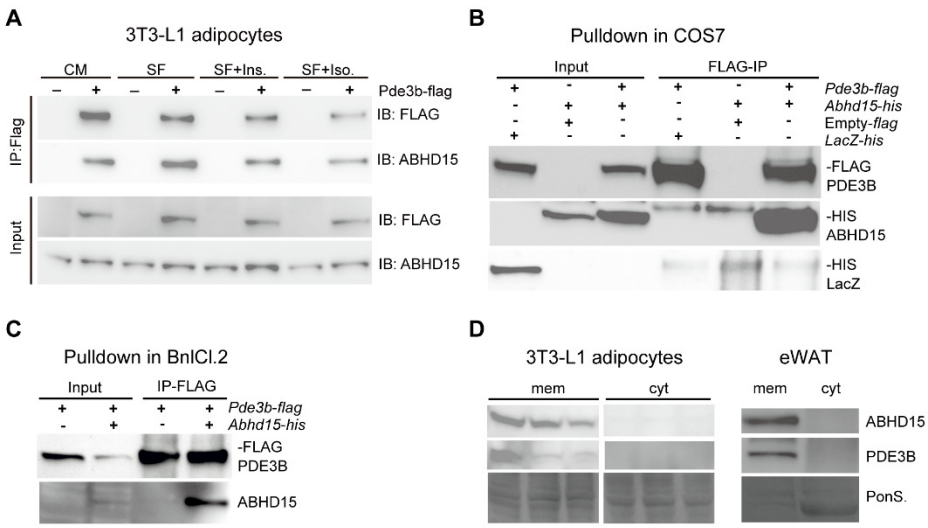

Figure 31. The interaction between ABHD15 and PDE3B in cells. (A) Pull down of ABHD15 from *Pde3b* overexpressing 3T3-L1 adipocytes under complete medium (CM), serum fasting (SF), SF with 100nM insulin and SF with 10nM isoproterenol treatments. (B-C) Pull down of ABHD15 and PDE3B in BnlCl2 and COS-7 cells. (M) ABHD15 and PDE3B expression in the membrane faction of 3T3-L1 adipocytes and eWAT.

3.6.2 The regulation of ABHD15 on PDE3B expression.

In *Abhd15*-ko and *Abhd15*-ako mice, mRNA and protein expression of PDE3B were both significantly reduced in WAT (fig. 16, D&E; fig. 32 C&D). The PDE3B protein expression was also ablated in fully differentiated SVCs of sWAT from Abhd15-ko mice compared to WT mice (fig. 32, A&B). To fully understand how PDE3B is reduced by *Abhd15* deletion, we examined PDE3B expression in ABHD15 knockdown adipocytes. Firstly, we checked the PDE3B expression in *Abhd15* heterozygous knockout (Het) mice, and found that with around 50% reduced ABHD15 expression, PDE3B level was comparable to WT mice (fig. 32, C&D). Alternatively, we knocked down ABHD15 expression transiently in 3T3-L1 adipocytes and immunoblotting result showed that with half amount of ABHD15 protein in the cells, PDE3B was as stable as in control cells (fig. 32, E-G). Next, we accessed whether the presence of ABHD15 is required for PDE3B protein, we rescued ABHD15 in knockout SVCs with *Abhd15* overexpressing retrovirus. With the introduction of ABHD15 in *Abhd15*-ko adipocytes, there was an approximately 50% increased PDE3B level (fig. 32, H-I). These data suggest that with the presence of ABHD15, no matter how much ABHD15 is there, PDE3B level is stable; and with the absence of ABHD15, PDE3B will be unstable and might be degraded via ubiquitination or lysosome system. Thus we followed with a protein half-life study to directly investigate whether ABHD15 stabilized PDE3B. When treated PDE3B expressing COS7 cells with cycloheximide (CHX), a protein synthesis inhibitor, PDE3B proteins start to degrade after 1 hour treatment (fig. 32, J left blot). When we added the same amount of CHX to the cells expressing both ABHD15 and PDE3B, both proteins are stable, at least, more than 1 hour (fig. 32, J right blot). We have shown that in COS7 cells, ABHD15 also interacts with PDE3B and likely to form a protein complex, thus it is possible this complex is more difficult to be broken down and this assumption was proposed by other group[63].

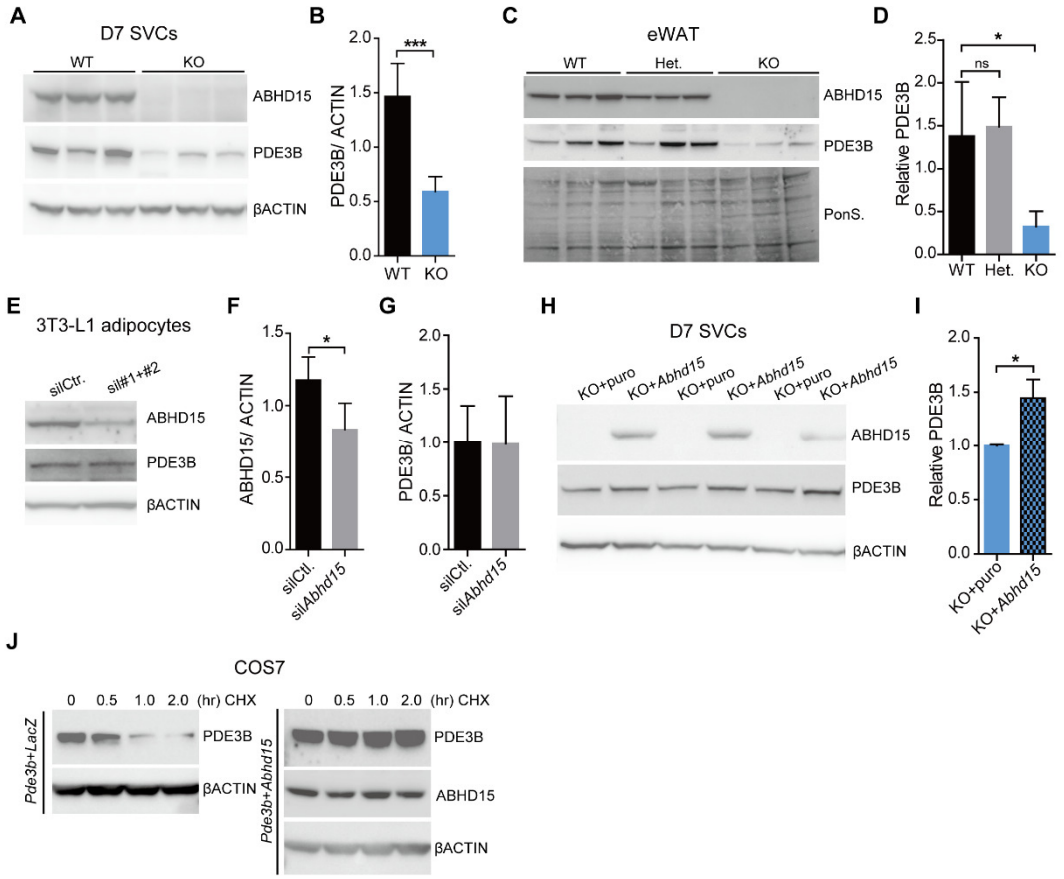

Figure 32. The regulation and stabilization of ABHD15 on PDE3B protein. (A&B) ABHD15 and PDE3B expression in the membrane fraction of eWAT from WT, heterozygous (Het), and homozygous (KO) *Abhd15*-ko mice. (C&D) ABHD15 and PDE3B expression in fully differentiated (day 7) SVCs. (E-G) ABHD15 and PDE3B expression in control and *Abhd15* silenced 3T3-L1 adipocytes. One representative WB is shown (n = 6). (H&I) ABHD15 and PDE3B expression in puro and *Abhd15* re-expressed fully differentiated *Abhd15*-ko SVCs. (J) ABHD15 and PDE3B expression in COS-7 cells co-transfected with *Pde3b* and *LacZ* or *Pde3b* and *Abhd15*, treated with or without 5 µg/mL CHX for 0-2 hours.

3.6.3 The impact of ABHD15 on PDE3B activity.

In addition to the evidence of reduced PDE3B protein and mRNA levels in *Abhd15* knockout cells, we also explored the impact of ABHD15 on PDE3B activity. Since both ABHD15 and PDE3B are membrane enriched proteins, we isolated the membrane fraction of Abhd15 and control plasmid (HMC) overexpressed COS7 cells and re-suspended the membrane lysates in PDE3B activity assay buffer. Immunoblotting confirmed the enrichment of ABHD15 protein in membrane lysates (fig. 33, A). The PDE3B activity assay showed that IBMX, a selective PDE3 inhibitor, significantly reduced PDE3B enzyme activity. However, compared to the control lysates, ABHD15 lysates did not change PDE3B enzyme activity (fig. 33, B). We further analyzed PDE3B activity with eWAT tissues from *Abhd15-ko* and WT mice injected with saline or insulin for 1 hour. However, we did not observe differences between WT and *Abhd15*-ko mice (fig. 33, C). Even though the impact of ABHD15 on PDE3B activity remains elusive, *Abhd15*-ko lysates showed trend of reduced PDE3B activity. Further sensitive activity assay needs to be applied.

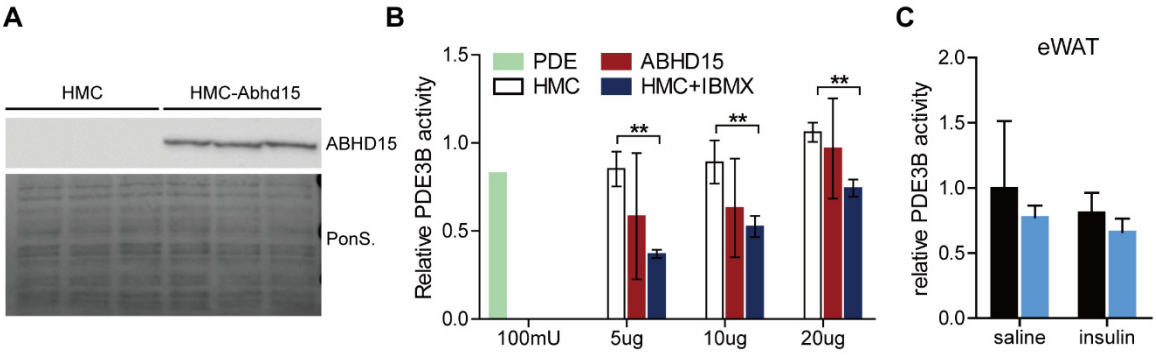

Figure 33. PDE3B activity assay. (A) ABHD15 expression in the membrane lysates used for PDE3B activity assay. (B) Relative PDE3B activity with different amount of lysate from HMC or HMC-Abhd15 transfected COS7 cell, IBMX was used as a negative control. (C) PDE3B activity in the membrane fractions of eWAT from Abhd15-ko and WT mice injected with saline or insulin.

3.6.4 The presence of PDE3B for the ABHD15 effect on lipolysis.

To further investigate whether PDE3B is required for ABHD15's effect on lipolysis, we silenced *Pde3b* transiently in *Abhd15* overexpressing 3T3-L1 adipocytes. Both PDE3B mRNA and protein were strongly reduced after 72 hours of *Pde3b*-siRNA (si*Pde3b*) electroporation (fig. 34, A-E). Intriguingly, the knock-down of PDE3B protein also reduced ABHD15 protein levels in both puro and *Abhd15* overexpressing adipocytes (fig. 34, C-E). Despite the successful deletion of PDE3B in ABHD15 overexpressed adipocytes, there is no defect on FFA and free glycerol release under basal and insulin conditions (fig. 34, F-G). Compared to the basal state, insulin treatment strongly reduced phosphorylation of HSL and PKA substrates (fig. 34, H). Silencing of Pde3b slightly increased the phosphorylation of HSL and PKA substrate in puro overexpressing cells when treated with insulin, however, this mild effect is not seen in ABHD15 overexpressing cells (fig. 34, G). It has been evidenced by published date[60] that insulin did not further reduce glycerol release in the absence of lipolytic stimuli in brown adipocytes. Indeed our data shows that without lipolytic stimulation (e.g. isoproterenol), insulin still reduced phosphorylation of HSL but did not potently reduce FFA release (fig.34, F-G). From above those results, we knew that insulin inhibited lipolysis is based on the pre-activation of lipolysis and both ABHD15 and PDE3B did not affect lipolysis under basal and insulin conditions when lipolysis is unstimulated.

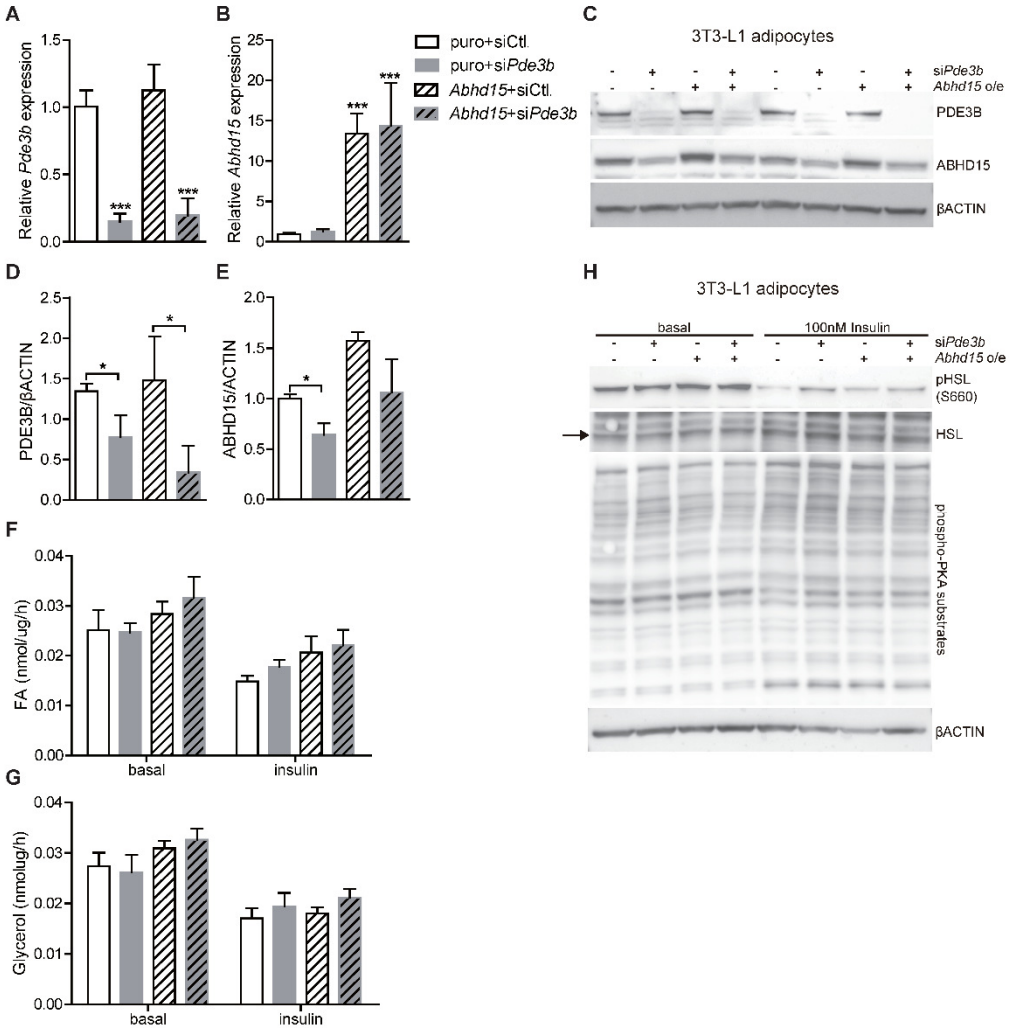

Figure 34. The impact of ABHD15 on lipolysis in the absence of PDE3B. (A&B) Relative *Abhd15* and *Pde3b* expression in adipocytes 48 hours after electroporation (n = 3). (C-E) ABHD15 and PDE3B expression in adipocytes 72 hours after electroporation (n = 4). (F-G) FA and glycerol release from cells 72 hours after electroporation; cells were incubated with 2% BSA medium for 3 hours (basal) or pre-treated with 100 nM insulin in 2% BSA medium for 1 hour and incubated with insulin for 2 hours (n = 3). (H) 72 hours after electroporation cells were serum starved for 6 hours, treated with or without 100nM insulin for 15 min and then harvested for western blotting. Arrow indicate the specific band of HSL. *<0.051, ***<0.001.

3.7 The role of ABHD15 in AT during the activation of BAT.

3.7.1 The *Abhd15*-ako mice are tolerant to acute and short-term cold exposure experiment.

Both cold exposure and β_3-AR agonist are known to be able to activate BAT in human and mouse models[17,108-110]. Before the prolonged cold exposure, we tested whether *Abhd15*-ako mice can survival in cold environment. In the first attempt of cold exposure experiment we used 5 male *Abhd15*-ako and 5 male *Abhd15*-flox (flox) homozygous control littermates. At the age of around 10 weeks, those mice were kept on chow diet after weaning. In the acute and short-term cold exposure experiments, the metal ear tags were not removed, two mice were housed together during the experiment. In the acute cold exposure, there were no differences on body temperature, body weight, food intake, blood glucose and FFA levels at different nutritional states (fig. 35, A-E). Later, we continued a short-term (7 days) cold exposure procedure and the mice always had access to water and food. In this 7-day cold exposure experiment, we did not observe a significant difference in body weight changes, food intake, tissues weight and O_2 consumption, blood glucose and FFA changes (fig. 35, F-M). Although there is a reduction of eWAT O_2 consumption (fig. 35, K), this might be due to a slightly increased eWAT weight (fig. 35, J). Also, there is no changes in the expression of browning genes and fatty acids oxidation genes in BAT (fig. 35, N). Together those data suggest that *Abhd15*-ako mice were tolerant to acute cold exposure which did not make changes between control and *Abhd15*-ako mice.

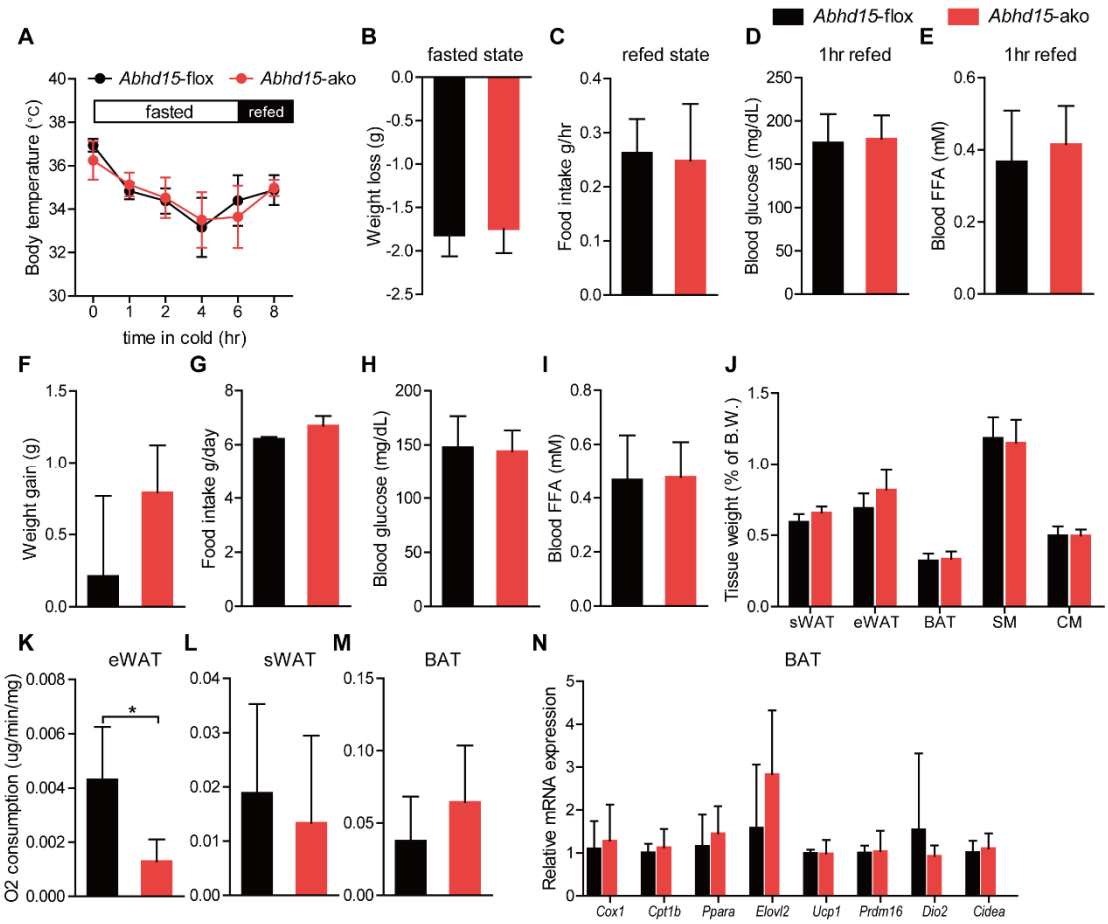

Figure 35. The body parameters of *Abhd15*-ako mice during acute or short-term cold exposure. (A) Rectal temperature of mice in cold chamber during fasting and refeeding. (B) Body weight loss of mice during 6 hours fasting in the cold. (C) Food intake during 2 hours refeeding after 6 hours fasting in cold. (D&E) Plasma glucose and FA levels after 1 hour refeeding in cold. (F&G) Body weight gain and food intake of mice during 7 days in cold. (H&I) Plasma glucose and FA levels of mice after 7 days cold exposure at fed *ad libitum* state. (J-M) Tissues weights of mice and tissue O^2 consumption after 7-day cold exposure. (N) Relative genes expression in BAT after 7-day cold exposure. n = 5-9 in each. *<0.05.

3.7.2 *Abhd15* deletion in BAT did not affect thermogenesis function.

To access whether *Abhd15* deletion affects BAT thermogenic function, we performed an acute cold exposure with *Abhd15*-bko and control mice. In the first experiment with *Abhd15*-bko mice, we were limited with 2 *Abhd15*-flox, 3 *Abhd15*-bko male mice and 2 *Abhd15*-flox, 3 *Abhd15*-bko female mice. We fasted the *Abhd15*-bko and flox mice at 4 °C for 3 hours, afterwards, the mice were refed with food until the experiment was done. During the acute cold exposure, male and female *Abhd15*-bko mice did not differ from control mice in body temperature, blood glucose and plasma FFA levels (fig. 36, A&B, D&E). Also all mice consumed comparable food amounts (fig. 36, C&F). Later, we repeated the acute 1 hour cold exposure with 5 flox and 6 *Abhd15*-bko male mice during fasting. Again, we did not observe any differences in body temperature, blood glucose and plasma FFA levels (fig. 36, G-I). Importantly, the acute cold exposure results imply that *Abhd15* deletion in ATs did not affect BAT thermogenesis function, and next we will try a prolonged cold exposure and acute or prolonged administration of β_3-AR agonist (CL-316,243) to explore ABHD15's role in those processes.

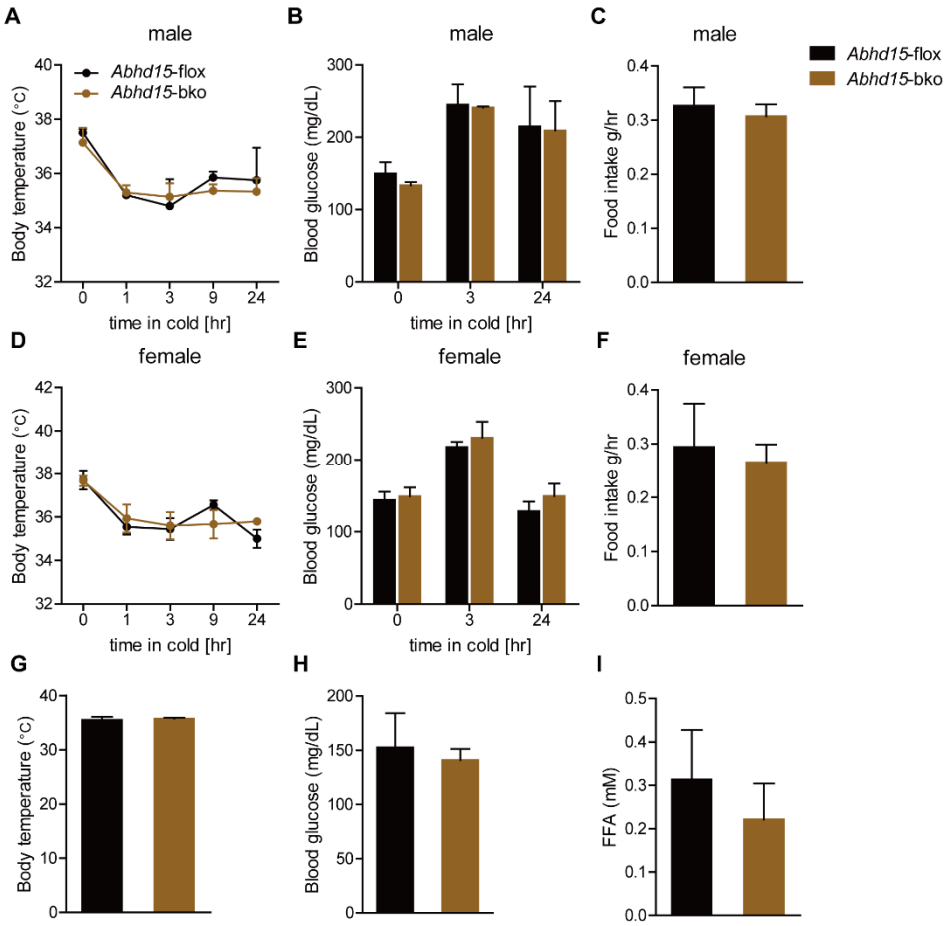

Figure 36. The body parameters of *Abhd15*-bko and control mice during acute cold exposure. (A&D) Rectal temperature of mice in cold chamber during fasting and refeeding. (B&E) Blood glucose levels during cold exposure. (C&F) Food intake during cold exposure. (D&E) Male rectal temperature, blood glucose and plasma FFA levels after 1 hour cold exposure when fasted (n = 2-3).

3.7.3 Long-term cold exposure activates sWAT FA oxidation in *Abhd15*-ako mice.

It has been shown that silencing or knockout of *Pde3b* promotes the white to beige conversion in eWAT[111]. Accordingly, the reduced expression of PDE3B in *Abhd15*-ko and *Abhd15*-ako mice led us to explore whether there is also a browning phenotype in *Abhd15* deficient mice. Cold exposure has been regarded as an efficient activator of BAT[9], as well as WAT[112], but this effect is indirect[112,113]. It was discussed that short-term cold exposure might not be sufficient to completely activate the browning of WAT[9] and indeed more than 7 days cold acclimation promotes almost 90% of UCP1 positive adipocytes in WAT[110]. Therefore, I performed a prolonged (2 weeks) cold exposure experiment with *Abhd15*-ako and control mice. In this experiment, 8 weeks old male mice were single housed and the metal ear tag was removed. Those mice were adapted to single housing for 3 days prior to the experiment and always had access to food and water during the experiment. After 2 weeks of cold exposure, there were no differences in body weight gain, food intake, blood glucose and triglyceride levels between knockouts and controls (fig. 37, A-D). And both genotypes consumed similar food amounts in the cold environment (fig. 37, B). Those cold stimulated mice were harvested at fed *ad libitum* state. Despite no differences on adipose tissues and muscles weight (fig. 37, E), the O_2 consumption of sWAT (fig. 37, G), not eWAT (fig.37, F) or BAT (fig. 37, H), was significantly increased in *Abhd15*-ako mice when compare to control mice. Adipocyte precursor cells (APs), which are defined as $Lin^-CD31^-CD45^-Sca\text{-}1^+PDGFR\alpha^+$ cells are bipotential precursor cells that are able to be differentiated into both white and brown adipocytes[114]. Real-time PCR analysis showed that the expression of brown adipocytes differentiation marker (*Prdm16*, *Cidea*, *Pparγ*), adipocyte precursor marker (*Pdgfrα*) and beige lineage markers (*Tmem26* and *Tnfrsf9*) was unchanged in *Abhd15*-ako mice compared to control mice (fig. 37, I). This result indicate

that *Abhd15* knockout did not affect the proliferation and *de novo* differentiation of beige precursor cells. However, the expression of thermogenic genes (*Ucp1* and *Dio2*) and *Fabp3*, which is essential for efficient fatty acid oxidation (FAO) in brown adipose tissue[115], was significantly upregulated in *Abhd15*-ako mice (fig. 37, I). These data suggest that ABHD15 might influence browning of WAT via the FAO pathway.

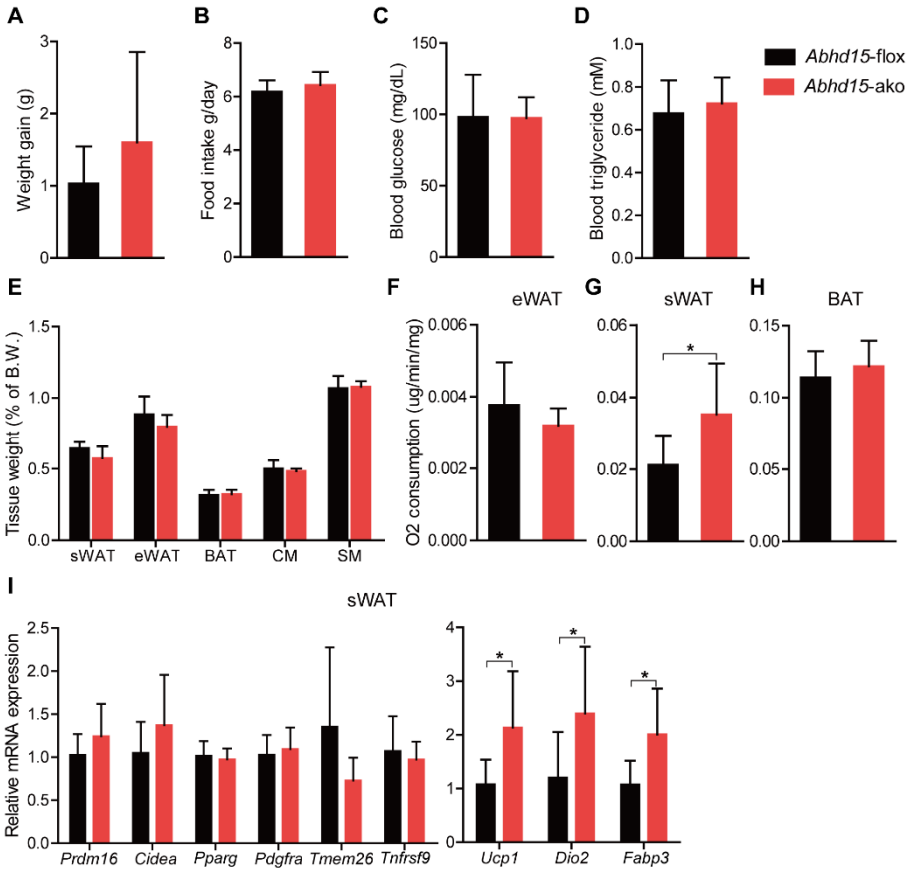

Figure 37. The increased expression of genes related with fatty acids oxidation in sWAT of *Abhd15*-ako mice after long-term cold exposure. (A&B) Body weight gain and food intake of mice after 2 week cold exposure. (C&D) Plasma glucose and TG levels of mice at fed *ad libitum* state after the cold exposure. (E-H) Tissues weight and O_2 consumption after cold exposure. (I) Relative genes expression in sWAT of mice after 2 weeks cold exposure, Prdm16: PR/SET domain 16; Cidea: cell death-inducing DFFA-like effector a; Pdgfra: platelet derived growth factor receptor, alpha polypeptide; Tmem26: transmembrane protein 26; Tnfrsf9: tumor necrosis factor receptor superfamily, member 9; Dio2: iodothyronine deiodinase 2; Fabp3: fatty acid binding protein 3. n = 5-8 in each. *<0.05.

3.7.4 β_3-AR agonist acutely enhances the energy metabolism in *Abhd15*-ako mice.

β_3-adrenergic activation has been found to activate BAT activity in both human and mouse[109,116]. CL-316,243 (referred as CL) is a β_3-adrenergic receptor agonist, the prolonged stimulation of CL also can activate BAT and promote the browning of WAT[117]. To examine CL induced BAT function and browning of WAT in *Abhd15*-ako mice, I injected CL to 10 weeks old male mice fed with CD and analyzed the metabolic changes during the treatment. In this experiment, *Abhd15*-ako and control (flox) mice had free access to food and water. Before the treatment, mice were single housed for 2 days in metabolic cages, from the third day of metabolic analysis, 0.5 mg/kg CL was i.p. injected over 3 consecutive days. On the 4th day, 1 mg/kg CL was injected and mice were harvested 20 min after injection. Compared to control mice, only the first CL administration strongly reduced RER in *Abhd15*-ako mice (fig. 38, A). And over the first 24 hours of CL treatment, the increased O_2 consumption and energy expenditure in *Abhd15*-ako only lasted for 10 hours (8 a.m. to 6 p.m.) (fig. 38, B-C). There were no differences on activity, food intake and water consumption between the two genotypes (fig. 38, D-F), although the CL injection seemed to reduce the activity of both mice (fig. 38, D) and food intake/water consumption of both mice gradually recovered from the first injection (fig. 38, E-F). After the treatment with CL, we did not observe any changes in blood glucose, plasma FFA and free glycerol levels in Abhd15-ako mice when compare to flox/control mice (fig. 38, G-I). Activated BAT has been shown to reduce circulating triglyceride levels via enhanced lipoprotein uptake[118], and we found that plasma triglyceride levels were significantly reduced in CL-treated *Abhd15*-ako mice (fig. 38, J). This result suggested that *Abhd15* deletion in BAT may enhance its activity. The fatty acid oxidation related genes were slightly increased in sWAT of Abhd15-ako mice when compared to flox mice (fig. 38, K). Together those data suggest

that CL injection acutely enhances the energy metabolism in *Abhd15*-ako mice.

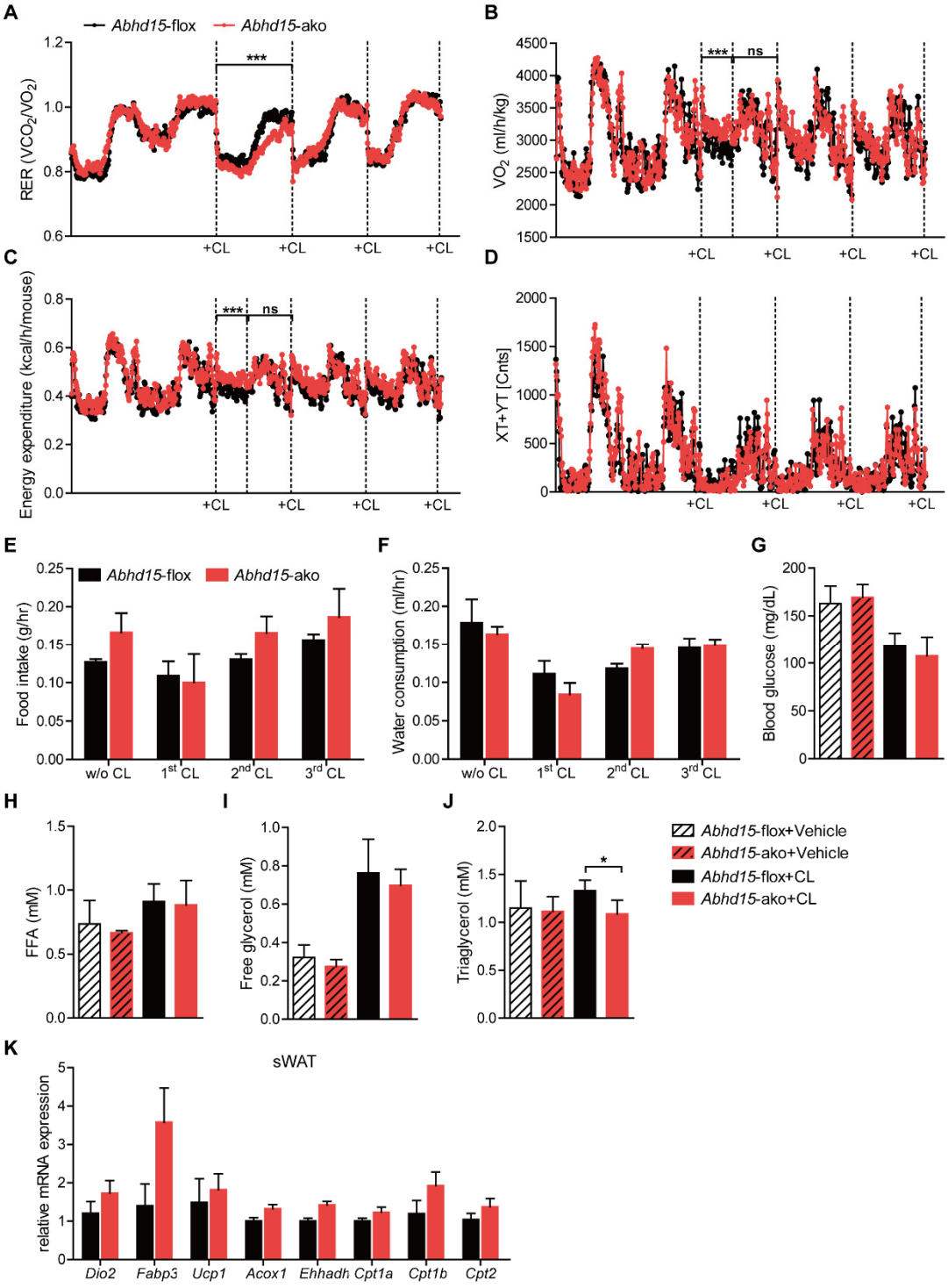

Figure 38. The metabolic parameters of *Abhd15*-ako mice during CL injection. (A-F) RER, O_2 consumption, energy expenditure, locomotor activity, food intake and water consumption of mice before and after CL injection. (G-J) Blood and plasma parameters in mice after 4 times CL injection. (K) Fatty acids oxidation genes expression in sWAT of mice after 4 times CL injection (n = 4-6). * < 0.05, ***< 0.001.

IV. Discussion

4 Discussion

Nature follows a cycle of daily sunrise and sunset which is similar to the circadian rhythm that occurs in almost all species living on earth. In vertebrates, eating, sleeping and movement are tightly controlled by the circadian system. For instance, the alternation of hunger and satiety in homeothermic vertebrates is not continuous over 24 hours, but is instead structured in time along the light and dark cycle. Thus, the dynamic nutritional transitions from feeding to fasting, and fasting to postprandial state are frequently happening in those vertebrates. Those changes are precisely regulated at molecular levels and of great importance for maintaining energy homeostasis.

4.1 The physiological function of ABHD15 in WAT and its contribution to the development of insulin resistance.

The major part of my thesis was to investigate the physiological function of ABHD15 in WAT based on whole body and adipose tissue specific knockout animal models. In those knockout models, we present ABHD15 as a novel and important player in regulating insulin-mediated suppression of lipolysis and the development of insulin resistance.

ABHD15 is one of the members of the ABHD family, which is part of a superfamily of proteins that contains various lipoases, esterases and proteases that share a common α/β-hydrolase fold[65]. The hydrolase activity arises from a catalytic triad build up with a nucleophile (Ser, Cys, or Asp), an acid (aspartate or glutamate), and a conserved histidine residue enabling hydrolase activity. The corresponding motif in most members of the ABHD family is GXSXG[119]. The majority of the ABHD proteins also have a conserved His-X4-Asp motif that has been related with acyltransferase activity[120,121]. However, ABHD15 lacks both of those motifs which makes it less possible to process a hydrolytic activity and difficult to predict its potential enzymatic activity.

ABHD15 has previously been described as a potential player in insulin signaling. In 3T3-L1 adipocytes, ABHD15 has been found as a phosphorylation substrate of Akt, with three indicated insulin-induced phosphorylation sites (T142, S425, S442)[66]. ABHD15 was considered to combine with PDE3B in 3T3L1 adipocytes, and regulates its expression[63]. Although those studies proposed ABHD15 as a substrate of Akt and a protein interacting with PDE3B in adipocytes, *in vivo* studies to confirm those assumptions and further studies on its physiological function were still missing.

Our study revealed that ABHD15 protein is highly enriched in adipose tissues, which are the major energy metabolising organs. Previously, we published that *Abhd15* mRNA expression is reduce in conditions of high circulating FFA levels[64]. In my thesis, we further confirmed that ABHD15 protein is reduced by fasting and induced by refeeding in WAT of lean and healthy mice. In addition, we found that *ABHD15* mRNA level is decreased in WAT of obese and diabetic patients compared to obese humans with normal glucose tolerance. In addition, we further confirmed the *ABHD15* expression is negatively correlated with insulin resistance markers in human. We used constitutive and AT-specific *Abhd15*-ko mouse models to further study the physiological function of ABHD15.

The most important discovery of our study was that loss of *Abhd15* in WAT leads to a failure of insulin to suppress FFA release at experimental (insulin administration) and physiological (oral glucose intake) conditions that is independent of diet and age. The unexpected discrepancy that plasma glycerol levels were unchanged in these mice could be explained by an increased glycerol uptake by the liver for gluconeogenesis. However, evidence to support this assumption needs to be further studied. Our microarray analysis revealed that *Pde3b* is strongly reduced in WAT of *Abhd15*-ko mice, thus, we hypothesized that unsuppressed FFA release by insulin upon *Abhd15* deletion might due a part of to the simultaneous

reduction of PDE3B in WAT. The most convincing evidence to support our hypothesis is a comparable unsuppressed lipolysis in *Pde3b*-null mice[58]. Supportively, we and others also showed an interaction of ABHD15 and PDE3B in adipocytes[63]. We even demonstrate that this interaction was not changed by hormonal stimulation and confirmed it in non-adipocytes[49]. Although the direct interaction evidence is still missing, given the fact that ABHD15 and PDE3B are both enriched in membrane fraction makes their interaction very possible. It has also been suggested that ABHD15 regulates PDE3B expression[63], however the mechanism remains unknown. Indeed, we found that *Abhd15* complete deletion leads to a striking reduction of PDE3B levels in WAT, while partial loss of ABHD15 protein was able to sustain PDE3B level. Of note, when we re-introduced ABHD15 in the knockout adipocytes, PDE3B protein expression was recovered by 50%. Our data indicates that ABHD15 and PDE3B formed a protein complex and ABHD15 seems to be required for the complex stability. In adipocytes, PDE3B has also been shown to form large macro-molecular complexes, so-called "signalosomes"[59,122-124]. Insulin-induced signalosomes included IRS-1, PI3K p85, HSP90, Akt, protein phosphatase 2A (PP2A), 14-3-3, perilipin and caveolin-1[125]. It's previously suggested that uncomplexed PDE3B protein properly has shorter half-life than complexed forms[63]. Thus, we tested whether the interacting partner-ABHD15 is important for PDE3B stability. Supporting this hypothesis, PDE3B protein degradation time is massively delayed when it binds to ABHD15. On the other hand, PDE3B seems to affect ABHD15 stability as well, because ABHD15 protein is reduced when PDE3B is partially knocked down. It would be interesting to know how ABHD15 expression is when PDE3B is completely knocked out. Together, our studies demonstrate that ABHD15 is required for insulin-regulated FFA release via stabilizing PDE3B (fig.39).

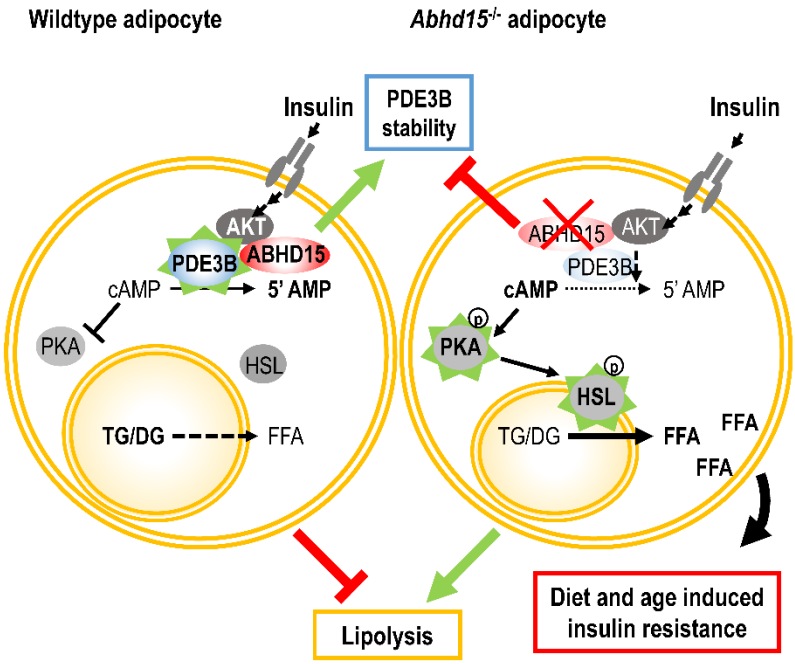

Figure 39. The working model of insulin resistance in *Abhd15*-ko mice[49].

Phosphodiesterases (PDEs) were identified right after the discovery of cAMP[50-52]. PDEs represent a super family of widely expressed hydrolases that regulate the intracellular levels of cyclic nucleotides by hydrolyzing cAMP and cGMP to 5'AMP and 5'GMP, respectively[53]. PDE3B and PDE3A have been described as two isoforms of the PDE3 subfamily due to their structural similarity. These two isoforms are highly conserved within the catalytic domains in the C-terminal region, while the N-terminal domains are very divergent, which leads to their different localization[57]. The structural homology would possibly make a compensatory rise by PDE3A when PDE3B is knocked out or down, however, we do not find an increased *Pde3a* expression although PDE3B content is massively reduced in *Abhd15*-ko mice. The failure of anti-lipolytic action by insulin in *Pde3b*-null mice directly demonstrate that PDE3B is the key node of insulin-suppressed lipolysis pathway[58]. Our study further support this generally accepted dogma that *Abhd15* deletion in AT leads to reduced PDE3B content, thus insulin fails to inhibit lipolysis. Although we did not study whether ABHD15 also affect the

phosphorylation of PDE3B, the other group's study showed that Akt and PKA phosphorylation sites in PDE3B seem to be dispensable for insulin's anti-lipolytic action[60].

Catecholamines are the main activators of fasting-activated lipolysis. The released catecholamine, such as norepinephrine, binds to and activates β_3-AR, the primary adrenergic receptor in adipocytes, on the plasma membrane. The activated β_3-AR releases its G-protein subunits that transmit a stimulatory signal to adenylyl cyclase to generate cAMP. It is unclear why there is no defect on fasting FFA levels in *Abhd15* deleted mice, however the fasted cAMP levels were unchanged as well. Although we also didn't detect differences of cAMP levels in *Abhd15*-ko mice upon injection of insulin, the PKA activity was highly enhanced. PKA has two lipolytic targets in adipocytes, HSL and perilipin A. HSL is the only known neutral lipid lipase regulated by PKA-mediated phosphorylation. It is well investigated that PKA phosphorylates HSL at Ser660 leading to its translocation from the cytosol to the lipid droplet surface where it hydrolyses DAG (and to a lesser extent also TAG). In line with increased PKA activity, the phosphorylation of HSL at Ser660 was increased and in turn explained the increased FFA release in *Abhd15*-ko mice under the conditions of insulin injection. In our *ex vivo* study, we applied small molecular inhibitor of HSL (iHSL) and ATGL (iATGL), separately. This HSL inhibitor is considered to work as a pseudosubstrate inhibitor which competitively occupies HSL instead its substrate[126]. We found that iHSL can further inhibit FFA release in both WT and *Abhd15*-ko fat pads when treated with insulin, however, there is no difference between WT and *Abhd15*-ko with HSL and ATGL inhibitors. This result suggests that *Abhd15* deletion do not affect HSL and ATGL lipase activity, while it more likely regulates the phosphorylation of HSL. HSL can be phosphorylated by PKA and dephosphorylated by protein phosphatases. In adipocytes, protein phosphatase 2A (PP2A) is mainly responsible for dephosphorylating HSL[127], thus the increased HSL phosphorylation might also due to the decreased

PP2A activity in *Abhd*15-ko adipocytes. It would be interesting for future study that to check the PP2A activity and supply a PP2A agonist (if available) to rescue the unsuppressed HSL phosphorylation in *Abhd15*-ko WAT. It's discussed that insulin can reduce lipolysis via a cAMP-independent mechanism whereby insulin reduces *Atgl* mRNA expression[34,128], however, another review pointed out that mRNA expression is not an appropriate indicator for ATGL's lipase activity[129]. Despite the debating of this cAMP-independent mechanism, we didn't find changes on ATGL activity or its expression in *Abhd15*-ko mice.

The inability to respond to normal circulating levels of insulin called insulin resistance which will develop into type 2 diabetes[130,131]. Insulin serves as an important physiological anabolic hormone, inhibiting the energy release (e.g. lipolysis) and promoting the energy storage (e.g. glucose uptake and lipogenesis)[132]. It's worth mentioning that not only FFA release is disrupted, we also found that glucose uptake and lipogenesis were impacted in WAT of *Abhd15*-ko mice. Glucose metabolism in WAT is largely dependent on Akt activation by insulin[101]. Akt promotes the translocation of glucose transporter 4 (Glut4) to plasma membrane, thus the uptake of glucose into AT. The accumulation of glucose inside the cells will be oxidized and its metabolites will be used for DNL. Intriguingly, in WAT of *Abhd15*-ko mice, the activation of Akt by insulin is reduced and thus might be responsible for the reduced glucose uptake and DNL. Adipose tissue DNL was mainly considered to store excess energy in form of lipids, which are more energy-dense than carbohydrates, thus representing an efficient form of energy storage. While increased DNL in the liver often correlates with insulin resistance[133,134], increased DNL in AT is associated with insulin sensitivity[42,135-137]. Moreover, emerging evidence suggests that WAT DNL is reduced in obese mice and humans[43,44,138,139], whereas increased DNL in WAT showed favorable metabolic effects in mice[140,141]. Considering the massive quantities of lipids stored in adipocytes, DNL is unlikely to contribute significantly to the lipid

composition of WAT, but may play an important regulatory role, perhaps generating a specific signaling lipid(s) or other factors that improve insulin sensitivity and reduce inflammation in other fat depots, liver or skeletal muscle[136,137,142].

Together with the dysregulated lipid and glucose metabolism pathways in *Abhd15*-ko mice eventually displayed impaired insulin sensitivity and glucose tolerance. Unrestrained circulating FFA levels and dysregulated glucose metabolism are the causes for insulin resistance in both animals and humans[143-147]. Recently, it has been reported that the failure of insulin to cut off the supply of FFAs as substrate for liver gluconeogenesis leads to systemic insulin resistance[96]. Reduced adiponectin levels are an early indicator for insulin resistance[102,104], and *Adipq* knockout mice developed severe insulin resistance[148] and supplement of adiponectin enhance insulin sensitivity[149]. Decreased adiponectin levels in *Abhd15*-ko mice might further support the development of insulin resistance. PDE3B has been suggested to play a role in the secretion of adiponectin in adipocytes by an uncertain mechanism[150]. The level of *PDE3B* is reduced in adipocytes of diabetic patients[151], and *Pde3b*-null mice developed insulin resistance[58]. However, these mice have elevated plasma adiponectin levels. Moreover, in our *Abhd15*-ko mice, both PDE3B and plasma adiponectin levels were reduced. The discrepancy among different model imply that a directly role of PDE3B in regulating adiponectin production unlikely. Many factors has been connected with adiponectin secretion[152-155], nevertheless, the mechanism by which lower adiponectin level in insulin resistance objects yet to be elucidated[156]. In our case, it might be true that reduced adiponectin in *Abhd15*-ko mice is caused by insulin resistance.

Although many proteins involved in insulin signalling have been identified, the detailed molecular mechanisms how insulin suppresses lipolysis in adipocytes is still elusive. Our studies demonstrate that AT ABHD15 is required for insulin-mediated suppression of lipolysis and its ablation in AT

contributes to the development of insulin resistance in mice. These findings, supported by the reduced *ABHD15* level in obese and diabetic patients, identify ABHD15 as a promising therapeutic target for treating age- and obesity-associated insulin resistance.

4.2 The potential role of ABHD15 in brown/beige adipocytes.

Recently, BAT became an attractive target for treating obesity and type 2 diabetes because of its high energy expenditure capability[157]. Our published data revealed a physiological function of ABHD15 in WAT[49]. ABHD15 is expressed the highest in human and murine BAT[49,65], while the impact of ABHD15 on BAT function is not yet known. Our unpublished data also suggest that ABHD15 expression is increasing during brown/beige adipocytes differentiation. Therefore, we have designed preliminary experiments to explore the function of ABHD15 in brown/beige adipocytes. The *Abhd15*-ako and *Abhd15*-bko mice were both tolerant to cold exposure and didn't differ from control mice with acute and short-term cold stimulation. During acute and short-term cold exposure, heat production mainly comes from muscle shivering[158], this might explain no defects in *Abhd15*-ako and control mice in this condition. After a prolonged cold exposure, the sWAT of *Abhd15*-ako mice showed increased O_2 consumption and genes related with fatty acid oxidation. These results suggest that upon cold exposure *Abhd15* deleted adipocytes have higher oxidation capacity than control mice. Also, the acute increase of O_2 consumption and energy expenditure by CL treatment might also due to increased FAO in *Abhd15*-ako mice. Interestingly, with the prolonged treatment of CL, we didn’t observe differences any longer. Given the fact that catecholamine resistance in obese[159-162] might due to the PDE3B activation by inflammation[163], we assumed that *Abhd15*-ako mice, which had reduced PDE3B level[49], might be more catecholamine sensitive than control mice. However with prolonged CL treatment, control mice catched up the defect and compensated the difference.

In summary, these *in vivo* preliminary data strongly suggest that in BAT

ABDH15 might play a different role from WAT. The mechanism whereby *Abhd15* deficiency promotes AT FAO is elusive, thus further study are important to confirm the changes at molecular levels.

V. Figure Legend

5 Figure Legends

VI. Reference

6 References

1 Kahn, S. E., Hull, R. L. & Utzschneider, K. M. Mechanisms linking obesity to insulin resistance and type 2 diabetes. *Nature* **444**, 840-846, doi:10.1038/nature05482 (2006).

2 Boden, G. Obesity, insulin resistance and free fatty acids. *Current opinion in endocrinology, diabetes, and obesity* **18**, 139-143, doi:10.1097/MED.0b013e3283444b09 (2011).

3 Peirce, V., Carobbio, S. & Vidal-Puig, A. The different shades of fat. *Nature* **510**, 76-83, doi:10.1038/nature13477 (2014).

4 Galic, S., Oakhill, J. S. & Steinberg, G. R. Adipose tissue as an endocrine organ. *Molecular and cellular endocrinology* **316**, 129-139, doi:10.1016/j.mce.2009.08.018 (2010).

5 Reddy, N. L., Tan, B. K., Barber, T. M. & Randeva, H. S. Brown adipose tissue: endocrine determinants of function and therapeutic manipulation as a novel treatment strategy for obesity. *BMC obesity* **1**, 13, doi:10.1186/s40608-014-0013-5 (2014).

6 Villarroya, J., Cereijo, R. & Villarroya, F. An endocrine role for brown adipose tissue? *American journal of physiology. Endocrinology and metabolism* **305**, E567-572, doi:10.1152/ajpendo.00250.2013 (2013).

7 Armani, A. *et al.* Cellular models for understanding adipogenesis, adipose dysfunction, and obesity. *Journal of cellular biochemistry* **110**, 564-572, doi:10.1002/jcb.22598 (2010).

8 Enerback, S. Human brown adipose tissue. *Cell metabolism* **11**, 248-252, doi:10.1016/j.cmet.2010.03.008 (2010).

9 Cannon, B. & Nedergaard, J. Brown adipose tissue: function and physiological significance. *Physiological reviews* **84**, 277-359, doi:10.1152/physrev.00015.2003 (2004).

10 Rousset, S. *et al.* The biology of mitochondrial uncoupling proteins. *Diabetes* **53 Suppl 1**, S130-135 (2004).

11 Brown, G. C. Control of respiration and ATP synthesis in mammalian mitochondria and cells. *The Biochemical journal* **284 (Pt 1)**, 1-13 (1992).

12 Klingenspor, M., Herzig, S. & Pfeifer, A. Brown fat develops a brite future. *Obesity facts* **5**, 890-896, doi:10.1159/000346337 (2012).

13 Bartelt, A. & Heeren, J. Adipose tissue browning and metabolic health. *Nature reviews. Endocrinology* **10**, 24-36, doi:10.1038/nrendo.2013.204 (2014).

14 Ouellet, V. *et al.* Brown adipose tissue oxidative metabolism contributes to energy expenditure during acute cold exposure in humans. *The Journal of clinical investigation* **122**, 545-552, doi:10.1172/JCI60433 (2012).

15 Saito, M. *et al.* High incidence of metabolically active brown adipose tissue in healthy adult humans: effects of cold exposure and adiposity. *Diabetes* **58**, 1526-1531, doi:10.2337/db09-0530 (2009).

16 Yoneshiro, T. *et al.* Brown adipose tissue, whole-body energy expenditure, and thermogenesis in healthy adult men. *Obesity* **19**, 13-16, doi:10.1038/oby.2010.105 (2011).

17 van Marken Lichtenbelt, W. D. *et al.* Cold-activated brown adipose tissue in healthy men. *The New England journal of medicine* **360**, 1500-1508,

doi:10.1056/NEJMoa0808718 (2009).

18 Virtanen, K. A. *et al.* Functional brown adipose tissue in healthy adults. *The New England journal of medicine* **360**, 1518-1525, doi:10.1056/NEJMoa0808949 (2009).

19 Ouellet, V. *et al.* Outdoor temperature, age, sex, body mass index, and diabetic status determine the prevalence, mass, and glucose-uptake activity of 18F-FDG-detected BAT in humans. *The Journal of clinical endocrinology and metabolism* **96**, 192-199, doi:10.1210/jc.2010-0989 (2011).

20 Nedergaard, J., Bengtsson, T. & Cannon, B. Unexpected evidence for active brown adipose tissue in adult humans. *American journal of physiology. Endocrinology and metabolism* **293**, E444-452, doi:10.1152/ajpendo.00691.2006 (2007).

21 Cypess, A. M. *et al.* Identification and importance of brown adipose tissue in adult humans. *The New England journal of medicine* **360**, 1509-1517, doi:10.1056/NEJMoa0810780 (2009).

22 Zingaretti, M. C. *et al.* The presence of UCP1 demonstrates that metabolically active adipose tissue in the neck of adult humans truly represents brown adipose tissue. *FASEB journal : official publication of the Federation of American Societies for Experimental Biology* **23**, 3113-3120, doi:10.1096/fj.09-133546 (2009).

23 Pfannenberg, C. *et al.* Impact of age on the relationships of brown adipose tissue with sex and adiposity in humans. *Diabetes* **59**, 1789-1793, doi:10.2337/db10-0004 (2010).

24 Ukropec, J., Anunciado, R. P., Ravussin, Y., Hulver, M. W. & Kozak, L. P. UCP1-independent thermogenesis in white adipose tissue of cold-acclimated Ucp1-/- mice. *The Journal of biological chemistry* **281**, 31894-31908, doi:10.1074/jbc.M606114200 (2006).

25 Granneman, J. G., Burnazi, M., Zhu, Z. & Schwamb, L. A. White adipose tissue contributes to UCP1-independent thermogenesis. *American journal of physiology. Endocrinology and metabolism* **285**, E1230-1236, doi:10.1152/ajpendo.00197.2003 (2003).

26 Kazak, L. *et al.* A creatine-driven substrate cycle enhances energy expenditure and thermogenesis in beige fat. *Cell* **163**, 643-655, doi:10.1016/j.cell.2015.09.035 (2015).

27 Ikeda, K. *et al.* UCP1-independent signaling involving SERCA2b-mediated calcium cycling regulates beige fat thermogenesis and systemic glucose homeostasis. *Nature medicine* **23**, 1454-1465, doi:10.1038/nm.4429 (2017).

28 Luo, L. & Liu, M. Adipose tissue in control of metabolism. *The Journal of endocrinology* **231**, R77-R99, doi:10.1530/JOE-16-0211 (2016).

29 Zimmermann, R. *et al.* Fat mobilization in adipose tissue is promoted by adipose triglyceride lipase. *Science* **306**, 1383-1386 (2004).

30 Zechner, R., Strauss, J. G., Haemmerle, G., Lass, A. & Zimmermann, R. Lipolysis: pathway under construction. *Current opinion in lipidology* **16**, 333-340 (2005).

31 Carmen, G. Y. & Victor, S. M. Signalling mechanisms regulating lipolysis. *Cellular signalling* **18**, 401-408, doi:10.1016/j.cellsig.2005.08.009 (2006).

32 Langin, D. Adipose tissue lipolysis as a metabolic pathway to define pharmacological strategies against obesity and the metabolic syndrome.

Pharmacological research **53**, 482-491, doi:10.1016/j.phrs.2006.03.009 (2006).

33 Kuriyama, H. *et al.* Coordinated regulation of fat-specific and liver-specific glycerol channels, aquaporin adipose and aquaporin 9. *Diabetes* **51**, 2915-2921 (2002).

34 Duncan, R. E., Ahmadian, M., Jaworski, K., Sarkadi-Nagy, E. & Sul, H. S. Regulation of lipolysis in adipocytes. *Annual review of nutrition* **27**, 79-101, doi:10.1146/annurev.nutr.27.061406.093734 (2007).

35 Zimmermann, R. *et al.* Fat mobilization in adipose tissue is promoted by adipose triglyceride lipase. *Science* **306**, 1383-1386, doi:10.1126/science.1100747 (2004).

36 Haemmerle, G. *et al.* Hormone-sensitive lipase deficiency in mice causes diglyceride accumulation in adipose tissue, muscle, and testis. *The Journal of biological chemistry* **277**, 4806-4815, doi:10.1074/jbc.M110355200 (2002).

37 Marcinkiewicz, A., Gauthier, D., Garcia, A. & Brasaemle, D. L. The phosphorylation of serine 492 of perilipin a directs lipid droplet fragmentation and dispersion. *The Journal of biological chemistry* **281**, 11901-11909, doi:10.1074/jbc.M600171200 (2006).

38 Brasaemle, D. L. Thematic review series: adipocyte biology. The perilipin family of structural lipid droplet proteins: stabilization of lipid droplets and control of lipolysis. *Journal of lipid research* **48**, 2547-2559, doi:10.1194/jlr.R700014-JLR200 (2007).

39 Karlsson, M., Contreras, J. A., Hellman, U., Tornqvist, H. & Holm, C. cDNA cloning, tissue distribution, and identification of the catalytic triad of monoglyceride lipase. Evolutionary relationship to esterases, lysophospholipases, and haloperoxidases. *The Journal of biological chemistry* **272**, 27218-27223 (1997).

40 Kim, J. B. *et al.* Nutritional and insulin regulation of fatty acid synthetase and leptin gene expression through ADD1/SREBP1. *The Journal of clinical investigation* **101**, 1-9, doi:10.1172/JCI1411 (1998).

41 Nadeau, K. J., Leitner, J. W., Gurerich, I. & Draznin, B. Insulin regulation of sterol regulatory element-binding protein-1 expression in L-6 muscle cells and 3T3 L1 adipocytes. *The Journal of biological chemistry* **279**, 34380-34387, doi:10.1074/jbc.M403596200 (2004).

42 Herman, M. A. *et al.* A novel ChREBP isoform in adipose tissue regulates systemic glucose metabolism. *Nature* **484**, 333-338, doi:10.1038/nature10986 (2012).

43 Kursawe, R. *et al.* Decreased transcription of ChREBP-alpha/beta isoforms in abdominal subcutaneous adipose tissue of obese adolescents with prediabetes or early type 2 diabetes: associations with insulin resistance and hyperglycemia. *Diabetes* **62**, 837-844, doi:10.2337/db12-0889 (2013).

44 Eissing, L. *et al.* De novo lipogenesis in human fat and liver is linked to ChREBP-beta and metabolic health. *Nature communications* **4**, 1528, doi:10.1038/ncomms2537 (2013).

45 Swierczynski, J. *et al.* Comparative study of the lipogenic potential of human and rat adipose tissue. *Metabolism: clinical and experimental* **49**, 594-599 (2000).

46 Letexier, D., Pinteur, C., Large, V., Frering, V. & Beylot, M. Comparison of the expression and activity of the lipogenic pathway in human and rat adipose tissue. *Journal of lipid research* **44**, 2127-2134, doi:10.1194/jlr.M300235-JLR200 (2003).

47 Golay, A. *et al.* Glucose-induced thermogenesis in nondiabetic and diabetic obese subjects. *Diabetes* **31**, 1023-1028 (1982).

48 Vallerand, A. L., Lupien, J. & Bukowiecki, L. J. Cold exposure reverses the diabetogenic effects of high-fat feeding. *Diabetes* **35**, 329-334 (1986).

49 Xia, W. *et al.* Loss of ABHD15 Impairs the Anti-lipolytic Action of Insulin by Altering PDE3B Stability and Contributes to Insulin Resistance. *Cell Rep* **23**, 1948-1961, doi:10.1016/j.celrep.2018.04.055 (2018).

50 Ashman, D. F., Lipton, R., Melicow, M. M. & Price, T. D. Isolation of adenosine 3', 5'-monophosphate and guanosine 3', 5'-monophosphate from rat urine. *Biochemical and biophysical research communications* **11**, 330-334 (1963).

51 Butcher, R. W. & Sutherland, E. W. Adenosine 3',5'-phosphate in biological materials. I. Purification and properties of cyclic 3',5'-nucleotide phosphodiesterase and use of this enzyme to characterize adenosine 3',5'-phosphate in human urine. *The Journal of biological chemistry* **237**, 1244-1250 (1962).

52 Sutherland, E. W. & Rall, T. W. Fractionation and characterization of a cyclic adenine ribonucleotide formed by tissue particles. *The Journal of biological chemistry* **232**, 1077-1091 (1958).

53 Azevedo, M. F. *et al.* Clinical and molecular genetics of the phosphodiesterases (PDEs). *Endocrine reviews* **35**, 195-233, doi:10.1210/er.2013-1053 (2014).

54 Bender, A. T. & Beavo, J. A. Cyclic nucleotide phosphodiesterases: molecular regulation to clinical use. *Pharmacological reviews* **58**, 488-520, doi:10.1124/pr.58.3.5 (2006).

55 Keravis, T. & Lugnier, C. Cyclic nucleotide phosphodiesterases (PDE) and peptide motifs. *Current pharmaceutical design* **16**, 1114-1125 (2010).

56 Omori, K. & Kotera, J. Overview of PDEs and their regulation. *Circulation research* **100**, 309-327, doi:10.1161/01.RES.0000256354.95791.f1 (2007).

57 Degerman, E., Belfrage, P. & Manganiello, V. C. Structure, localization, and regulation of cGMP-inhibited phosphodiesterase (PDE3). *The Journal of biological chemistry* **272**, 6823-6826 (1997).

58 Choi, Y. H. *et al.* Alterations in regulation of energy homeostasis in cyclic nucleotide phosphodiesterase 3B-null mice. *The Journal of clinical investigation* **116**, 3240-3251, doi:10.1172/jci24867 (2006).

59 Rondinone, C. M. *et al.* Phosphorylation of PDE3B by phosphatidylinositol 3-kinase associated with the insulin receptor. *Journal of Biological Chemistry* **275**, 10093-10098 (2000).

60 DiPilato, L. M. *et al.* The Role of PDE3B Phosphorylation in the Inhibition of Lipolysis by Insulin. *Molecular and cellular biology* **35**, 2752-2760, doi:10.1128/MCB.00422-15 (2015).

61 Prokesch, A. *et al.* Arxes: retrotransposed genes required for adipogenesis. *Nucleic acids research* **39**, 3224-3239, doi:10.1093/nar/gkq1289 (2011).

62 Bogner-Strauss, J. G. *et al.* Reconstruction of gene association network reveals

a transmembrane protein required for adipogenesis and targeted by PPARgamma. *Cellular and molecular life sciences : CMLS* **67**, 4049-4064, doi:10.1007/s00018-010-0424-5 (2010).

63 Chavez, J. A., Gridley, S., Sano, H., Lane, W. S. & Lienhard, G. E. The 47kDa Akt substrate associates with phosphodiesterase 3B and regulates its level in adipocytes. *Biochemical and biophysical research communications* **342**, 1218-1222, doi:10.1016/j.bbrc.2006.02.091 (2006).

64 Walenta, E. *et al.* alpha/beta-hydrolase domain containing protein 15 (ABHD15)--an adipogenic protein protecting from apoptosis. *PloS one* **8**, e79134, doi:10.1371/journal.pone.0079134 (2013).

65 Lord, C. C., Thomas, G. & Brown, J. M. Mammalian alpha beta hydrolase domain (ABHD) proteins: Lipid metabolizing enzymes at the interface of cell signaling and energy metabolism. *Biochimica et biophysica acta* **1831**, 792-802, doi:10.1016/j.bbalip.2013.01.002 (2013).

66 Gridley, S., Lane, W. S., Garner, C. W. & Lienhard, G. E. Novel insulin-elicited phosphoproteins in adipocytes. *Cellular signalling* **17**, 59-66, doi:10.1016/j.cellsig.2004.05.013 (2005).

67 Aune, U. L., Ruiz, L. & Kajimura, S. Isolation and differentiation of stromal vascular cells to beige/brite cells. *JoVE (Journal of Visualized Experiments)*, e50191-e50191 (2013).

68 Itariu, B. K. *et al.* Long-chain n-3 PUFAs reduce adipose tissue and systemic inflammation in severely obese nondiabetic patients: a randomized controlled trial. *The American journal of clinical nutrition* **96**, 1137-1149, doi:10.3945/ajcn.112.037432 (2012).

69 Mari, A., Pacini, G., Murphy, E., Ludvik, B. & Nolan, J. J. A model-based method for assessing insulin sensitivity from the oral glucose tolerance test. *Diabetes care* **24**, 539-548 (2001).

70 Matsuda, M. & DeFronzo, R. A. Insulin sensitivity indices obtained from oral glucose tolerance testing: comparison with the euglycemic insulin clamp. *Diabetes care* **22**, 1462-1470 (1999).

71 Anderwald, C. *et al.* The Clamp-Like Index: a novel and highly sensitive insulin sensitivity index to calculate hyperinsulinemic clamp glucose infusion rates from oral glucose tolerance tests in nondiabetic subjects. *Diabetes care* **30**, 2374-2380, doi:10.2337/dc07-0422 (2007).

72 Matthews, D. R. *et al.* Homeostasis model assessment: insulin resistance and beta-cell function from fasting plasma glucose and insulin concentrations in man. *Diabetologia* **28**, 412-419 (1985).

73 Su, H., Mills, A. A., Wang, X. & Bradley, A. A targeted X‐linked CMV‐Cre line. *Genesis* **32**, 187-188 (2002).

74 Eguchi, J. *et al.* Transcriptional control of adipose lipid handling by IRF4. *Cell metabolism* **13**, 249-259, doi:10.1016/j.cmet.2011.02.005 (2011).

75 Rosenwald, M., Perdikari, A., Rulicke, T. & Wolfrum, C. Bi-directional interconversion of brite and white adipocytes. *Nature cell biology* **15**, 659-667, doi:10.1038/ncb2740 (2013).

76 Huang, D. W., Sherman, B. T. & Lempicki, R. A. Systematic and integrative analysis of large gene lists using DAVID bioinformatics resources. *Nature protocols* **4**, 44-57 (2009).

77 Sturn, A., Quackenbush, J. & Trajanoski, Z. Genesis: cluster analysis of microarray data. *Bioinformatics* **18**, 207-208 (2002).

78 Davis, S. & Meltzer, P. S. GEOquery: a bridge between the Gene Expression Omnibus (GEO) and BioConductor. *Bioinformatics* **23**, 1846-1847 (2007).

79 Livak, K. J. & Schmittgen, T. D. Analysis of relative gene expression data using real-time quantitative PCR and the 2− ΔΔCT method. *methods* **25**, 402-408 (2001).

80 Schweiger, M. *et al.* Measurement of lipolysis. *Methods in enzymology* **538**, 171 (2014).

81 Schweiger, M. *et al.* Pharmacological inhibition of adipose triglyceride lipase corrects high-fat diet-induced insulin resistance and hepatosteatosis in mice. *Nature communications* **8**, 14859, doi:10.1038/ncomms14859 (2017).

82 Galarraga, M. *et al.* Adiposoft: automated software for the analysis of white adipose tissue cellularity in histological sections. *Journal of lipid research* **53**, 2791-2796, doi:10.1194/jlr.D023788 (2012).

83 Schreiber, R. *et al.* Hypophagia and metabolic adaptations in mice with defective ATGL-mediated lipolysis cause resistance to HFD-induced obesity. *Proceedings of the National Academy of Sciences* **112**, 13850-13855 (2015).

84 Pessentheiner, A. R. *et al.* NAT8L (N-acetyltransferase 8-like) accelerates lipid turnover and increases energy expenditure in brown adipocytes. *The Journal of biological chemistry* **288**, 36040-36051, doi:10.1074/jbc.M113.491324 (2013).

85 Folch, J., Lees, M. & Sloane-Stanley, G. A simple method for the isolation and purification of total lipids from animal tissues. *The Journal of biological chemistry* **226**, 497-509 (1957).

86 Knittelfelder, O. L., Weberhofer, B. P., Eichmann, T. O., Kohlwein, S. D. & Rechberger, G. N. A versatile ultra-high performance LC-MS method for lipid profiling. *Journal of Chromatography B* **951**, 119-128 (2014).

87 Elia, M. & Livesey, G. in *Metabolic Control of Eating, Energy Expenditure and the Bioenergetics of Obesity* 68-131 (Karger Publishers, 1992).

88 Ruiz-Ojeda, F. J., Ruperez, A. I., Gomez-Llorente, C., Gil, A. & Aguilera, C. M. Cell Models and Their Application for Studying Adipogenic Differentiation in Relation to Obesity: A Review. *International journal of molecular sciences* **17**, doi:10.3390/ijms17071040 (2016).

89 Wolins, N. E. *et al.* OP9 mouse stromal cells rapidly differentiate into adipocytes: characterization of a useful new model of adipogenesis. *Journal of lipid research* **47**, 450-460, doi:10.1194/jlr.D500037-JLR200 (2006).

90 Liang, G. *et al.* Diminished hepatic response to fasting/refeeding and liver X receptor agonists in mice with selective deficiency of sterol regulatory element-binding protein-1c. *Journal of Biological Chemistry* **277**, 9520-9528 (2002).

91 Zmuda-Trzebiatowska, E., Oknianska, A., Manganiello, V. & Degerman, E. Role of PDE3B in insulin-induced glucose uptake, GLUT-4 translocation and lipogenesis in primary rat adipocytes. *Cellular signalling* **18**, 382-390 (2006).

92 Holm, C. Molecular mechanisms regulating hormone-sensitive lipase and lipolysis. *Biochemical Society transactions* **31**, 1120-1124, doi:10.1042/ (2003).

93 Watt, M. J. *et al.* Regulation of HSL serine phosphorylation in skeletal muscle and adipose tissue. *American journal of physiology. Endocrinology and metabolism* **290**, E500-508, doi:10.1152/ajpendo.00361.2005 (2006).

94 Anthonsen, M. W., Ronnstrand, L., Wernstedt, C., Degerman, E. & Holm, C. Identification of novel phosphorylation sites in hormone-sensitive lipase that are phosphorylated in response to isoproterenol and govern activation properties in vitro. *The Journal of biological chemistry* **273**, 215-221 (1998).

95 Chitraju, C. *et al.* Triglyceride Synthesis by DGAT1 Protects Adipocytes from Lipid-Induced ER Stress during Lipolysis. *Cell metabolism* **26**, 407-418 e403, doi:10.1016/j.cmet.2017.07.012 (2017).

96 Perry, R. J. *et al.* Hepatic acetyl CoA links adipose tissue inflammation to hepatic insulin resistance and type 2 diabetes. *Cell* **160**, 745-758 (2015).

97 Samuel, V. T. & Shulman, G. I. Mechanisms for insulin resistance: common threads and missing links. *Cell* **148**, 852-871, doi:10.1016/j.cell.2012.02.017 (2012).

98 Saltiel, A. R. & Kahn, C. R. Insulin signalling and the regulation of glucose and lipid metabolism. *Nature* **414**, 799-806 (2001).

99 Kahn, B. B. & Flier, J. S. Obesity and insulin resistance. *The Journal of clinical investigation* **106**, 473-481, doi:10.1172/JCI10842 (2000).

100 Brewer, P. D., Habtemichael, E. N., Romenskaia, I., Mastick, C. C. & Coster, A. C. Insulin-regulated Glut4 translocation: membrane protein trafficking with six distinctive steps. *The Journal of biological chemistry* **289**, 17280-17298, doi:10.1074/jbc.M114.555714 (2014).

101 Kohn, A. D., Summers, S. A., Birnbaum, M. J. & Roth, R. A. Expression of a constitutively active Akt Ser/Thr kinase in 3T3-L1 adipocytes stimulates glucose uptake and glucose transporter 4 translocation. *Journal of Biological Chemistry* **271**, 31372-31378 (1996).

102 Cnop, M. *et al.* Relationship of adiponectin to body fat distribution, insulin sensitivity and plasma lipoproteins: evidence for independent roles of age and sex. *Diabetologia* **46**, 459-469, doi:10.1007/s00125-003-1074-z (2003).

103 Kadowaki, T. *et al.* Adiponectin and adiponectin receptors in insulin resistance, diabetes, and the metabolic syndrome. *The Journal of clinical investigation* **116**, 1784-1792, doi:10.1172/jci29126 (2006).

104 Hotta, K. *et al.* Circulating concentrations of the adipocyte protein adiponectin are decreased in parallel with reduced insulin sensitivity during the progression to type 2 diabetes in rhesus monkeys. *Diabetes* **50**, 1126-1133 (2001).

105 Wang, C. Y. & Liao, J. K. A mouse model of diet-induced obesity and insulin resistance. *Methods in molecular biology* **821**, 421-433, doi:10.1007/978-1-61779-430-8_27 (2012).

106 Surwit, R. S., Kuhn, C. M., Cochrane, C., McCubbin, J. A. & Feinglos, M. N. Diet-induced type II diabetes in C57BL/6J mice. *Diabetes* **37**, 1163-1167 (1988).

107 Oka, Y., Akanuma, Y., Kasuga, M. & Kosaka, K. Effect of a high glucose diet on insulin binding and insulin action in rat adipocytes. A longitudinal study. *Diabetologia* **19**, 468-474 (1980).

108 van der Lans, A. A. *et al.* Cold acclimation recruits human brown fat and

increases nonshivering thermogenesis. *The Journal of clinical investigation* **123**, 3395-3403, doi:10.1172/JCI68993 (2013).

109 Cypess, A. M. *et al.* Activation of human brown adipose tissue by a beta3-adrenergic receptor agonist. *Cell metabolism* **21**, 33-38, doi:10.1016/j.cmet.2014.12.009 (2015).

110 Vitali, A. *et al.* The adipose organ of obesity-prone C57BL/6J mice is composed of mixed white and brown adipocytes. *Journal of lipid research* **53**, 619-629, doi:10.1194/jlr.M018846 (2012).

111 Chung, Y. W. *et al.* White to beige conversion in PDE3B KO adipose tissue through activation of AMPK signaling and mitochondrial function. *Scientific reports* **7**, 40445, doi:10.1038/srep40445 (2017).

112 Nedergaard, J. & Cannon, B. The browning of white adipose tissue: some burning issues. *Cell metabolism* **20**, 396-407, doi:10.1016/j.cmet.2014.07.005 (2014).

113 Morrison, S. F., Madden, C. J. & Tupone, D. Central control of brown adipose tissue thermogenesis. *Frontiers in endocrinology* **3**, doi:10.3389/fendo.2012.00005 (2012).

114 Lee, Y. H., Petkova, A. P., Mottillo, E. P. & Granneman, J. G. In vivo identification of bipotential adipocyte progenitors recruited by beta3-adrenoceptor activation and high-fat feeding. *Cell metabolism* **15**, 480-491, doi:10.1016/j.cmet.2012.03.009 (2012).

115 Vergnes, L., Chin, R., Young, S. G. & Reue, K. Heart-type fatty acid-binding protein is essential for efficient brown adipose tissue fatty acid oxidation and cold tolerance. *The Journal of biological chemistry* **286**, 380-390, doi:10.1074/jbc.M110.184754 (2011).

116 Himms-Hagen, J. *et al.* Multilocular fat cells in WAT of CL-316243-treated rats derive directly from white adipocytes. *American journal of physiology. Cell physiology* **279**, C670-681, doi:10.1152/ajpcell.2000.279.3.C670 (2000).

117 Bauters, D. *et al.* Loss of ADAMTS5 enhances brown adipose tissue mass and promotes browning of white adipose tissue via CREB signaling. *Molecular metabolism* **6**, 715-724, doi:10.1016/j.molmet.2017.05.004 (2017).

118 Bartelt, A. *et al.* Brown adipose tissue activity controls triglyceride clearance. *Nature medicine* **17**, 200-205 (2011).

119 Nardini, M. & Dijkstra, B. W. Alpha/beta hydrolase fold enzymes: the family keeps growing. *Current opinion in structural biology* **9**, 732-737 (1999).

120 Ghosh, A. K., Ramakrishnan, G., Chandramohan, C. & Rajasekharan, R. CGI-58, the causative gene for Chanarin-Dorfman syndrome, mediates acylation of lysophosphatidic acid. *The Journal of biological chemistry* **283**, 24525-24533, doi:10.1074/jbc.M801783200 (2008).

121 Montero-Moran, G. *et al.* CGI-58/ABHD5 is a coenzyme A-dependent lysophosphatidic acid acyltransferase. *Journal of lipid research* **51**, 709-719, doi:10.1194/jlr.M001917 (2010).

122 Ahmad, F. *et al.* Insulin-induced formation of macromolecular complexes involved in activation of cyclic nucleotide phosphodiesterase 3B (PDE3B) and its interaction with PKB. *Biochemical Journal* **404**, 257-268 (2007).

123 Kitamura, T. *et al.* Insulin-induced phosphorylation and activation of cyclic nucleotide phosphodiesterase 3B by the serine-threonine kinase Akt.

Molecular and cellular biology **19**, 6286-6296 (1999).

124 Ahmad, F., Degerman, E. & Manganiello, V. Cyclic nucleotide phosphodiesterase 3 signaling complexes. *Hormone and metabolic research* **44**, 776-785 (2012).

125 Ahmad, F. *et al.* Differential regulation of adipocyte PDE3B in distinct membrane compartments by insulin and the beta3-adrenergic receptor agonist CL316243: effects of caveolin-1 knockdown on formation/maintenance of macromolecular signalling complexes. *The Biochemical journal* **424**, 399-410, doi:10.1042/BJ20090842 (2009).

126 Ebdrup, S., Sorensen, L. G., Olsen, O. H. & Jacobsen, P. Synthesis and structure-activity relationship for a novel class of potent and selective carbamoyl-triazole based inhibitors of hormone sensitive lipase. *Journal of medicinal chemistry* **47**, 400-410, doi:10.1021/jm031004s (2004).

127 Wood, S. L., Emmison, N., Borthwick, A. C. & Yeaman, S. J. The protein phosphatases responsible for dephosphorylation of hormone-sensitive lipase in isolated rat adipocytes. *The Biochemical journal* **295 (Pt 2)**, 531-535 (1993).

128 Kershaw, E. E. *et al.* Adipose triglyceride lipase: function, regulation by insulin, and comparison with adiponutrin. *Diabetes* **55**, 148-157 (2006).

129 Zechner, R. *et al.* FAT SIGNALS--lipases and lipolysis in lipid metabolism and signaling. *Cell metabolism* **15**, 279-291, doi:10.1016/j.cmet.2011.12.018 (2012).

130 Kadowaki, T. *et al.* Risk factors for worsening to diabetes in subjects with impaired glucose tolerance. *Diabetologia* **26**, 44-49 (1984).

131 Martin, B. C. *et al.* Role of glucose and insulin resistance in development of type 2 diabetes mellitus: results of a 25-year follow-up study. *Lancet* **340**, 925-929 (1992).

132 Saltiel, A. R. Insulin Signaling in the Control of Glucose and Lipid Homeostasis. *Handbook of experimental pharmacology* **233**, 51-71, doi:10.1007/164_2015_14 (2016).

133 Matsuzaka, T. & Shimano, H. Molecular mechanisms involved in hepatic steatosis and insulin resistance. *Journal of diabetes investigation* **2**, 170-175, doi:10.1111/j.2040-1124.2011.00111.x (2011).

134 Sanders, F. W. & Griffin, J. L. De novo lipogenesis in the liver in health and disease: more than just a shunting yard for glucose. *Biological reviews of the Cambridge Philosophical Society* **91**, 452-468, doi:10.1111/brv.12178 (2016).

135 Tang, Y. *et al.* Adipose tissue mTORC2 regulates ChREBP-driven de novo lipogenesis and hepatic glucose metabolism. *Nature communications* **7**, 11365, doi:10.1038/ncomms11365 (2016).

136 Cao, H. *et al.* Identification of a lipokine, a lipid hormone linking adipose tissue to systemic metabolism. *Cell* **134**, 933-944, doi:10.1016/j.cell.2008.07.048 (2008).

137 Yore, M. M. *et al.* Discovery of a class of endogenous mammalian lipids with anti-diabetic and anti-inflammatory effects. *Cell* **159**, 318-332, doi:10.1016/j.cell.2014.09.035 (2014).

138 Nadler, S. T. *et al.* The expression of adipogenic genes is decreased in obesity and diabetes mellitus. *Proceedings of the National Academy of Sciences of the*

United States of America **97**, 11371-11376, doi:10.1073/pnas.97.21.11371 (2000).

139 Moraes, R. C. *et al.* Study of the alteration of gene expression in adipose tissue of diet-induced obese mice by microarray and reverse transcription-polymerase chain reaction analyses. *Endocrinology* **144**, 4773-4782, doi:10.1210/en.2003-0456 (2003).

140 Bruss, M. D., Khambatta, C. F., Ruby, M. A., Aggarwal, I. & Hellerstein, M. K. Calorie restriction increases fatty acid synthesis and whole body fat oxidation rates. *American journal of physiology. Endocrinology and metabolism* **298**, E108-116, doi:10.1152/ajpendo.00524.2009 (2010).

141 Nuotio-Antar, A. M. *et al.* FABP4-Cre Mediated Expression of Constitutively Active ChREBP Protects Against Obesity, Fatty Liver, and Insulin Resistance. *Endocrinology* **156**, 4020-4032, doi:10.1210/en.2015-1210 (2015).

142 Moraes-Vieira, P. M., Saghatelian, A. & Kahn, B. B. GLUT4 Expression in Adipocytes Regulates De Novo Lipogenesis and Levels of a Novel Class of Lipids With Antidiabetic and Anti-inflammatory Effects. *Diabetes* **65**, 1808-1815, doi:10.2337/db16-0221 (2016).

143 Savage, D. B., Petersen, K. F. & Shulman, G. I. Disordered lipid metabolism and the pathogenesis of insulin resistance. *Physiological reviews* **87**, 507-520, doi:10.1152/physrev.00024.2006 (2007).

144 Boden, G. Role of fatty acids in the pathogenesis of insulin resistance and NIDDM. *Diabetes* **46**, 3-10 (1997).

145 Kelley, D. E., Mokan, M., Simoneau, J.-A. & Mandarino, L. J. Interaction between glucose and free fatty acid metabolism in human skeletal muscle. *Journal of Clinical Investigation* **92**, 91 (1993).

146 Gandotra, S. *et al.* Human frame shift mutations affecting the carboxyl terminus of perilipin increase lipolysis by failing to sequester the adipose triglyceride lipase (ATGL) coactivator AB-hydrolase-containing 5 (ABHD5). *The Journal of biological chemistry* **286**, 34998-35006, doi:10.1074/jbc.M111.278853 (2011).

147 Gandotra, S. *et al.* Perilipin deficiency and autosomal dominant partial lipodystrophy. *The New England journal of medicine* **364**, 740-748, doi:10.1056/NEJMoa1007487 (2011).

148 Maeda, N. *et al.* Diet-induced insulin resistance in mice lacking adiponectin/ACRP30. *Nature medicine* **8**, 731-737, doi:10.1038/nm724 (2002).

149 Yamauchi, T. *et al.* Adiponectin stimulates glucose utilization and fatty-acid oxidation by activating AMP-activated protein kinase. *Nature medicine* **8**, 1288-1295, doi:10.1038/nm788 (2002).

150 Cong, L. *et al.* Regulation of adiponectin and leptin secretion and expression by insulin through a PI3K-PDE3B dependent mechanism in rat primary adipocytes. *Biochemical Journal* **403**, 519-525 (2007).

151 Engfeldt, P., Arner, P., Bolinder, J. & Ostman, J. Phosphodiesterase activity in human subcutaneous adipose tissue in insulin- and noninsulin-dependent diabetes mellitus. *The Journal of clinical endocrinology and metabolism* **55**, 983-988, doi:10.1210/jcem-55-5-983 (1982).

152 He, Y. *et al.* The multimerization and secretion of adiponectin are regulated by

TNF-alpha. *Endocrine* **51**, 456-468, doi:10.1007/s12020-015-0741-4 (2016).

153 Jin, D. *et al.* Peroxisome proliferator-activated receptor gamma enhances adiponectin secretion via up-regulating DsbA-L expression. *Molecular and cellular endocrinology* **411**, 97-104, doi:10.1016/j.mce.2015.04.015 (2015).

154 Landrier, J. F. *et al.* Reduced adiponectin expression after high-fat diet is associated with selective up-regulation of ALDH1A1 and further retinoic acid receptor signaling in adipose tissue. *FASEB journal : official publication of the Federation of American Societies for Experimental Biology* **31**, 203-211, doi:10.1096/fj.201600263RR (2017).

155 DeClercq, V., d'Eon, B. & McLeod, R. S. Fatty acids increase adiponectin secretion through both classical and exosome pathways. *Biochimica et biophysica acta* **1851**, 1123-1133, doi:10.1016/j.bbalip.2015.04.005 (2015).

156 Ruan, H. & Dong, L. Q. Adiponectin signaling and function in insulin target tissues. *Journal of molecular cell biology* **8**, 101-109, doi:10.1093/jmcb/mjw014 (2016).

157 Cypess, A. M. & Kahn, C. R. Brown fat as a therapy for obesity and diabetes. *Current opinion in endocrinology, diabetes, and obesity* **17**, 143-149, doi:10.1097/MED.0b013e328337a81f (2010).

158 Duchamp, C. & Barre, H. Skeletal muscle as the major site of nonshivering thermogenesis in cold-acclimated ducklings. *The American journal of physiology* **265**, R1076-1083, doi:10.1152/ajpregu.1993.265.5.R1076 (1993).

159 Reynisdottir, S., Wahrenberg, H., Carlstrom, K., Rossner, S. & Arner, P. Catecholamine resistance in fat cells of women with upper-body obesity due to decreased expression of beta 2-adrenoceptors. *Diabetologia* **37**, 428-435 (1994).

160 Stallknecht, B., Bulow, J., Frandsen, E. & Galbo, H. Desensitization of human adipose tissue to adrenaline stimulation studied by microdialysis. *The Journal of physiology* **500 (Pt 1)**, 271-282 (1997).

161 Jocken, J. W. *et al.* Effect of beta-adrenergic stimulation on whole-body and abdominal subcutaneous adipose tissue lipolysis in lean and obese men. *Diabetologia* **51**, 320-327, doi:10.1007/s00125-007-0866-y (2008).

162 Horowitz, J. F. & Klein, S. Whole body and abdominal lipolytic sensitivity to epinephrine is suppressed in upper body obese women. *American journal of physiology. Endocrinology and metabolism* **278**, E1144-1152, doi:10.1152/ajpendo.2000.278.6.E1144 (2000).

163 Mowers, J. *et al.* Inflammation produces catecholamine resistance in obesity via activation of PDE3B by the protein kinases IKKepsilon and TBK1. *eLife* **2**, e01119, doi:10.7554/eLife.01119 (2013).

Ⅶ. Appendix

7 Appendix

7.1 Abbreviation list

Abcg1	ATP binding cassette subfamily G member 1
ABHD15	α/β-hydrolase domain containing protein 15
ACC	acetyl-CoA carboxylase
AceCS	acetyl-coenzyme A synthetase
Acot3	acyl-CoA thioesterase 3
Acot4	acyl-CoA thioesterase 4
Acsl1	acyl-CoA synthetase long chain family member 1
AMPK	5'AMP-activated protein kinase
AR	adrenergic receptor
AT	adipose tissue
ATGL	adipose triglyceride lipase
AUC	area under the curve
BAT	brown adipose tissue
cAMP	cyclic AMP
CD	chow diet
CE	cholesteryl esters
ChREBP	carbohydrate response element binding protein
CHX	cycloheximide
Cidea	cell death-inducing DFFA-like effector a
CLIX	clamp-like index
CM	cardiac muscle
DAG	diacylglycerol
Dgat1	diacylglycerol O-acyltransferase 1
Dio2	iodothyronine deiodinase 2
DMEM	dulbecco's modified eagle medium
DNL	de novo lipogenesis
ECL	enhanced chemiluminescence
ES	embryonic stem cells
eWAT	epididymal white adipose tissue

Fabp3	fatty acid binding protein 3
FAO	fatty acid oxidation
Fas	fatty acid synthase
FFA	free fatty acid
Gck	glucose kinase
GEO	gene expression omnibus
GTT	glucose tolerance test
HFD	high fat diet
HGD	high glucose diet
HLM	hypotonic lysis medium
Hmgcs1	3-hydroxy-3-methylglutaryl-CoA synthase 1
HOMA-IR	homeostatic model assessment for insulin resistance
HSL	hormone-sensitive lipase
IBMX	isobutylmethylxanthine
IQR	inter-quartile range
IR	insulin receptor
IRS	insulin receptor substrate
ISI	insulin sensitivity index
ITT	insulin tolerance test
ko	knockout
Ldlr	low density lipoprotein receptor
MAG	monoacylglycerol
MGL	monoglyceride lipase
mTORC1	mTOR complex 2
NEFA	non-esterified fatty acid
NMR	nuclear magnetic resonance
NST	non-shivering thermogenesis
o/n	overnight
OGIS	oral glucose insulin sensitivity
OGTT	oral glucose tolerance test
OWAT	omental white adipose tissue
PDE3B	Phosphodiesterase 3B

Pdgfrα	platelet derived growth factor receptor, alpha polypeptide
PDK1	phosphoinositide-dependent kinase-1
PI3K	phosphatidylinositol-3-kinase
PIC	protease inhibitor cocktail
PIP3	phosphatidylinositol 3,4,5-triphosphate
PKA	cAMP-dependent protein kinase A
PKA	protein kinase A
PKB/Akt	protein kinase B
PM	plasma membrane
PP2A	protein phosphatase 2A
PPARγ	peroxisome proliferator-activated receptor γ
Prdm16	PR/SET domain 16
RER	respiratory exchange ratio
RMA	robust multi-array average
RT	room temperature
RT-PCR	reverse transcription polymerase chain reaction
SDS	sodium dodecyl sulfate
SERCA2b	sarcoplasmic/endoplasmic reticulum calcium ATPase 2
SM	skeletal muscle
SNS	sympathetic nervous system
SREBP1	sterol regulatory element-binding protein 1
SVCs	stromal vascular cells
sWAT	subcutaneous white adipose tissue
TAG	triacylglycerol
TG	triglyceride
TLC	thin layer chromatography
Tmem26	transmembrane protein 26
Tnfrsf9	tumor necrosis factor receptor superfamily, member 9
UCP1	uncoupling protein 1
WAT	white adipose tissue
WT	wild type

7.2 Nomenclature

Murine genes are written in lowercase italics, human genes in uppercase italics. All proteins are expressed as uppercase letters.

7.3 Publication list

1. **Xia W**, Pessentheiner AR, Hofer DC, Amor M, Schreiber R, Schoiswohl G, Eichmann TO, Walenta E, Itariu B, Prager G, Hackl H, Stulnig T, Kratky D, Rülicke T, Bogner-Strauss JG. Loss of ABHD15 impairs the anti-lipolytic action of insulin by altering PDE3B stability and contributes to insulin resistance. ***Cell Rep.*** 2018 May; 23(7):1948-1961. PMID: 29768196
2. Skorobogatko Y, Dragan M, Cordon C, Reilly S, Hung CW, **Xia W**, Zhao P, Wallace M, Lackey DE, Chen XW, Osborn O, Bogner-Strauss JG, Theodorescu D, Christian M. Metallo CM, Olefsky JM, Saltiel A. RalA controls glucose homeostasis by regulating glucose uptake in brown fat. ***Proc Natl Acad Sci U S A.*** 2018 June; PMID: 29915037
3. Duta-Mare M, Sachdev V, Leopold C, Kolb D, Vujic N, Korbelius M, Hofer DC, **Xia W**, Huber K, Auer M, Gottschalk B, Magnes C, Graier WF, Prokesch A, Radovic B, Bogner-Strauss JG, Kratky D. Lysosomal acid lipase regulates fatty acid channeling in brown adipose tissue to maintain thermogenesis. ***Biochim Biophys Acta.*** 2018 April; 1863(4):467-478. PMID: 29374543